NAVAL POSTGRADUATE SCHOOL
MONTEREY, CALIFORNIA

THESIS

EXPERIMENTAL AND COMPUTATIONAL INVESTIGATION OF FLOW THROUGH AN ANNULAR TURBINE CASCADE

by

William Howard Donovan, Jr.

June 1995

Thesis Advisor: Garth V. Hobson

Approved for public release; distribution is unlimited.

DISCLAIMER NOTICE

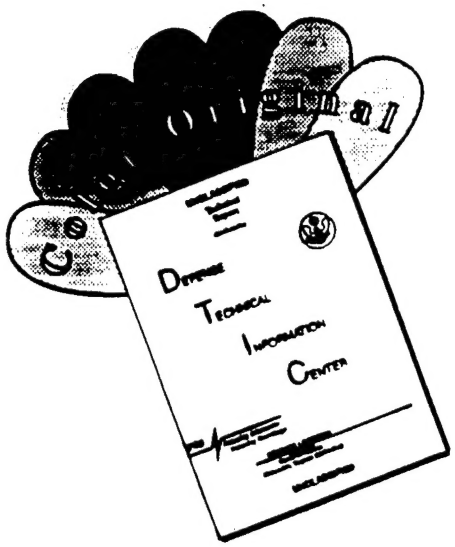

THIS DOCUMENT IS BEST QUALITY AVAILABLE. THE COPY FURNISHED TO DTIC CONTAINED A SIGNIFICANT NUMBER OF COLOR PAGES WHICH DO NOT REPRODUCE LEGIBLY ON BLACK AND WHITE MICROFICHE.

REPORT DOCUMENTATION PAGE

Form Approved OMB No. 0704-0188

1. AGENCY USE ONLY *(Leave blank)*	2. REPORT DATE	3. REPORT TYPE
	June 1995	Master's Thesis

4. TITLE AND SUBTITLE EXPERIMENTAL AND COMPUTATIONAL INVESTIGATION OF FLOW THROUGH AN ANNULAR TURBINE CASCADE

5. FUNDING NUMBERS

6. AUTHOR(S)

Donovan, William H. Jr.

7. PERFORMING ORGANIZATION NAME(S) AND ADDRESS(ES)

Naval Postgraduate School
Monterey CA 93943-5000

8. PERFORMING ORGANIZATION

9. SPONSORING/MONITORING AGENCY NAME(S) AND ADDRESS(ES)

Naval Air Warfare Center Aircraft Division, AIR-4.4.3.1 (Attn: D. Parish), Patuxent River, MD 20670-5304

10. SPONSORING/MONITORING AGENCY REPORT NUMBER

11. SUPPLEMENTARY NOTES The views expressed in this thesis are those of the author and do not reflect the official policy or position of the Department of Defense or the U.S. Government.

12a. DISTRIBUTION/AVAILABILITY STATEMENT

Approved for public release; distribution is unlimited.

12b. DISTRIBUTION CODE

13. ABSTRACT *(maximum 200 words)*

The purpose of this research was to compare numerical predictions with experimental results and to devise an accurate laser anemometry technique to measure in the endwall region of a confined annulus. Flowfield characteristics were computed using a three-dimensional flow solver with the numerical plane coincident with the experimental measurement location. An annular turbine cascade, designed for laser-Doppler velocimetry, was modified to obtain blade passage midspan surface pressure measurements. A range of predicted subsonic and transonic midspan surface pressures were compared favorably with experimental measurements. Two-dimensional Mach number, flow angle, and turbulence intensity measurements were obtained with a fiber-optics laser-Doppler velocimeter. These measurements were performed through a 1.0922 millimeter opening in the endwall at depths ranging from 0.01 mm to 3.34 mm and the results were compared with numerical predictions.

14. SUBJECT TERMS	15. NUMBER OF PAGES
Computational Fluid Dynamics, Annular Turbine Cascade, Surface Pressure Measurement, Laser-Doppler Velocimetry	96
	16. PRICE CODE

17. SECURITY CLASSIFICATION OF REPORT	18. SECURITY CLASSIFICATION OF THIS PAGE	19. SECURITY CLASSIFICATION OF ABSTRACT	20. LIMITATION OF ABSTRACT
Unclassified	Unclassified	Unclassified	UL

NSN 7540-01-280-5500

Standard Form 298 (Rev. 2-89)
Prescribed by ANSI Std. 239-18 298-102

Approved for public release; distribution is unlimited.

EXPERIMENTAL AND COMPUTATIONAL INVESTIGATION OF FLOW THROUGH AN ANNULAR TURBINE CASCADE

William H. Donovan, Jr.
Lieutenant, United States Navy
B.S., United States Naval Academy, 1986

Submitted in partial fulfillment of the
requirements for the degree of

MASTER OF SCIENCE IN AERONAUTICAL ENGINEERING

from the

NAVAL POSTGRADUATE SCHOOL
June 1995

Author: William H. Donovan, Jr.
William H. Donovan, Jr.

Approved by: Garth V. Hobson
Garth V. Hobson, Thesis Advisor

Raymond P Shreeve
Raymond P. Shreeve, Second Reader

Daniel J Collins
Daniel J. Collins, Chairman
Department of Aeronautics and Astronautics

ABSTRACT

The purpose of this research was to compare numerical predictions with experimental results and to devise an accurate laser anemometry technique to measure in the endwall region of a confined annulus. Flowfield characteristics were computed using a three-dimensional flow solver with the numerical plane coincident with the experimental measurement location. An annular turbine cascade, designed for laser-Doppler velocimetry, was modified to obtain blade passage midspan surface pressure measurements. A range of predicted subsonic and transonic midspan surface pressures were compared favorably with experimental measurements. Two-dimensional Mach number, flow angle, and turbulence intensity measurements were obtained with a fiber-optics laser-Doppler velocimeter. The measurements were performed through a 1.0922 millimeter opening in the endwall at depths ranging from 0.01 mm to 3.34 mm and the results were compared with numerical predictions.

TABLE OF CONTENTS

LIST OF FIGURES

LIST OF TABLES

ACKNOWLEDGMENTS

This work would not have been possible without the guidance and support of several dedicated individuals. I wish to thank Professor Garth Hobson for his friendship, patience, and everlasting motivation. His ability to share knowledge and spark individual interest will always be appreciated. The technical expertise, sense of humor, and friendly working environment provided by Professor Raymond Shreeve, Rick Still, and Thad Best made my work an enjoyable and worthwhile experience.

My greatest thanks goes to my immediate family. The instilled work ethic and undying support provided by my parents will guide me for life. Nothing I have accomplished has come without the unselfish sacrifice and never-ending support provided by my best friend and wife, Elaine, and three children, Megan, Brady, and Kelsey.

I. INTRODUCTION

Advanced aeropropulsion systems have required substantial technological improvements in turbomachinery. These depend on the availability of complex analysis and experimental tools. A thorough understanding of the generation and development of secondary flows in annular blade rows has provided insight into the design and performance of turbomachinery. Secondary flows, together with tip leakage flows, produce considerable flow distortions and losses in the endwall region. [Ref. 1] These losses can be minimized and turbomachinery efficiency can be improved with a more precise understanding of the flow mechanics and the ability to numerically predict the flow field. The current emphasis on turbomachinery design centers on numerical analysis.

This report specifically documents the investigation of the flow through an annular turbine cascade (ATC). References 2 through 4 include continuing research in the field of laser-Doppler velocimetry (LDV) and numerical prediction in a large annular turbine cascade. The authors provided experimental two and three-dimensional velocity, flow angle, and turbulence intensity at constant axial positions within an ATC passage. These measurements, in addition to vane surface static pressure measurements, supplied a test case for three-dimensional turbomachinery computer programs. They concentrated on obtaining comparisons ahead of, inside, and downstream of the blade passage and concluded that the largest difference between experimental and computational results was in the endwall region where viscous and secondary flow effects were the greatest.

Two previous investigations of the flow through the ATC have been conducted at the Naval Postgraduate School. Reference 5 included design and manufacturing information of the annular turbine cascade that was developed to determine the limitations of LDV measurements in a confined annulus. Reference 6 included additional laser and pressure probe access modifications and initial LDV measurements to the same ATC. This report includes further ATC modifications for midspan blade surface pressure measurements and LDV measurement techniques of the endwall flow. Radial two-dimensional fiber-optic probe traverses were performed, through a small access hole in the outer casing, to coincide with the numerical exit plane. Circumferential surveys were obtained at different radial locations close to the endwall. Blade midspan surface pressures were measured within one blade passage at various inlet total-to-downstream hub-static pressure ratios. Blade surface pressure and endwall flow measurements were compared with numerical predictions obtained using a three-dimensional viscous computer program.

The two most noteworthy comparisons were at a subsonic pressure ratio and a pressure ratio corresponding to sonic exit conditions. Comparisons with the LDV data were performed at the subsonic flow condition. The numerical blade surface pressure distributions compared well with the experimental results, particularly for the sonic exit condition for which trailing edge shocks were predicted.

II. EXPERIMENTAL SETUP

A. TEST FACILITY AND ANNULAR TURBINE CASCADE

Airflow for the annular turbine cascade experiment was provided by a VA-312 Allis-Chalmers 12-stage axial-flow compressor located at the Turbopropulsion Laboratory of the Naval Postgraduate School. The compressor was operated at 12,000 rpm at various discharge pressures and provided metered air to a plenum chamber. Air from the plenum was routed to a 232.918 mm (9.170 in) diameter bellmouth and test section through honeycomb flow straighteners in a 254 mm (10 in) flanged steel pipe as shown in Figures 1 and 2.

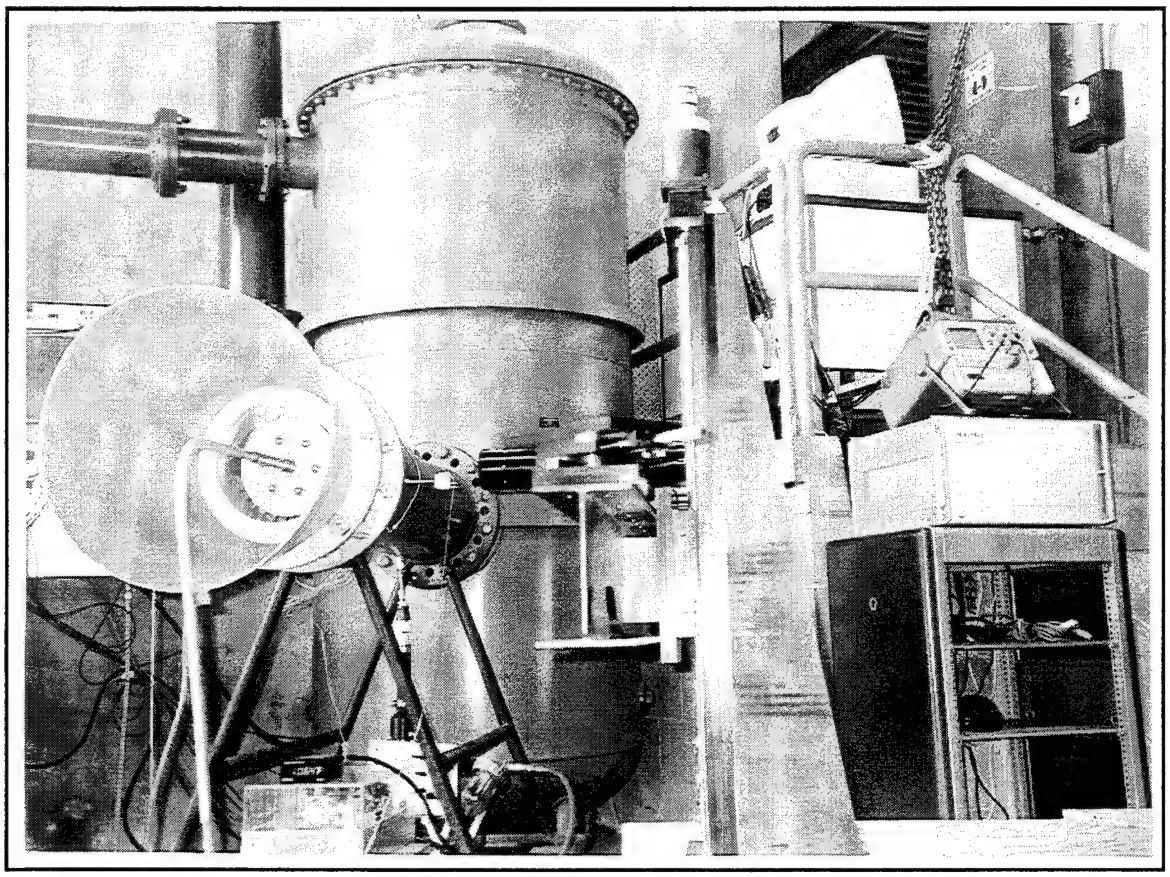

Figure 1. Front View of Experimental Apparatus

Flow stagnation pressure was measured at two upstream locations. One combination probe provided pressure-setting information to a mercury manometer board and a digital readout of flow stagnation temperature, while the second probe was connected to a Scanivalve (Figure 2, lower right). Four (averaged) upstream static ports and four (averaged) inner hub

downstream (one-half axial chord) static ports were also connected to a Scanivalve for automated pressure data acquisition.

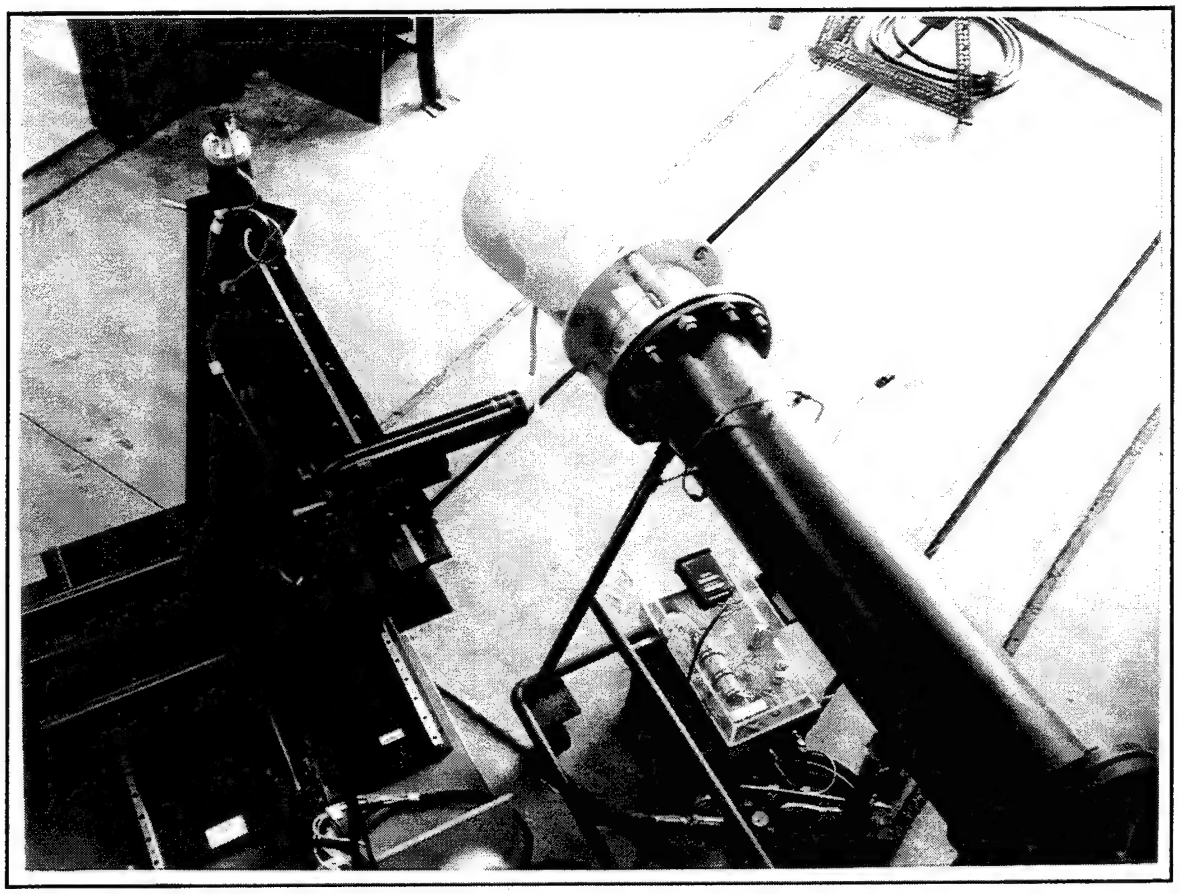

Figure 2. Top View of Experimental Apparatus

Atomized glycerin particles constituted the LDV seed material which were introduced through a 7.938 mm (0.313 in) diameter copper tube approximately 108 tube diameters upstream of the test section. Seed atomization was performed using a commercial TSI, Inc., Six-Jet Atomizer connected to the laboratory compressed air supply. Laser traverse mechanism buffet, caused by the exiting flow, was minimized with a prefabricated aluminum cone (Figure 2, upper center) and Reference 6 showed that flow characteristics were unaltered with the cone attached.

Each blade was designed with a combination of simple circular arcs and line segments and included a leading edge radius of 2.413 mm (0.095 in), trailing edge radius of 0.305 mm (0.012 in), and axial chord of 24.77 mm (0.975 in). The annular stator row was manufactured from 2218-T61 aluminum and consisted of 31 blades with a midspan spacing

of 21.77 mm (0.857 in), resulting in a blade solidity of 1.14. The inner hub radius was 98.93 mm (3.895 in) and the outer case radius was 116.46 mm (4.585 in) with the same profile at all radii. Reference 5 included the original set of manufacturing drawings and Reference 6 included a description of the wake positioning system.

B. PRESSURE MEASUREMENT MODIFICATIONS

The original ATC did not provide the capability to measure blade surface pressures. Within a single passage, seven suction-side static ports and four pressure-side static ports were drilled orthogonal to the blade surface at midspan. Figures 3 and 4 show front and rear views of the instrumented blades. As shown in Figure 5, each static port was 0.406 mm (0.016 in) in diameter and each spanwise hole was 1.321 mm (0.052 in) in diameter.

All spanwise holes were sealed at the tips and stainless steel tubes were cemented into the hub openings. The tubes were connected to the Scanivalve with plastic tubing which was fed out through a sting from the center body. (Figures 1 and 2) Each port's circumferential position was measured using a 2.375 mm (0.0935 in) diameter stylus and later converted graphically to an axial chord position to allow computational comparisons. Figure 5 shows port numbering and dimensions.

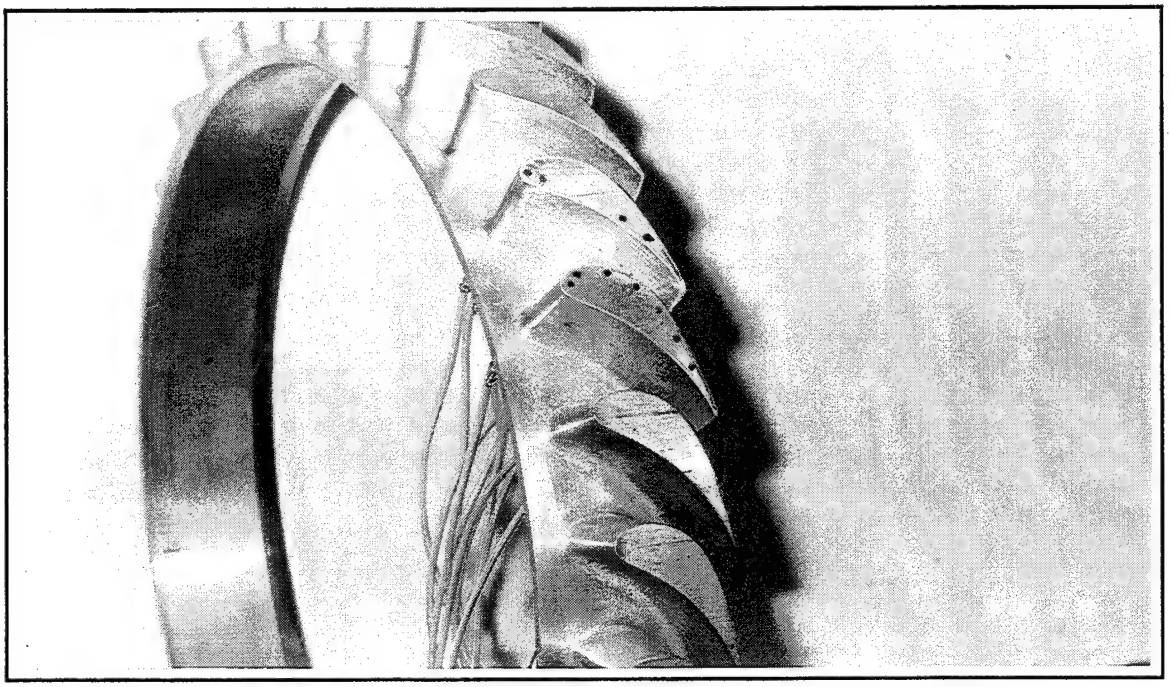

Figure 3. Blade Leading Edge View With Pressure Measurement Modifications

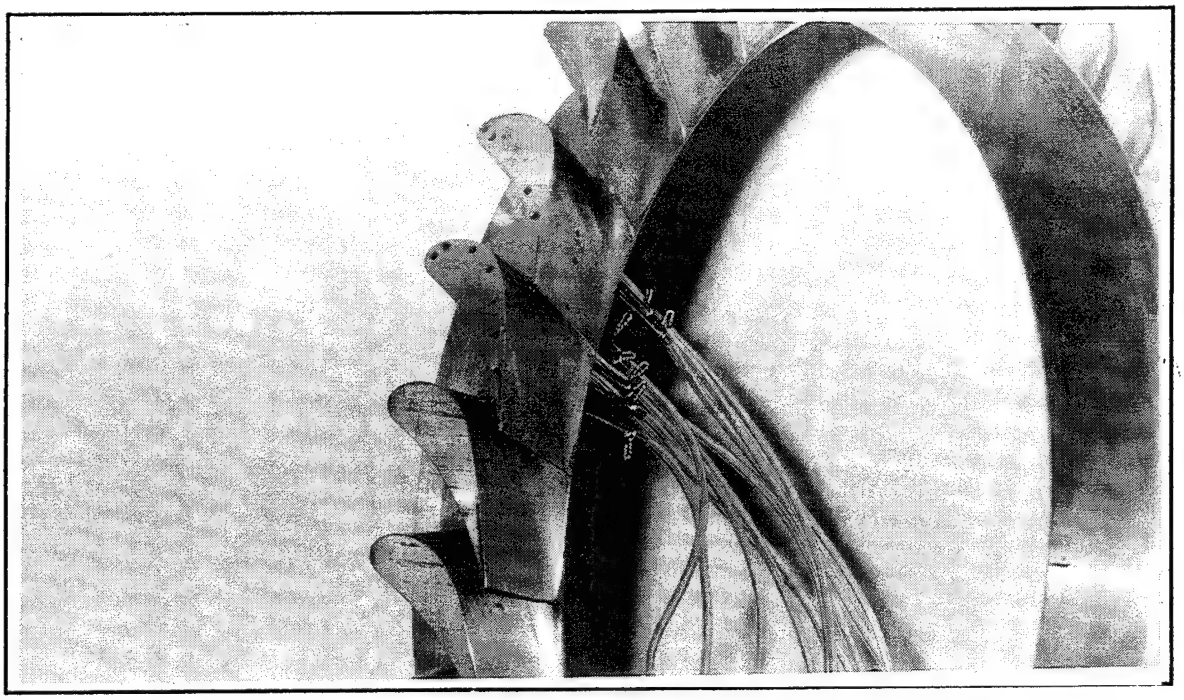

Figure 4. Blade Trailing Edge View With Pressure Measurement Modifications

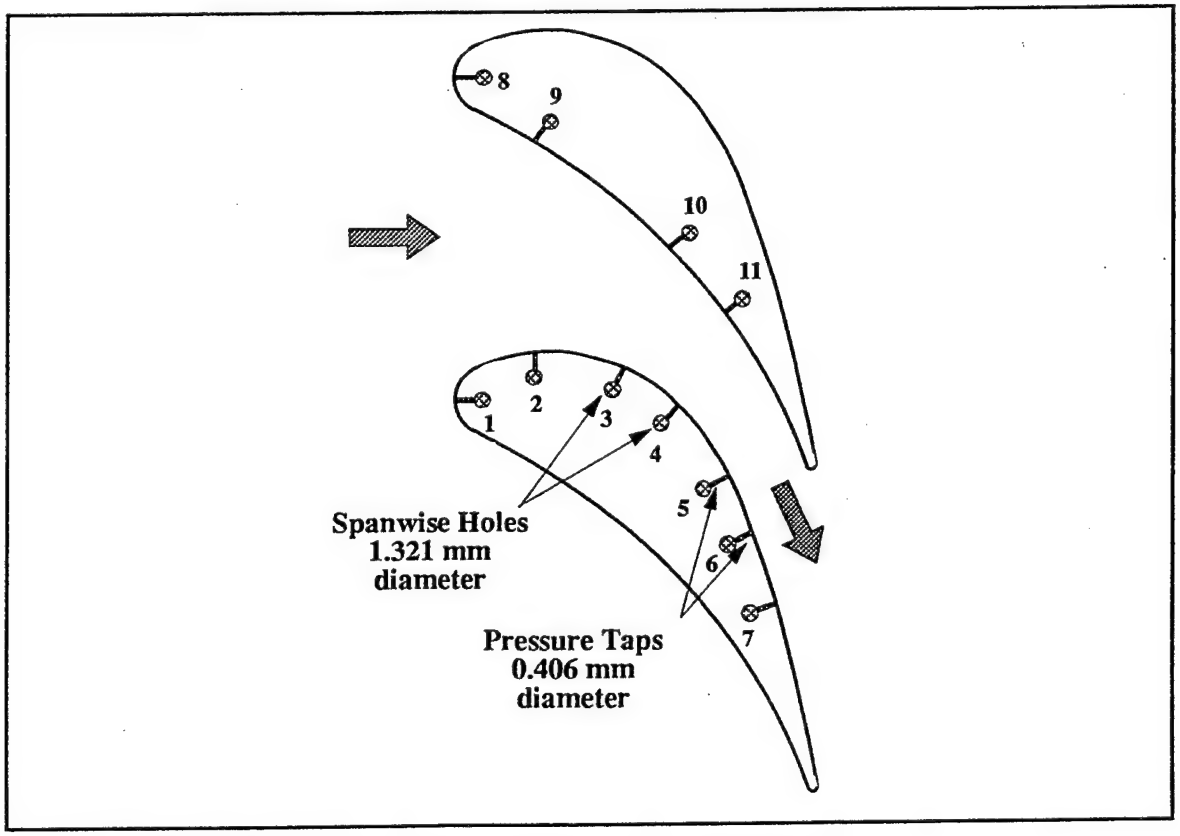

Figure 5. Blade Static Port Numbering Sequence And Dimensions

C. PRESSURE DATA ACQUISITION

The data acquisition system, for the pressure measurements, is shown schematically in Figure 6. All data acquisition was remotely controlled by a Hewlett-Packard 9000 computer system. Appendix A contains the program utilized to conduct all pressure data acquisition. A Scanivalve was connected to a Model HG-78K Scanivalve controller, which in turn was connected to a Hewlett-Packard, Model 3456A Digital Voltmeter and Model 3495A Scanner via a HP-IB instrument bus. Scanivalve calibration was performed to within an accuracy of +/- 0.1 inches mercury. Table A1 in Appendix A relates each Scanivalve port to its respective pressure measurement.

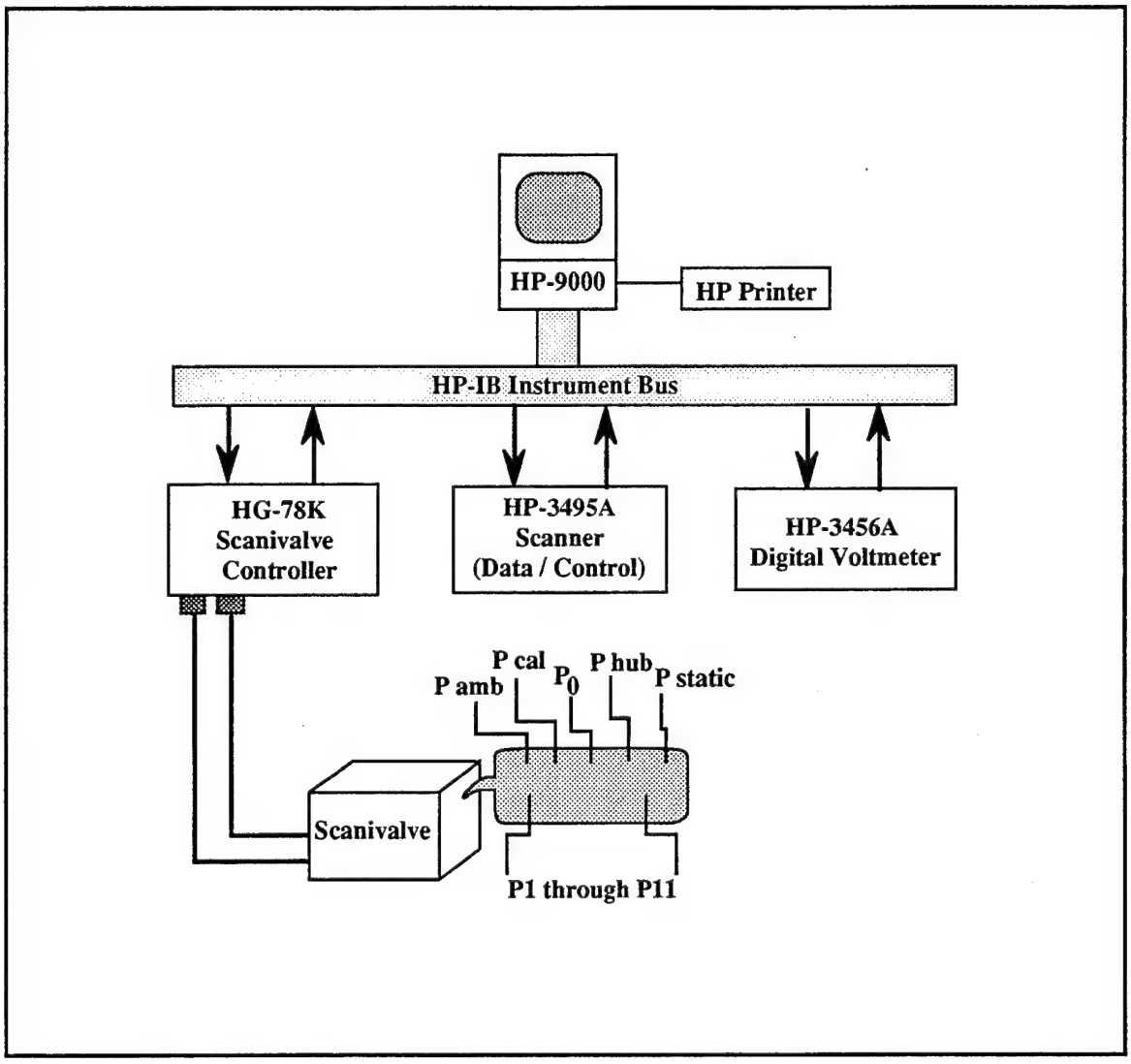

Figure 6. Pressure Data Acquisition Schematic

D. LASER-DOPPLER VELOCIMETER

Part of the laser apparatus is shown in Figure 7. The probe, processor, computer, and traverse mechanism are shown in Figures 1 and 2. The LDV system is shown schematically in Figure 8. A LEXEL Model 95 four-Watt argon-ion laser was connected to a TSI, Inc., Model 9201 ColorBurst multicolor beam separator. The beam separator divided the incoming light into shifted and unshifted beams, with the shifted beam receiving a 40 MHz frequency shift from a Bragg cell. The two beams were further split into three polarized pairs: green (514.5 nm), blue (488 nm), and violet (476.5 nm).

Individual couplers on the ColorBurst directed each beam to the laser probe via a fiber-optic cable. Each fiber-optic probe contained receiving optics which directed the return signal to a TSI, Inc., Model 9230 ColorLink multicolor receiver. The ColorLink provided photomultiplier and frequency-shifting functions. All conditioned ColorLink signals were sent to a TSI, Inc., IFA-750 digital burst correlator where valid Doppler signals were identified and digitized.

The fiber-optic probes were mounted to a LINTECH, Model 41583 traverse table. An Applied Motion Products System 1618 traverse controller was used manually to control traverse table movement. All ColorLink and IFA-750 functions and LDV data processing were accomplished remotely by computer using TSI's menu-driven software, FIND (FLOW INFORMATION DISPLAY) version 4.04.

E. EXPERIMENTAL PROCEDURE

1. Midspan Surface Pressure Measurements

Midspan surface pressure measurements were obtained with the pressure data acquisition system. The pressure ratio (P_{rat}) was defined as the downstream hub-static pressure (P_{hub}) divided by the upstream stagnation pressure (P_0). Each pressure ratio was set by metering the upstream stagnation pressure until a desired mercury manometer column height was achieved. Five pressure ratios (0.5070, 0.6041, 0.6815, 0.8077, and 0.9054) were considered and during each run all the blade surface pressures, P_0, and P_{hub} were recorded.

2. Laser Alignment

LDV alignment for endwall flow measurements was accomplished as shown in Figure 9. The objective of the LDV alignment procedure was to center the probe volume in the 1.0922 mm optical access hole at a known and repeatable radial distance. The two-dimensional fiber-optic probe was attached to a mounting-bracket micrometer which allowed

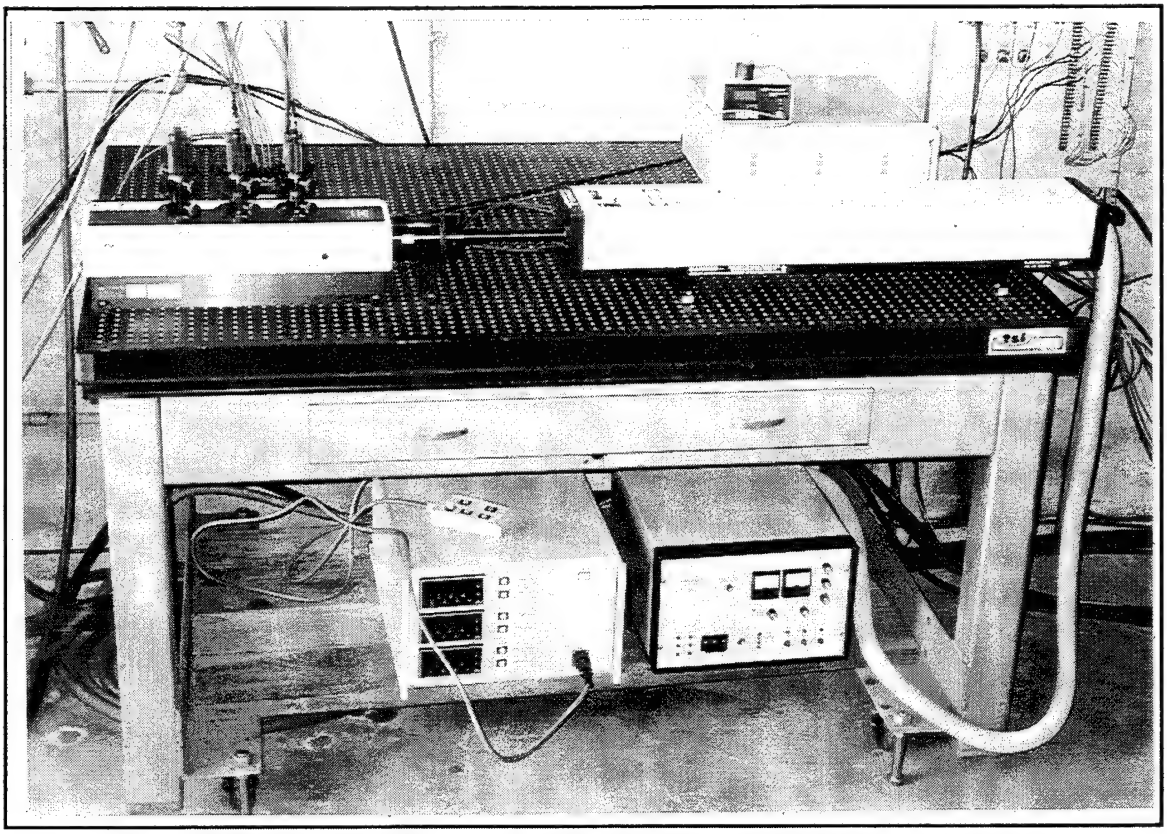

Figure 7. LDV Bread Board (with Laser, Color Separator, and Receiving Optics Module)

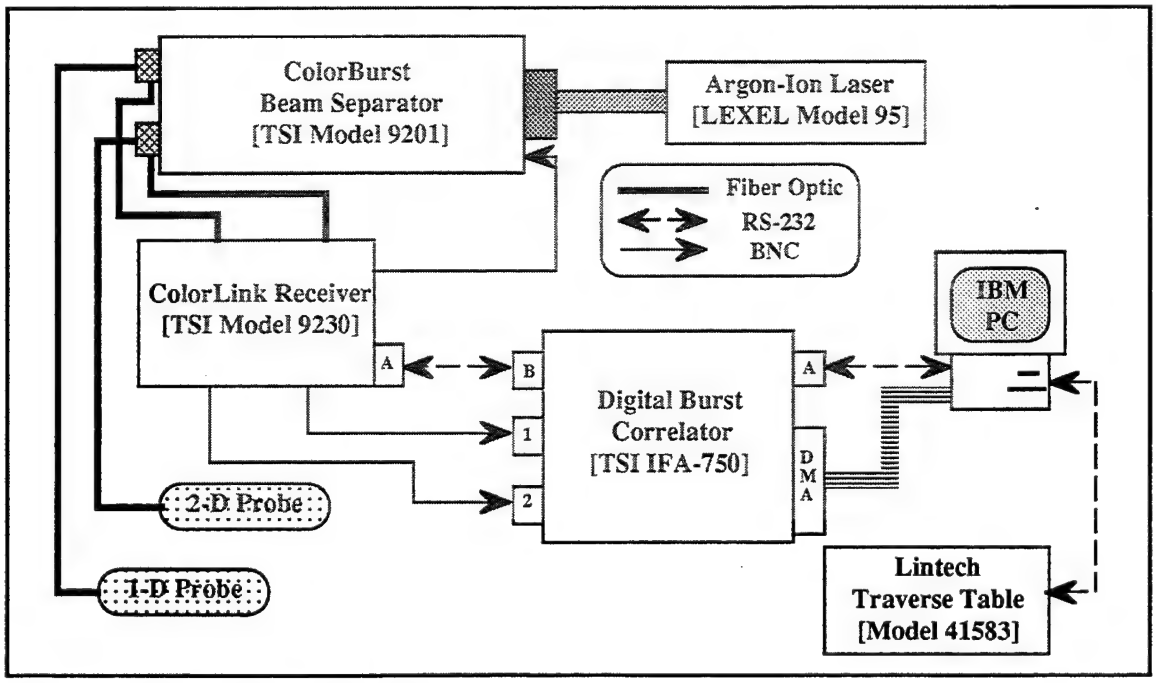

Figure 8. LDV System Schematic

probe radial travel in 0.01 mm increments. After zeroing the micrometer, the traverse table was manually advanced forward until the four beam separation was minimized, yet discernible with the naked eye (Figure 9, sketch A). The digital position-indicator reading on the traverse controller was noted and the process repeated for forward travel until the same image reappeared. The midpoint of the traverse table positions was defined as the center of the probe volume with the face of the optical access plate as a radial reference point. Reference 6 described complete dimensions of the optical access plate.

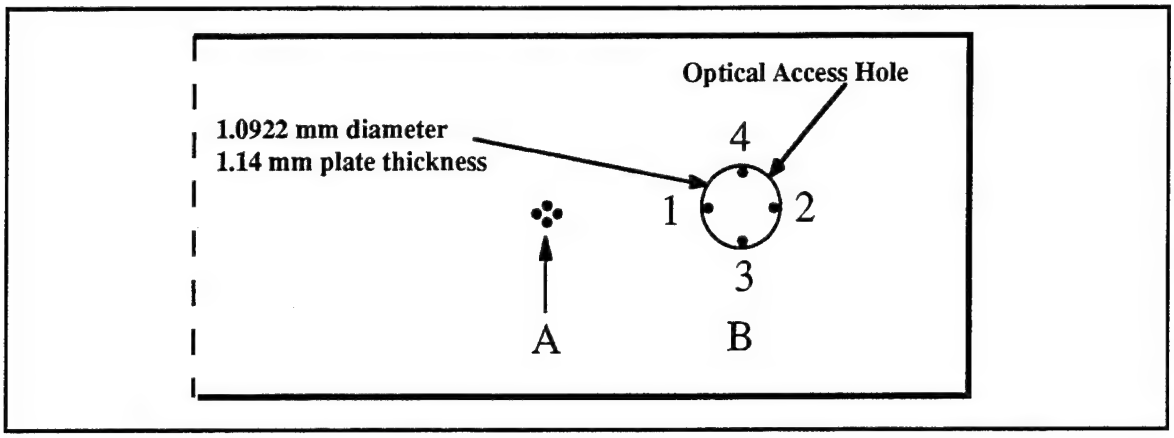

Figure 9. LDV Alignment Schematic

Horizontal and vertical alignment positions (Figure 9, sketch B) were obtained by noting the digital position indicator on the traverse controller as the probe volume touched the left(1), right(2), bottom(3), and top(4) inner edge of the optical access hole. The horizontal and vertical reference positions were defined as the center of the optical access hole. The probe was then traversed inward by 1.14 mm (the thickness of the optical access plate), at which point the center of the probe volume coincided with the outer (case) wall of the turbine cascade. This alignment technique was repeatable and ensured that the probe volume passed cleanly through the center of the optical access hole.

3. Endwall Measurements

All endwall measurements were conducted at a pressure ratio of 0.9054. The laser beams were aligned with the downstream optical access hole as described above, and then traversed manually using the mounting-bracket micrometer. Radial endwall surveys at 0.01, 0.06, 0.18, 0.42, 0.89, 1.78, and 3.34 millimeters from the tip casing were conducted for peripheral (wake) angular settings ranging from -8 degrees to +8 degrees. One degree (wake) position increments were achieved by circumferentially rotating the blade row and

center body within the outer casing. At each circumferential position the inner section was secured in place with a locking bolt arrangement, the design of which was documented in Reference 6. Seeding position, ColorLink, and IFA-750 settings were adjusted for an optimum LDV data rate and minimum noise. All settings ensured a minimum data rate of 100 samples per second, however; LDV data rate was extremely sensitive to position of the wand which introduced seed into the flow.

A 'random' mode processor setting allowed a total of 1,024 samples between the green and blue channels with no user control over sample distribution. The 'coincidence' mode acquired 1,024 samples for each channel. Repeatability measurements for endwall velocity, flow angle, and turbulence intensity were separately conducted at three wake positions for both modes. A minimum pressure ratio was determined before data rate conditions became unacceptable. Raw data were converted within FIND and manually transferred to a spreadsheet for further processing.

III. COMPUTATIONAL FLUID DYNAMICS

A. GRID GENERATION

Grid generation was completed using the FORTRAN language program "Turbomachinery C GRID (TCGRID)" [Ref. 7]. TCGRID inputs consisted of four lines of namelist inputs followed by a title, hub and tip geometry, and blade geometry. The blade geometry was input in cylindrical coordinates (z, theta, r) starting at the blade trailing edge and wrapping clockwise. The blade inputs were completed in stacked sections from the hub to the tip. The grid used, with resolution of 150 x 31 x 65 (i, j, k), was the same as that generated in Reference 6. The i-index was defined clockwise from the lower (pressure surface) exit to the upper (suction surface) exit, the j-index was defined from the blade surface to the periodic boundary, and the k-index was defined from the hub to the tip. All computational solutions were based on this gird. The final grid is shown in Figure 10. Appendix B contains the grid namelist input file and Figure B1 shows the blade geometry.

B. COMPUTATIONAL SCHEME

Flowfield solutions were obtained using two versions (206 and 208) of "Rotor Viscous Code 3-D (RVC3D)", a FORTRAN language program designed for analysis of three-dimensional viscous flows in turbomachinery. RVC3D was written to solve the thin-layer Navier-Stokes equations in Cartesian coordinates. The equations were discretized using second-order finite-differences in space and solved in time with a fourth-order Runge-Kutta scheme. Streamwise viscous terms were neglected using a thin-layer assumption, but cross-channel viscous terms were retained. A spatially-varying time step and implicit residual smoothing were used to accelerate convergence. [Refs. 8-10] Turbulence effects were modeled using a 3-D adaptation of the Baldwin-Lomax model and the Cebeci-Smith model.

RVC3D version 206 was used to predict the flowfield for pressure ratios of 0.6041, 0.6815, 0.8077, and 0.9054. The turbulence in the flowfield was computed with an adaptation of the Cebeci-Smith turbulence model. This version of RVC3D only accommodated subsonic exit boundary conditions whereby the hub static pressure was held at the pressure ratio and radial equilibrium was solved for the spanwise pressure distribution. Version 208 of RVC3D was used for the 0.5070 pressure ratio, which produced trailing edge shocks that extended to the exit plane. This newer version allowed for a supersonic exit boundary condition where the exit conditions were based on Giles' characteristic boundary conditions [Ref. 11]. The Baldwin-Lomax turbulence model was used for this test case since

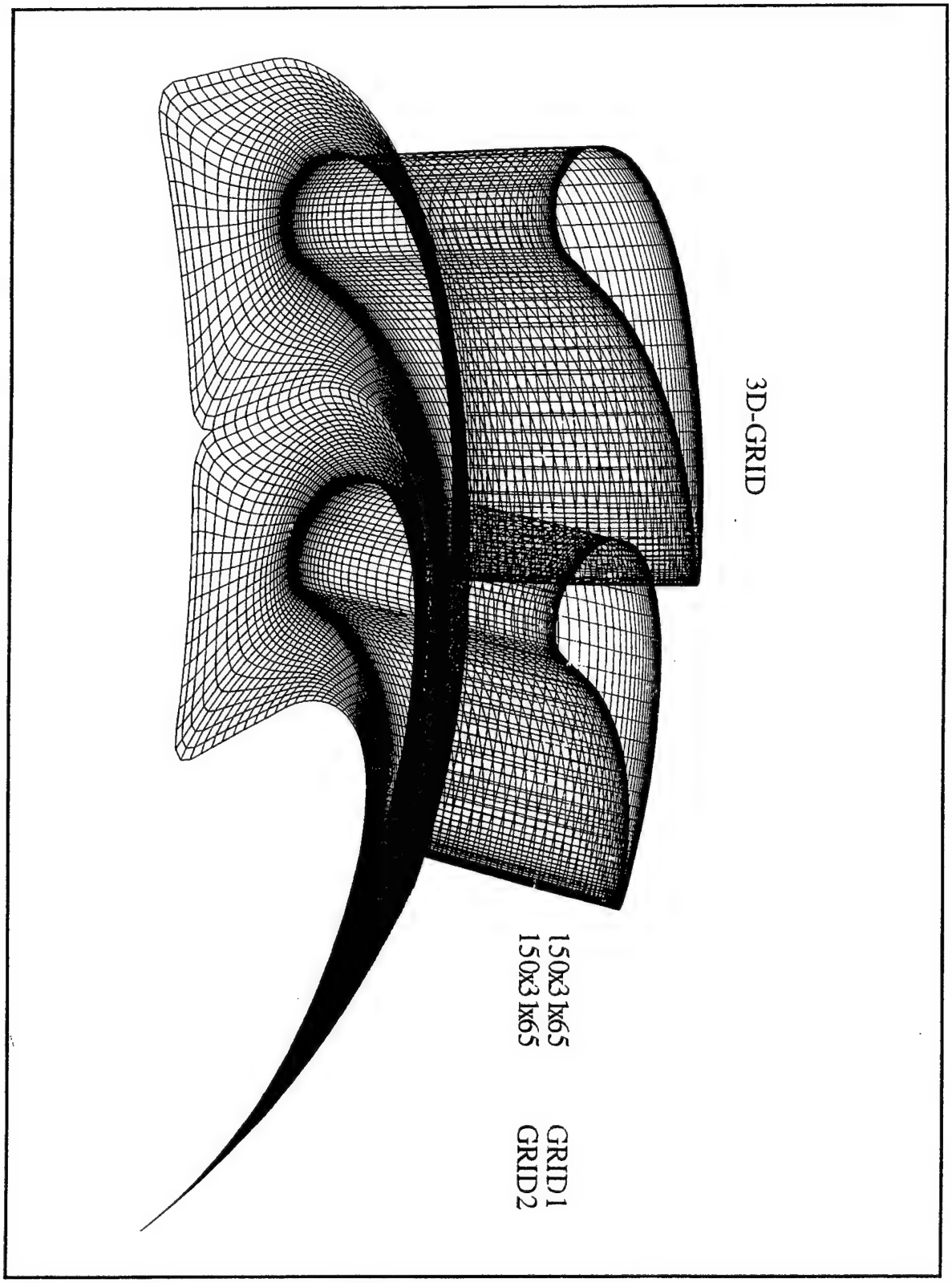

Figure 10. Three-Dimensional Multiple Grid (150 x 31 x 65)

a 'bug' was discovered that would not allow the code to properly recognize the Cebeci-Smith turbulence model [Ref. 12]. The code's author has since corrected the program.

Appendix C contains an example namelist input file used to obtain a flow solution and a description of the steps required to run the code on the Naval Postgraduate School (NPS) and National Aerodynamic Simulation Program (NAS) Cray supercomputers. Output solution file (fort.3) information was visually examined with FAST and PLOT3D graphics software [Refs. 13 and 14]. Solution residual files (fort.4), blade surface pressure files (fort.7), and Mach number and flow angle files (fort. 7-11) were calculated from the solution file with the FORTRAN programs "pxy.f" and "plane.f" (Appendix G) for final graphical representation.

IV. RESULTS AND DISCUSSION

A. BLADE MIDSPAN SURFACE PRESSURE MEASUREMENTS

Experimental blade-surface pressure measurements were averaged and a maximum repeatability error was calculated. Each blade static port reading was non-dimensionalized by the upstream stagnation pressure (P_0). In order to provide an experimental comparison with Reference 6 for the 0.6815 pressure ratio, experimental repeatability was confirmed by conducting six runs; three runs each on separate days (Tables D1 and D2 of Appendix D). The maximum repeatability error was 0.87%. All other mean pressure data were based on a three run average at each pressure ratio and resulted in a maximum repeatability error ranging from 0.66% at the lowest pressure ratio down to 0.22% at the highest pressure ratio. Table 1 contains each midspan static port location and non-dimensional pressure measurement for all experimental pressure ratios. Tables D3 through D6 of Appendix D contain pressure data for pressure ratios of 0.5070, 0.6041, 0.8077, and 0.9054 respectively.

Static Port Number	Fraction of Axial Chord (x/c)	Pressure Ratio = 0.5070	Pressure Ratio = 0.6041	Pressure Ratio = 0.6815	Pressure Ratio = 0.8077	Pressure Ratio = 0.9054
1	0.0000	1.0116	1.0019	0.9999	0.9996	1.0012
2	0.1322	0.9628	0.9576	0.9600	0.9729	0.9872
3	0.4615	0.8613	0.8646	0.8791	0.9171	0.9566
4	0.6604	0.6986	0.7223	0.7595	0.8433	0.9195
5	0.7757	0.5419	0.6216	0.6910	0.8113	0.9057
6	0.8542	0.5584	0.6358	0.7031	0.8190	0.9103
7	0.9183	0.5200	0.6166	0.6928	0.8169	0.9102
8	0.0000	1.0082	0.9987	0.9992	0.9993	1.0004
9	0.1322	0.9955	0.9878	0.9893	0.9923	0.9973
10	0.6274	0.9389	0.9362	0.9439	0.9600	0.9810
11	0.7508	0.8853	0.8874	0.9015	0.9327	0.9668

Table 1. Non-Dimensional Midspan Surface Pressure (P/P_0)

B. LASER-DOPPLER VELOCIMETRY MEASUREMENTS

Two-dimensional LDV measurements were obtained to an approximate depth of 3.34 mm through a 1.0922 mm (0.043 in) diameter hole located one-half axial chord downstream. All LDV data were acquired at a pressure ratio of 0.9054 and are tabulated in

Tables E1 through E5 of Appendix E. All data resulted from programmed editing of histograms by the FIND software and data outside two standard deviations were discarded.

The axial velocity (V_Z) and tangential velocity (V_{theta}) were combined to form the total velocity (V_{total}) as shown in Figure 11. Flow velocities are seen to decrease toward the case wall. The boundary layer was distorted due to secondary flows and wake and corner vortices that form within the blade passage. Two-dimensional endwall flow angle was defined as the arc tangent of the tangential velocity divided by the axial velocity and is shown graphically in Figure 12. Periodicity is evident over 11.6 degrees (31 blades).

Turbulence intensities were calculated with respect to the maximum downstream exit velocity (V_{exit}). Figures 13 and 14 show turbulence intensity in both the tangential and axial directions. The tangential turbulence intensity is seen to be higher, possibly due to the steep gradient of the V_{theta} mean-flow profile in the radial direction.

The 0.9054 pressure ratio provided excellent seeding conditions and ATC vibrations were low. Data rates ranged from approximately 300 samples per second at the 3.34 mm depth to 150 samples per second at the 0.01 mm depth. Seeding material slowly accumulated inside the lower portion of the optical access hole and interfered with LDV data acquisition. Occasionally, the atomizer was secured and seed material allowed to disperse. Hole alignment and laser power (1.5 Watts) were periodically verified as these could drift due to temperature changes. Endwall measurement techniques did not provide pressure equalization across the optical access hole. During one exploratory run a minimum pressure ratio of 0.80 was achieved before the data rates deteriorated to unacceptable levels.

A random mode comparison resulted in an average repeatability difference of 2.9%, 0.6%, 6.4%, and 7.0% for velocity, flow angle, tangential turbulence intensity, and axial turbulence intensity respectively. Figures 15 through 23 graphically depict velocity, flow angle, and turbulence intensity random mode repeatability data for wake positions of +7, 0, and -8 degrees. A random and coincidence mode comparison resulted in an average maximum difference of 0.4%, 0.2%, 4.1%, and 6.3% for velocity, flow angle, tangential turbulence intensity, and axial turbulence intensity respectively. Tables F1 and F2 of Appendix F contain LDV repeatability data.

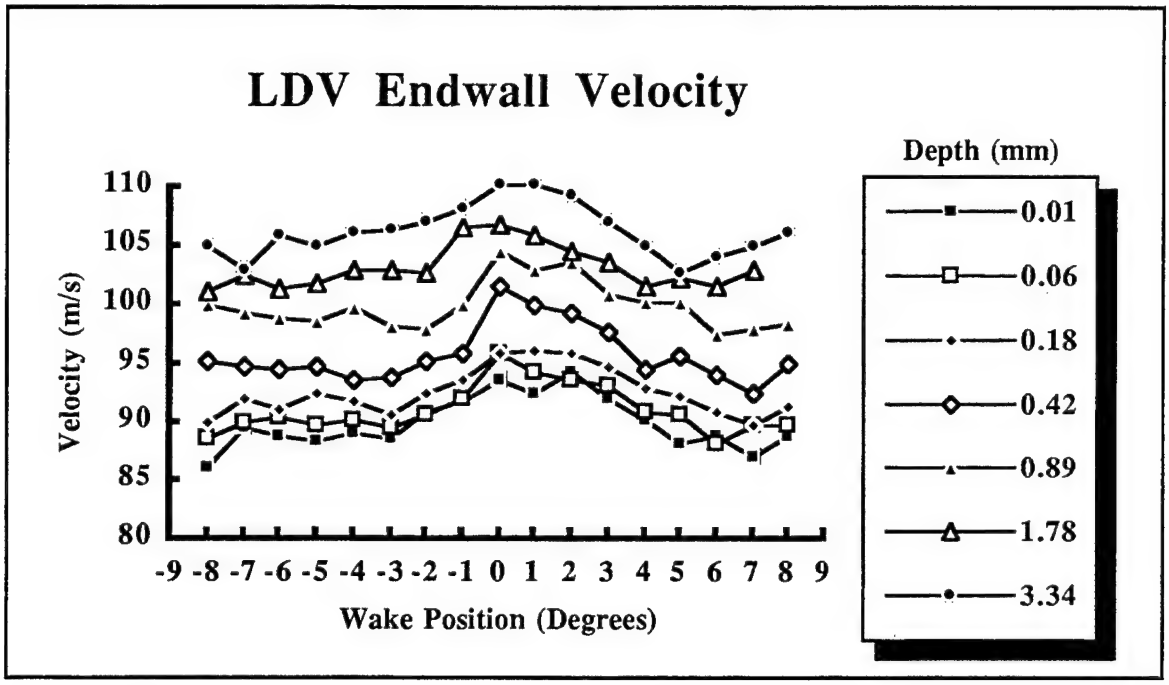

Figure 11. Two Component LDV Endwall Velocity

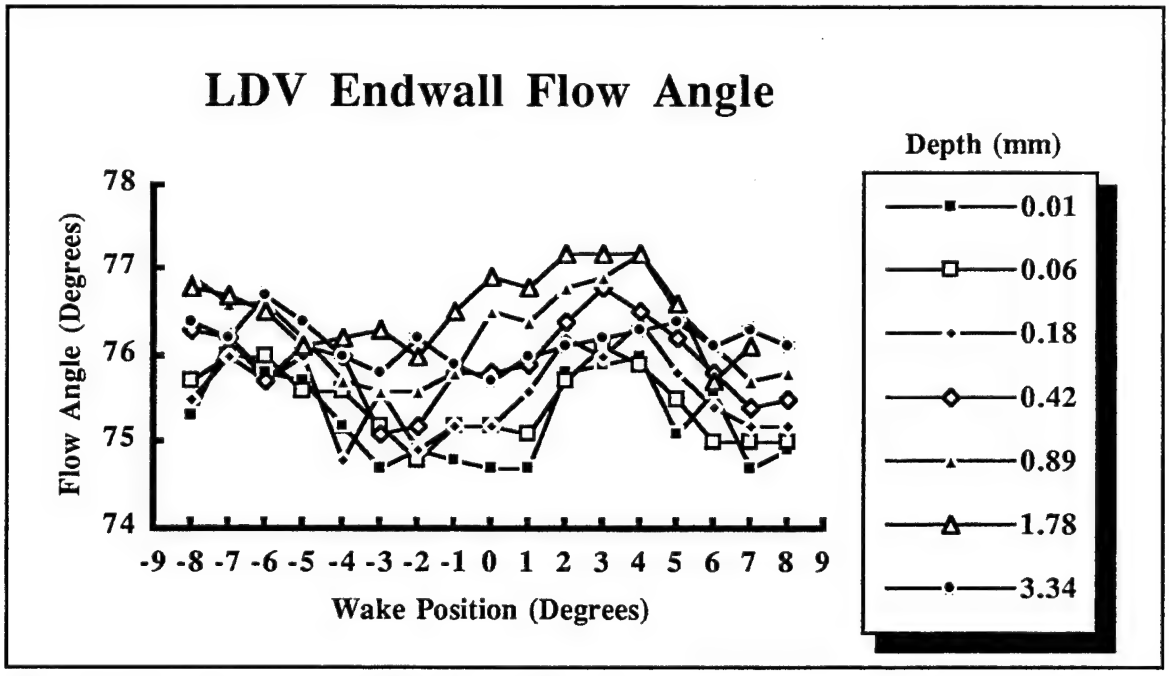

Figure 12. Two Component LDV Endwall Flow Angle

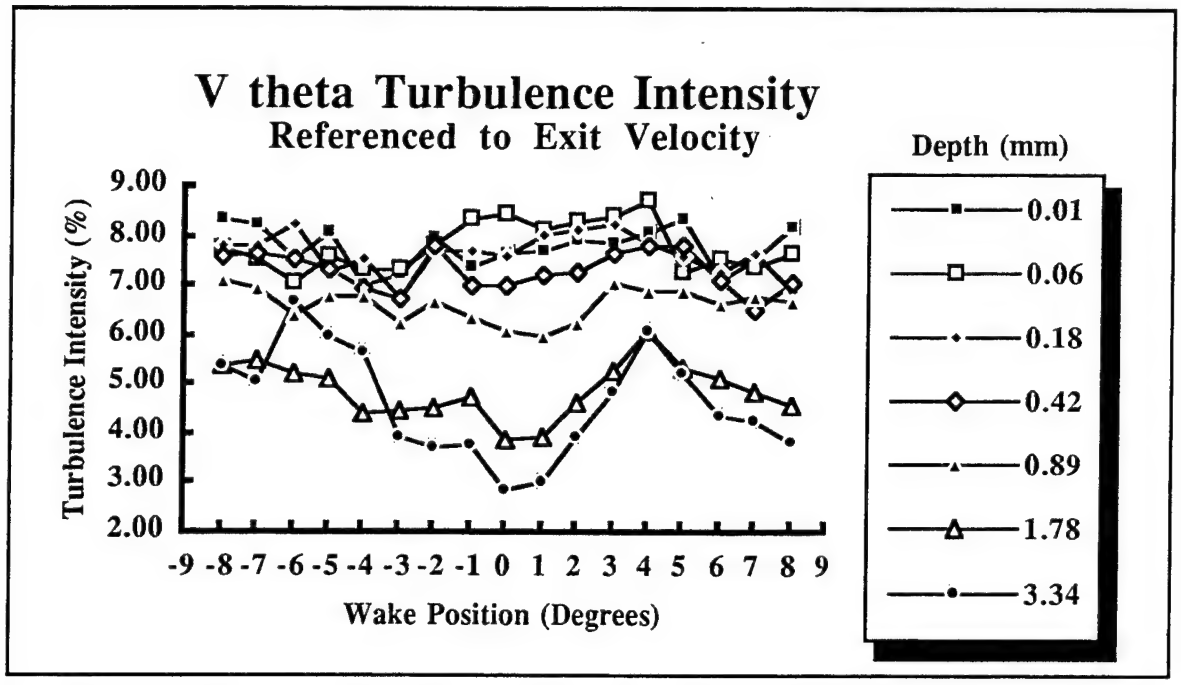

Figure 13. Two Component LDV Endwall Turbulence, V_{theta}

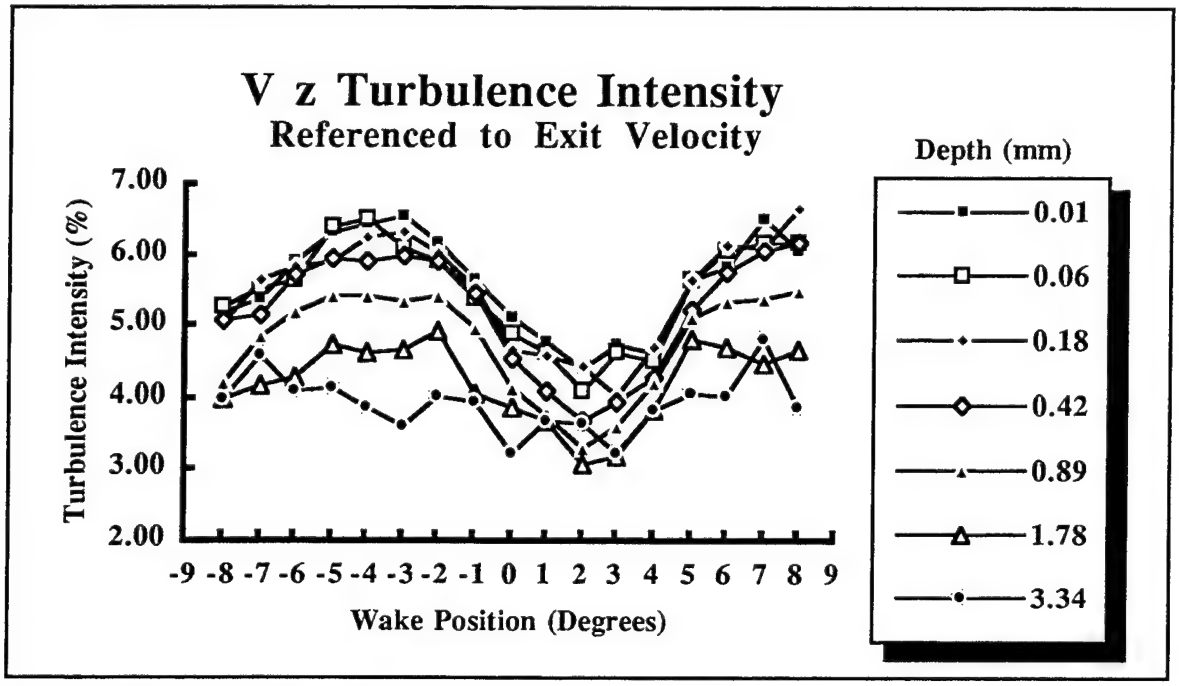

Figure 14. Two Component LDV Endwall Turbulence, V_Z

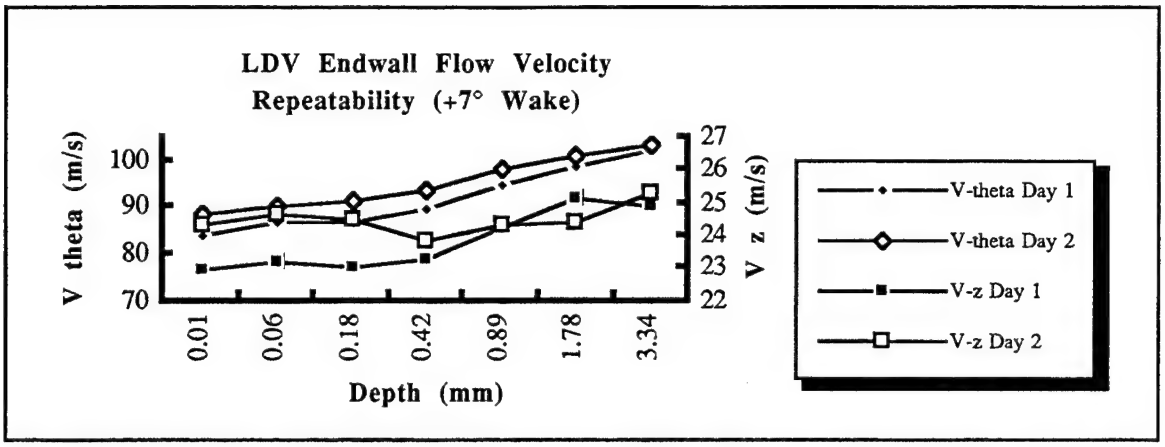

Figure 15. LDV Endwall Flow Velocity Repeatability At +7 Degrees Wake Position

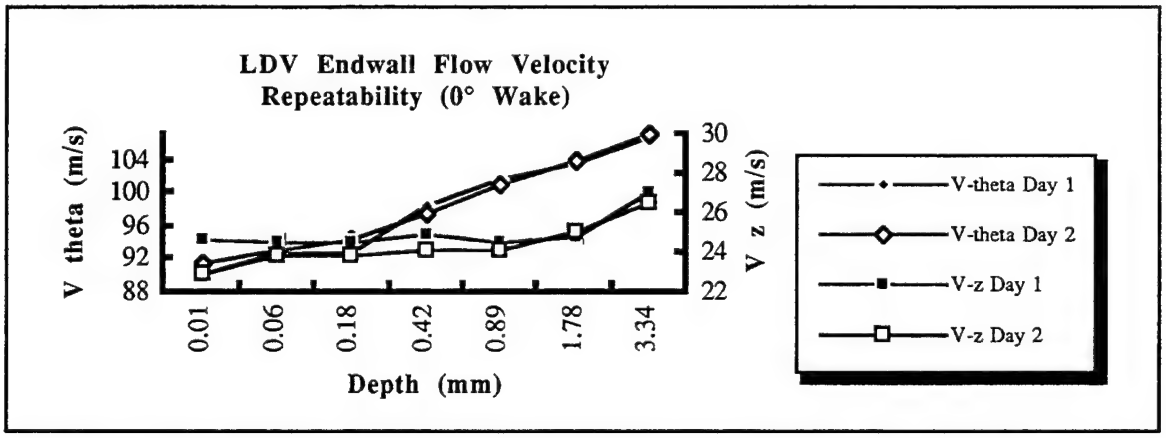

Figure 16. LDV Endwall Flow Velocity Repeatability At 0 Degrees Wake Position

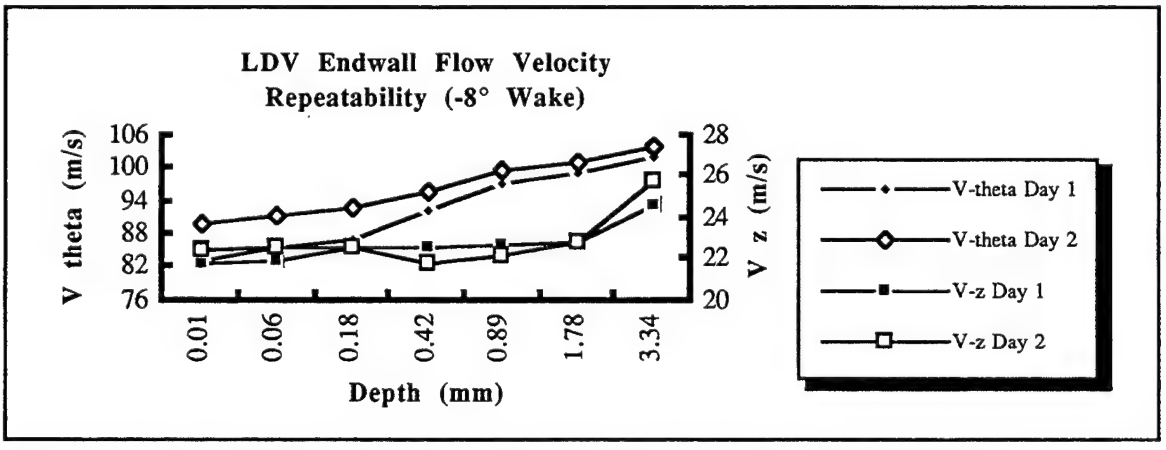

Figure 17. LDV Endwall Flow Velocity Repeatability At -8 Degrees Wake Position

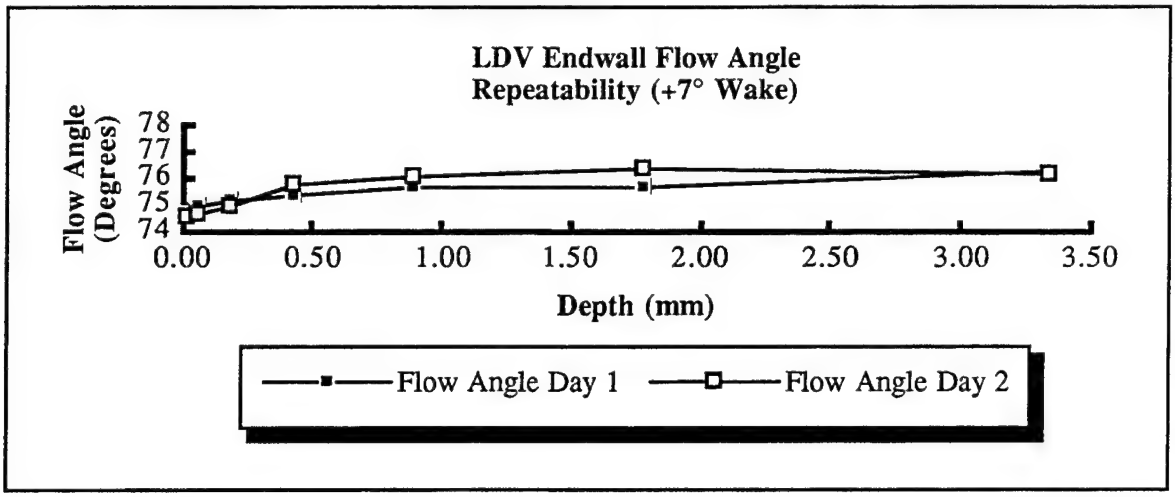

Figure 18. LDV Endwall Flow Angle Repeatability At +7 Degrees Wake Position

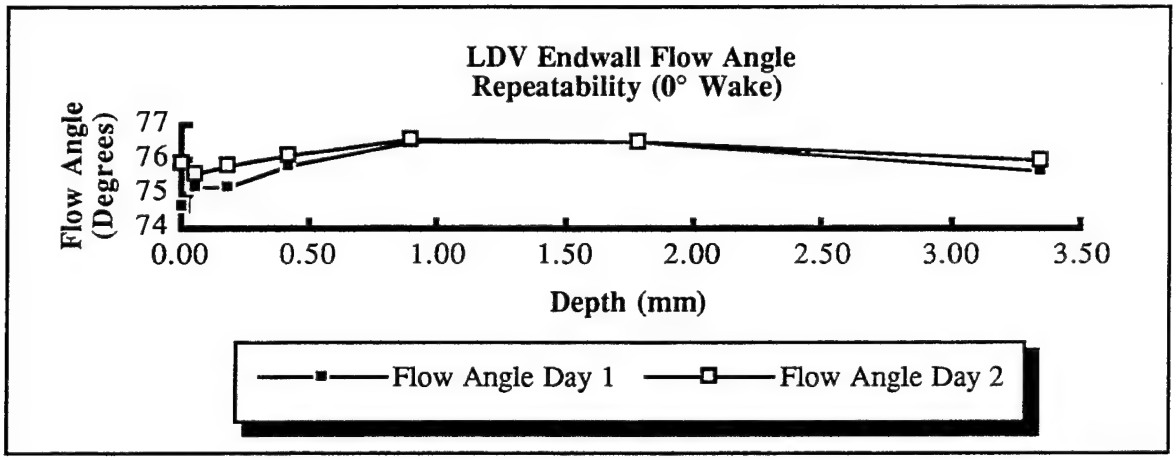

Figure 19. LDV Endwall Flow Angle Repeatability At 0 Degrees Wake Position

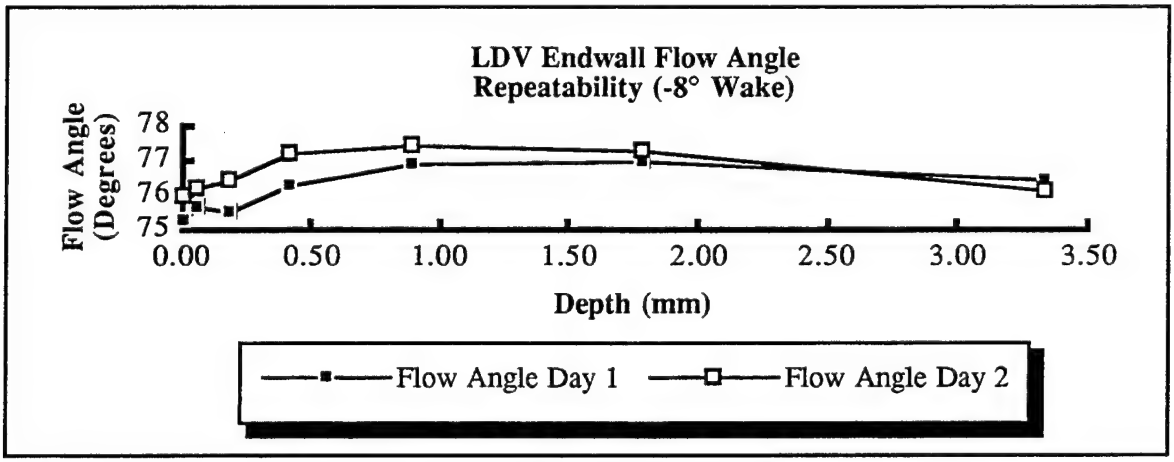

Figure 20. LDV Endwall Flow Angle Repeatability At -8 Degrees Wake Position

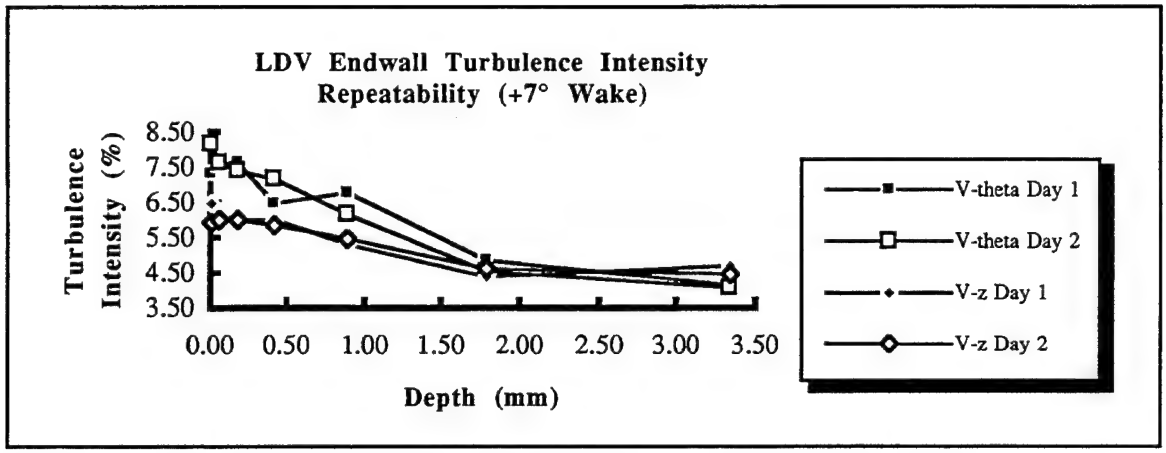

Figure 21. LDV Endwall Turbulence Repeatability At +7 Degrees Wake Position

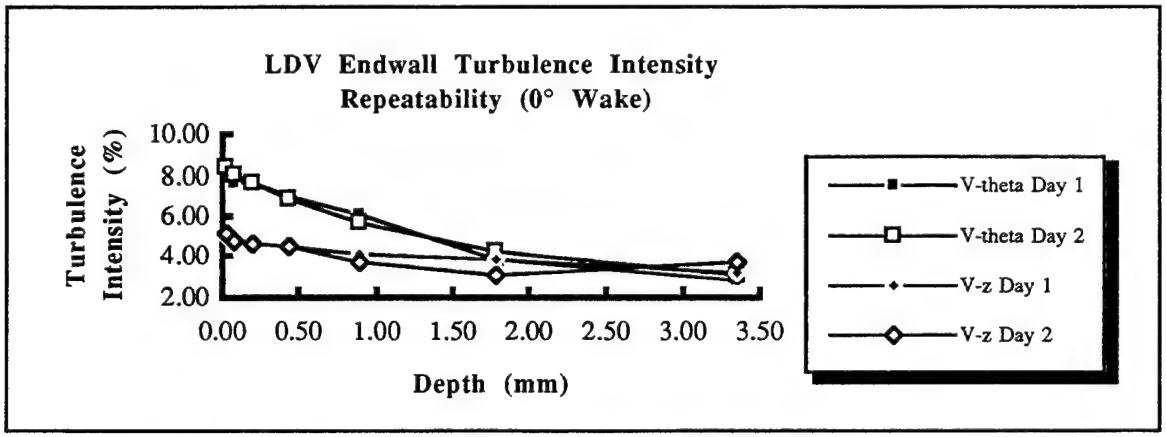

Figure 22 LDV Endwall Turbulence Repeatability At 0 Degrees Wake Position

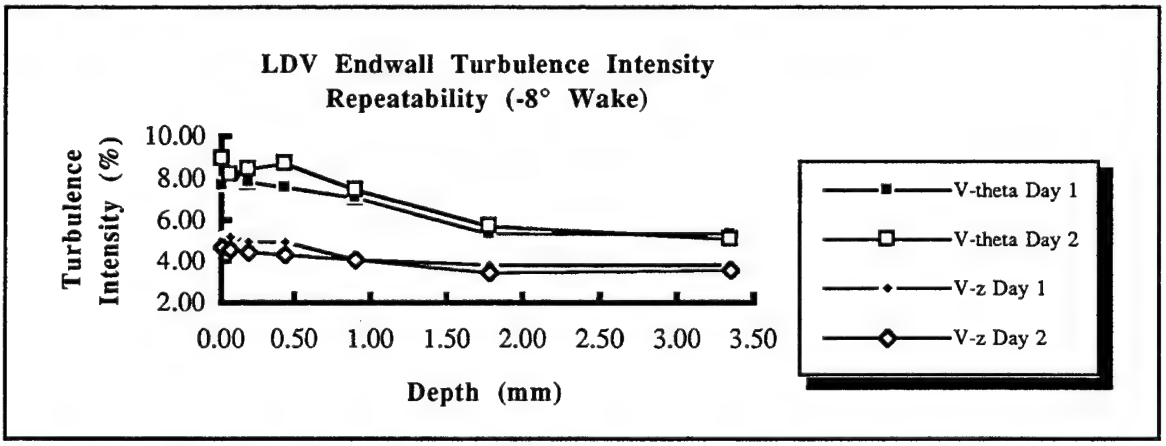

Figure 23. LDV Endwall Turbulence Repeatability At -8 Degrees Wake Position

C. NUMERICAL COMPARISON

Computational Fluid Dynamic (CFD) solutions were run with the same pressure ratios used in the experiments. Appendix G briefly describes the computational data reduction process and programs utilized. Graphical output of the numerical results was useful in obtaining a qualitative understanding of the flow characteristics.

1. Blade Midspan Surface Pressures

Reference 6 predicted hub, midspan and tip surface pressures at a pressure ratio of 0.68. Figure 24 shows a comparison between numerical and experimental blade surface pressures at midspan for a pressure ratio of 0.6815. The suction surface curve suggests that the position of the blade passage throat was at 0.8 of axial chord and, in fact, the throat was located between static ports five and six. The minimum and maximum values at static ports five, six, and seven may be due to the boundary layer interaction at the blade's blunt trailing edge. Figures 25 through 28 show a comparison between numerical and experimental blade midspan surface pressures at pressure ratios of 0.5070, 0.6041, 0.8077 and 0.9054 respectively. Comparison of the blade surface measurements and the computational results generally show excellent agreement.

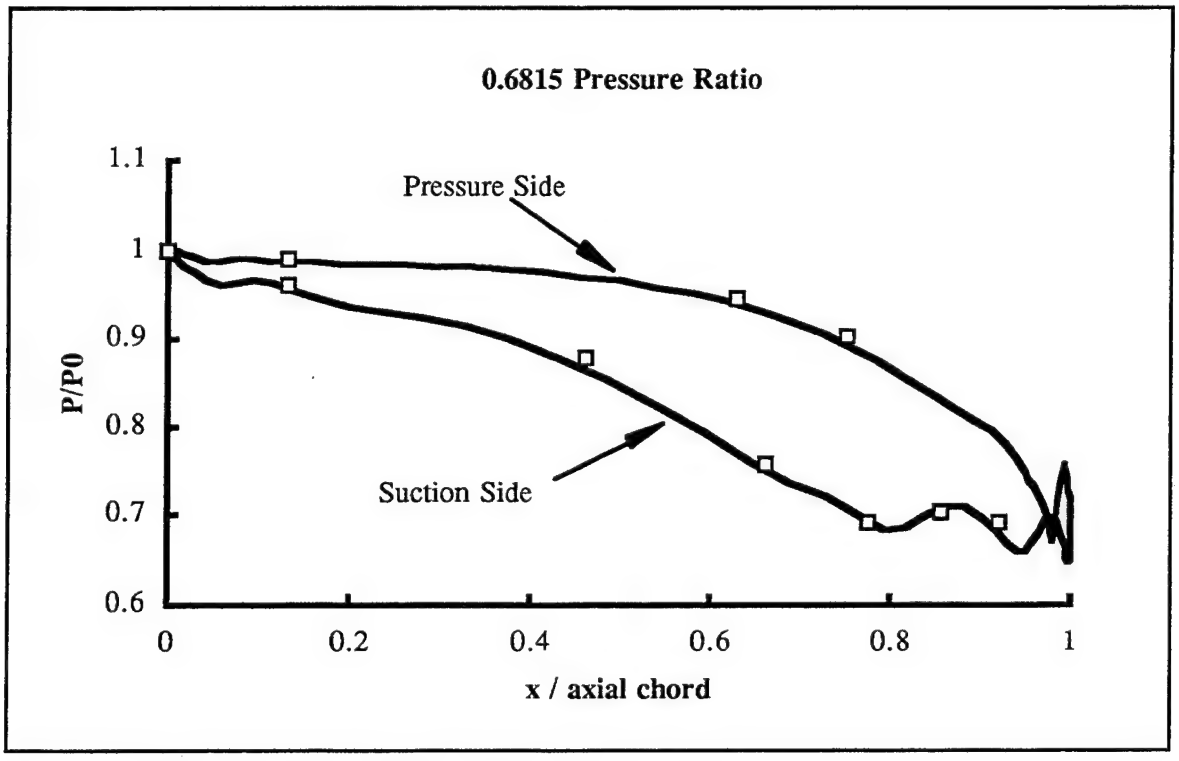

Figure 24. P/P_0 vs. x/c for 0.6815 Pressure Ratio

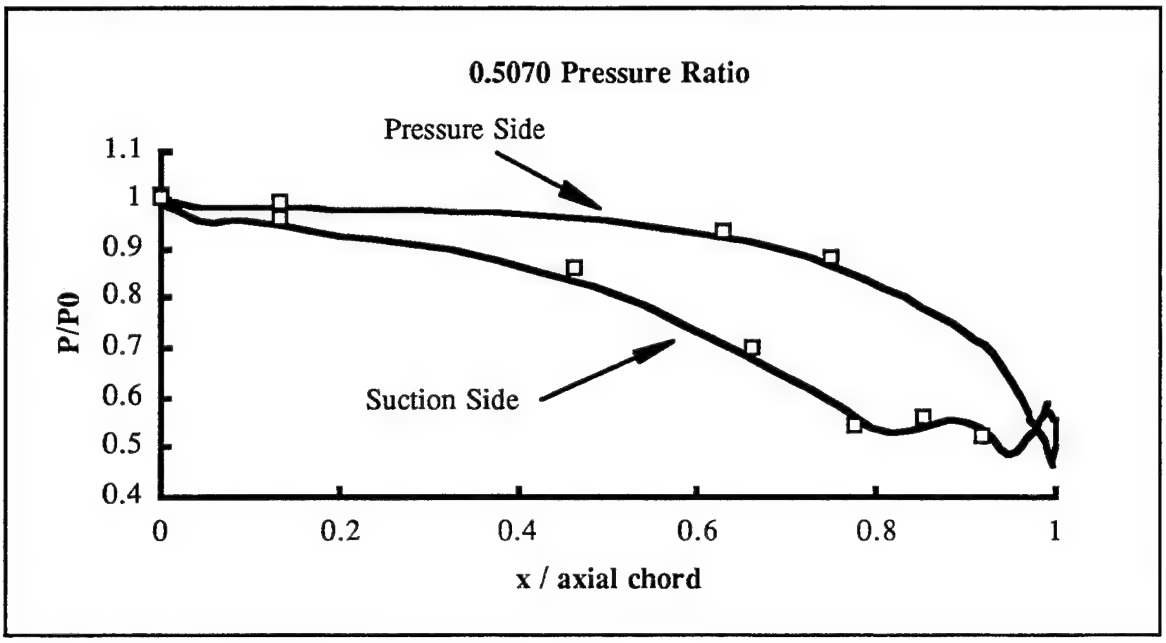

Figure 25. P/P_0 vs. x/c for 0.5070 Pressure Ratio

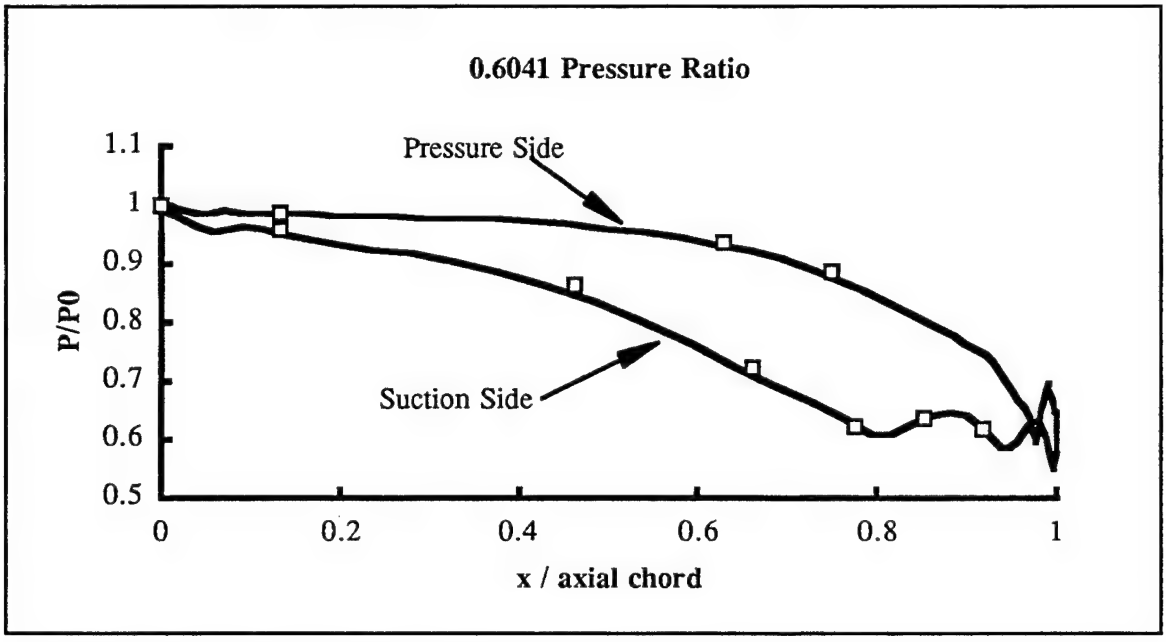

Figure 26 P/P_0 vs. x/c for 0.6041 Pressure Ratio

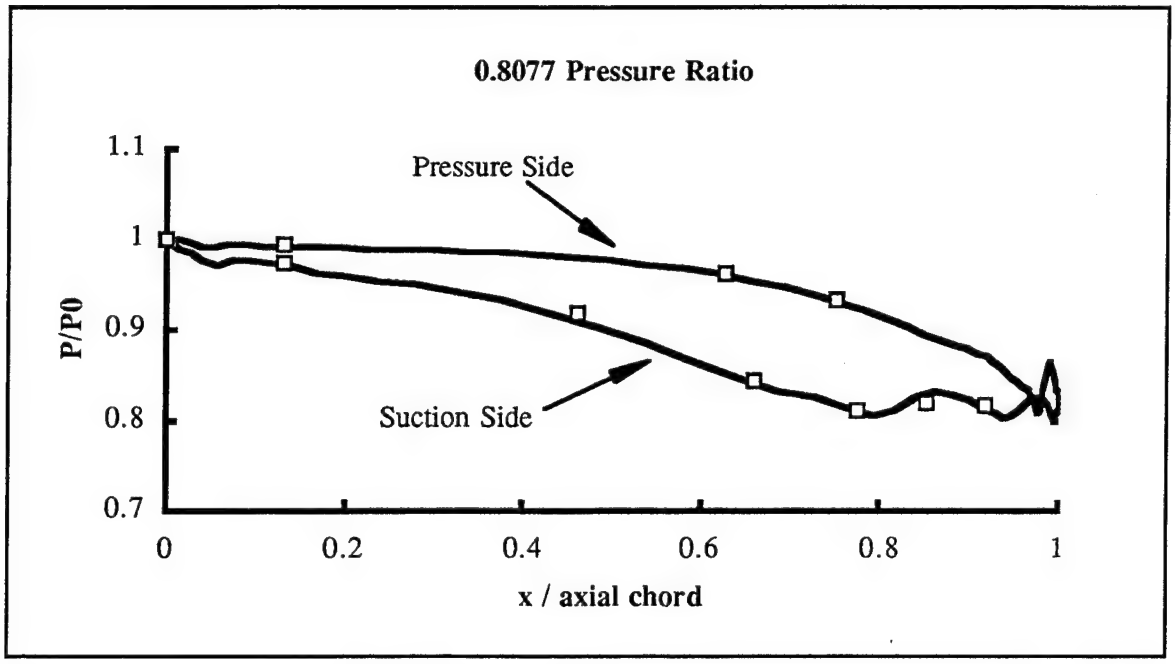

Figure 27. P/P_0 vs. x/c for 0.8077 Pressure Ratio

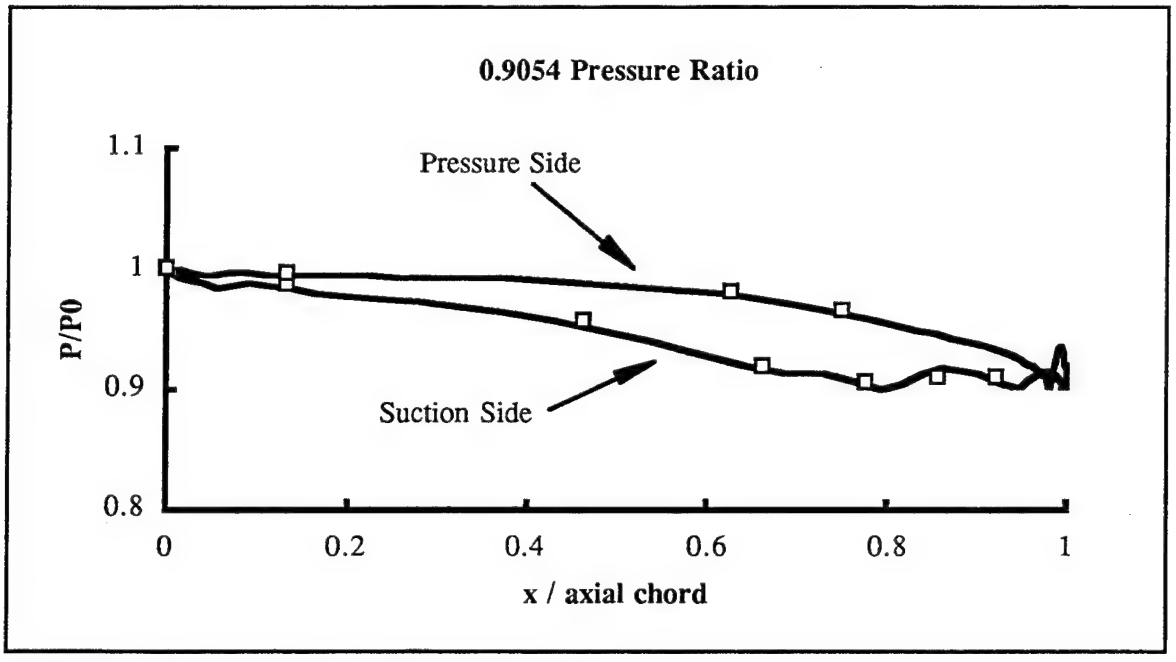

Figure 28. P/P_0 vs. x/c for 0.9054 Pressure Ratio

2. Mach Number and Flow Angle

Two-dimensional Mach number and flow angle comparisons were made between numerical and experimental results for the surveys at each of the seven radial positions. Figures 29 through 32 compare Mach number, while Figures 33 through 36 compare flow angle at four selected radial positions. The remaining comparisons are included in Appendix H. All comparisons were based on a circumferential match between the experiment and computation, by shifting the latter to coincide with the measured profile. The specific matching was based on the maximum Mach number at the deepest radial position (3.34 mm). This matching was kept constant for the circumferential comparisons at all other spanwise locations. To depict flow periodicity and equivalently compare with experimental wake positions, the numerical solutions were repeated over one and one-half blade passages.

Computed Mach numbers differed from the experimental values by an average 12.7% between the surveys at 0.18 mm and 3.34 mm. The difference increased to 70.8% near the endwall, possibly due to a combination of LDV data velocity biasing and insufficient grid resolution. Velocity biasing was estimated to cause an approximate 11.0% velocity increase in the endwall region. The numerical solution at the endwall (0.01 mm) was based on the last k grid point in the radial direction. Computed flow angles surprisingly only varied from the experimental values by an average 3.2% (2.3 degrees). This was in contrast to the measurements in Reference 6 (P_{rat} = 0.68) which showed poor comparison between measured and computed flow angles across the wake at 90 percent span.

The question of radial spatial error with the probe volume needed to be determined. The probe volume length and diameter (Figure 37) was calculated as 1.56 mm and 0.11 mm respectively. The probe volume had approximately 30 fringes across its minor axis and after data processing an average of 13 fringe crossings constituted a valid Doppler burst. Since the IFA-750 digital burst correlator automatically centered the valid signal within the probe volume, an effective probe volume with length 1.39 mm and diameter 0.04 mm was obtained. Figure 38 depicts, to scale, the radial survey resolution that results from endwall depth and effective probe volume dimensions. The decrease in relative spatial resolution close to the endwall also contributed to the lack of agreement between the Mach number profiles (Figure 32).

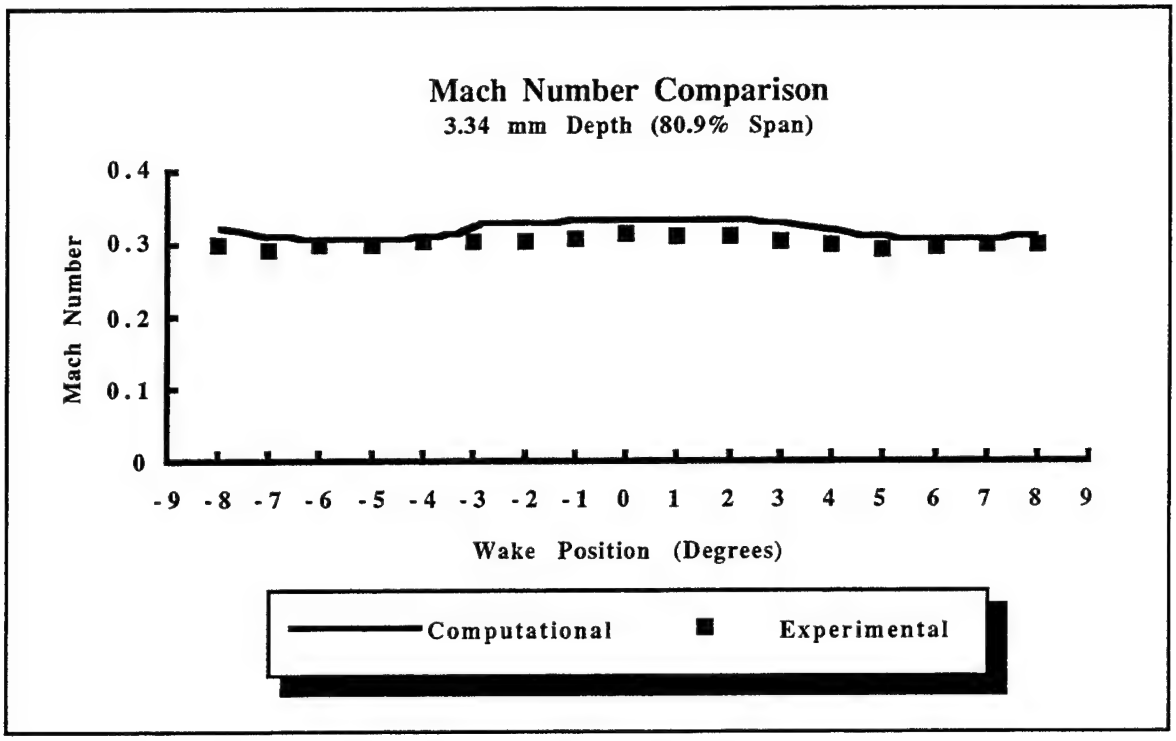

Figure 29. Mach Number Comparison At 3.34 mm Depth

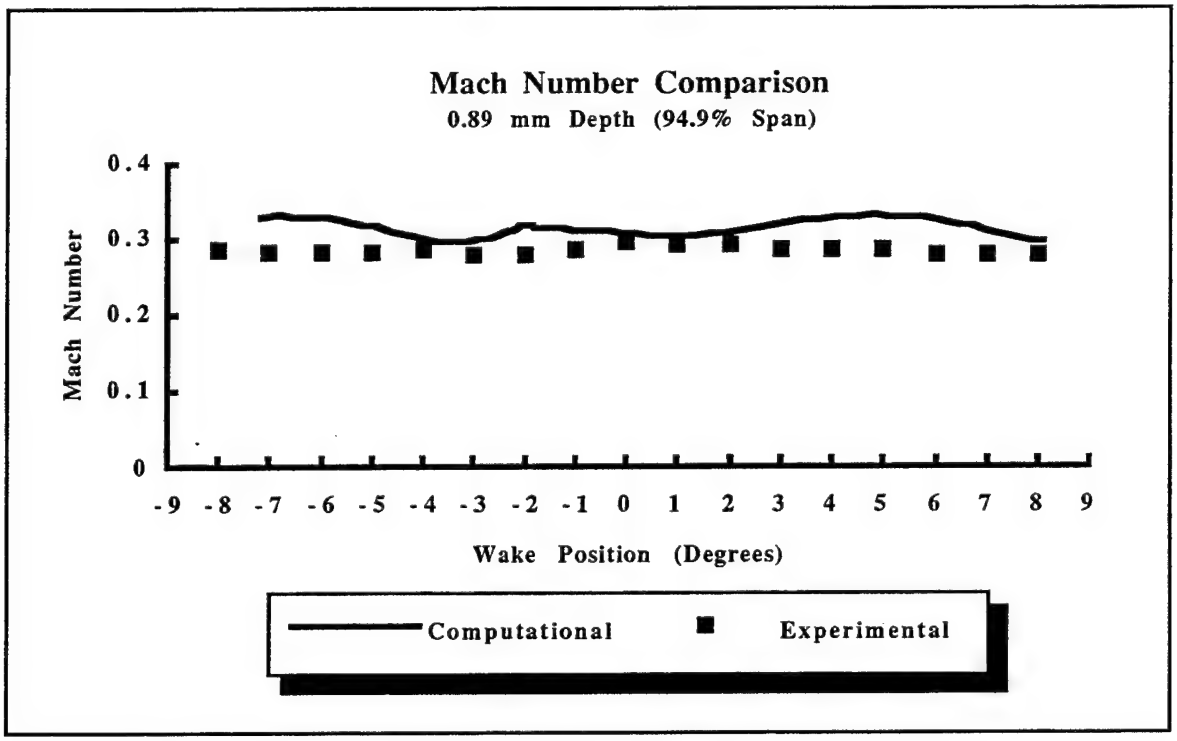

Figure 30. Mach Number Comparison At 0.89 mm Depth

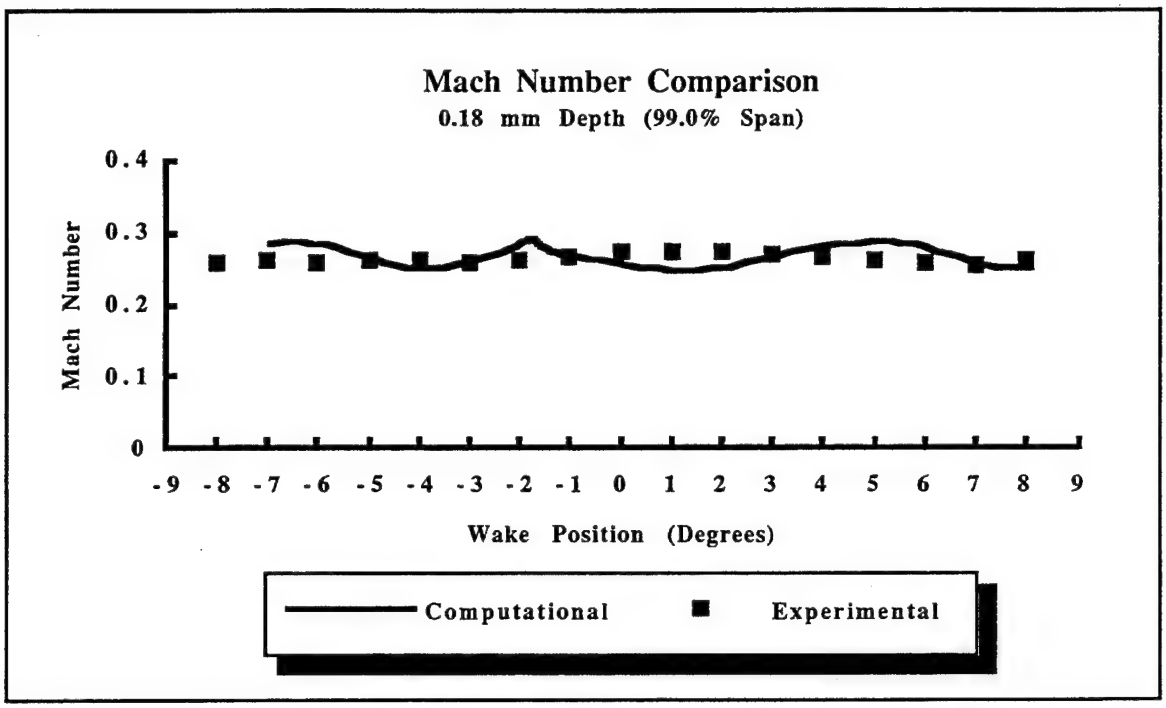

Figure 31. Mach Number Comparison At 0.18 mm Depth

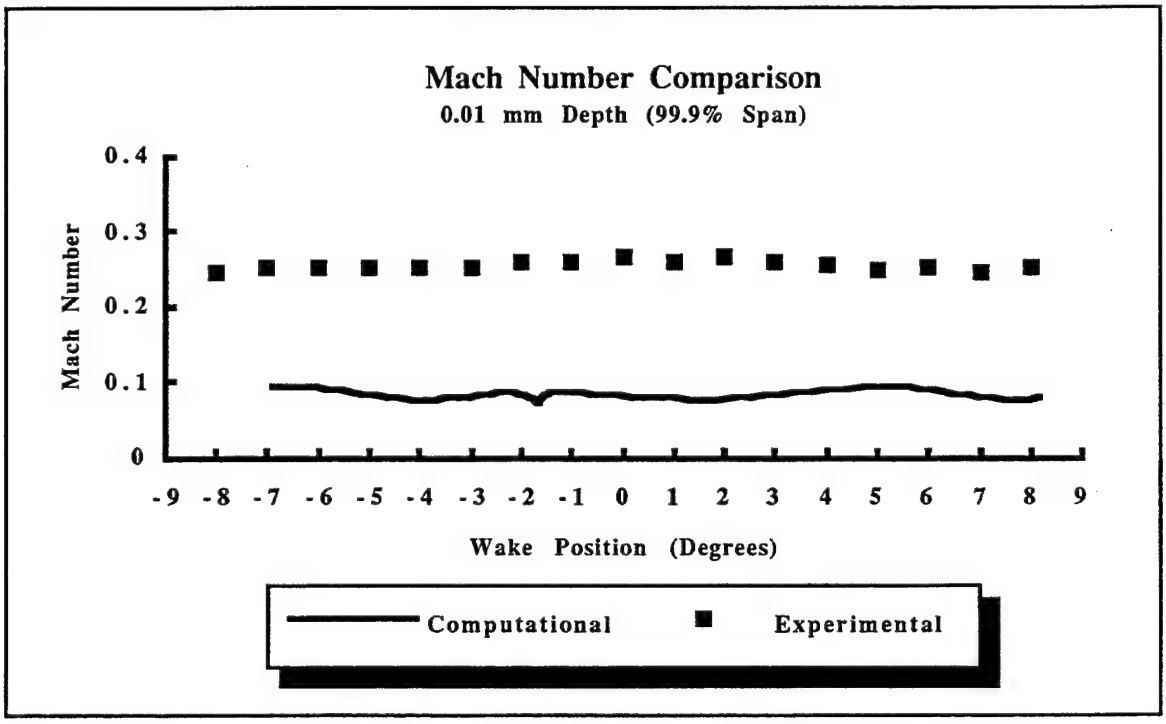

Figure 32. Mach Number Comparison At 0.01 mm Depth

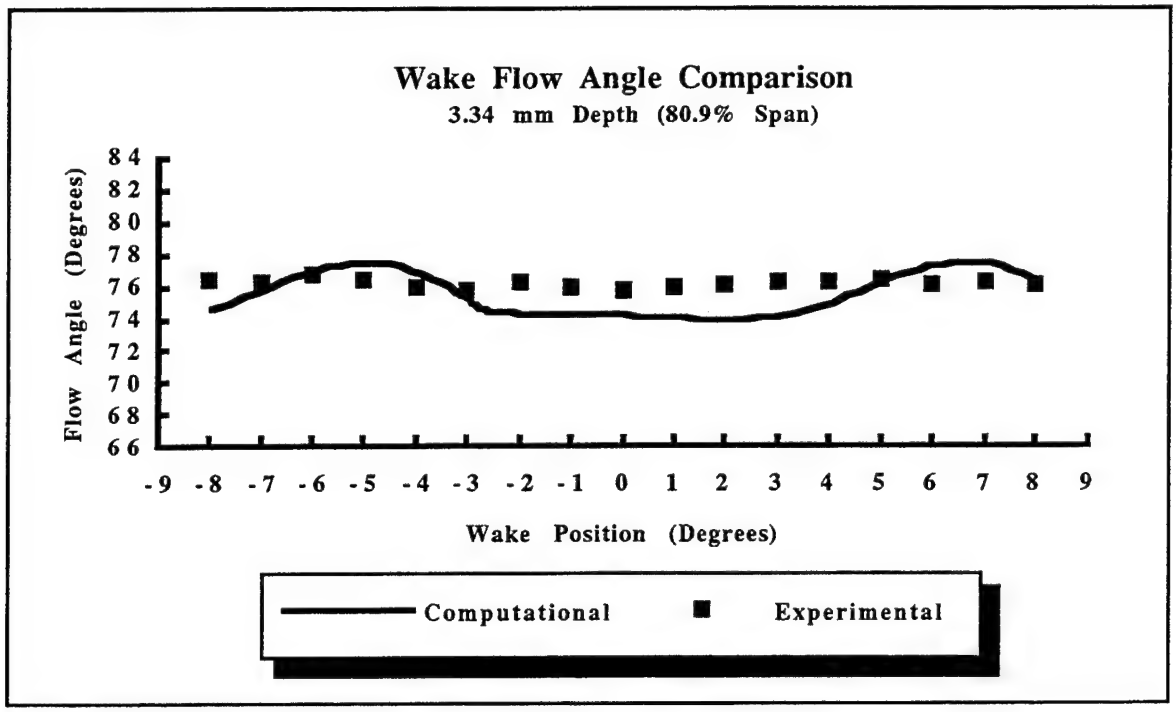

Figure 33. Wake Flow Angle Comparison At 3.34 mm Depth

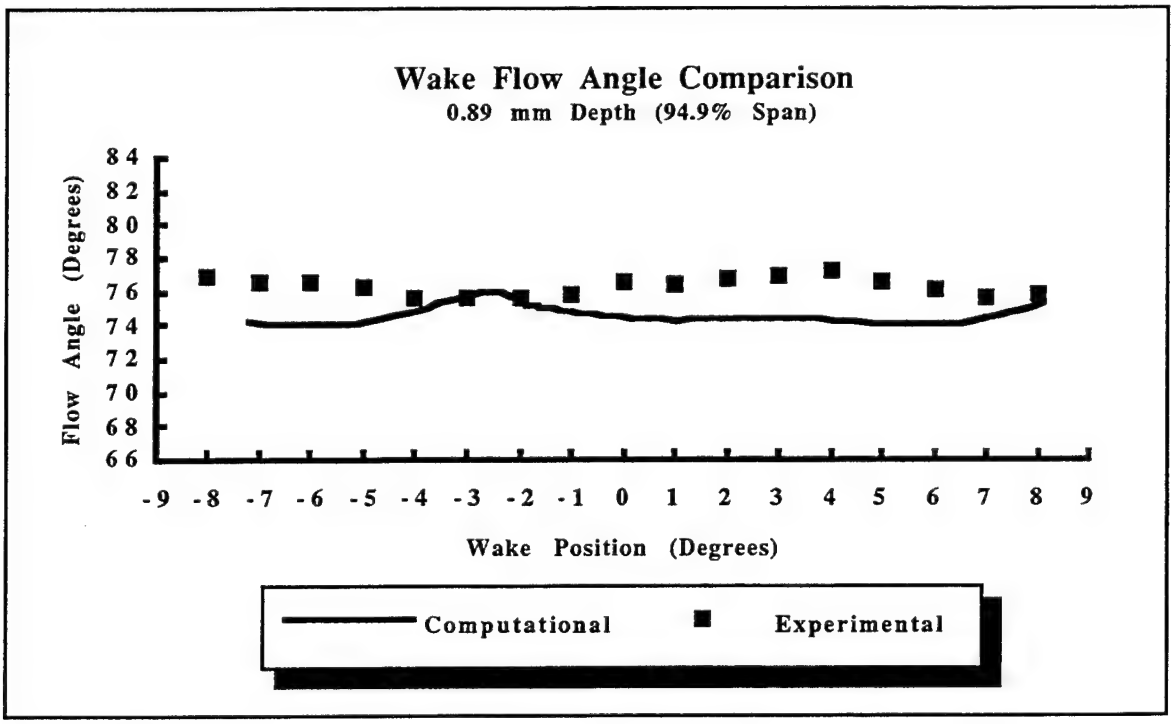

Figure 34. Wake Flow Angle Comparison At 0.89 mm Depth

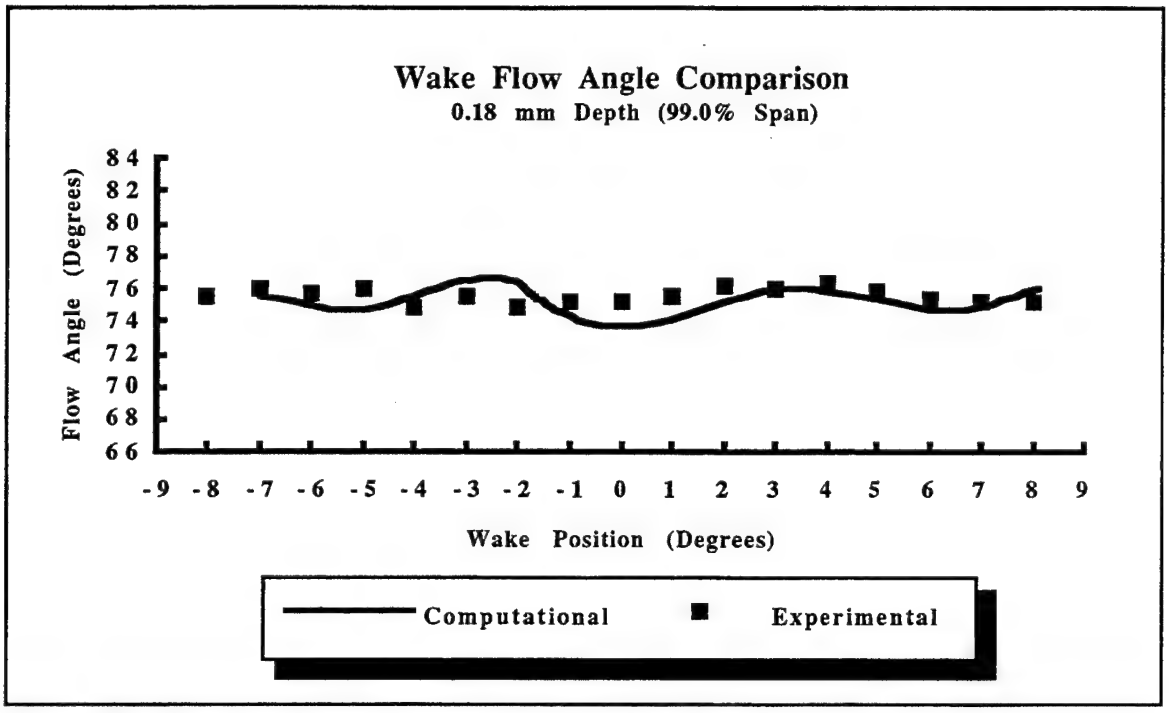

Figure 35. Wake Flow Angle Comparison At 0.18 mm Depth

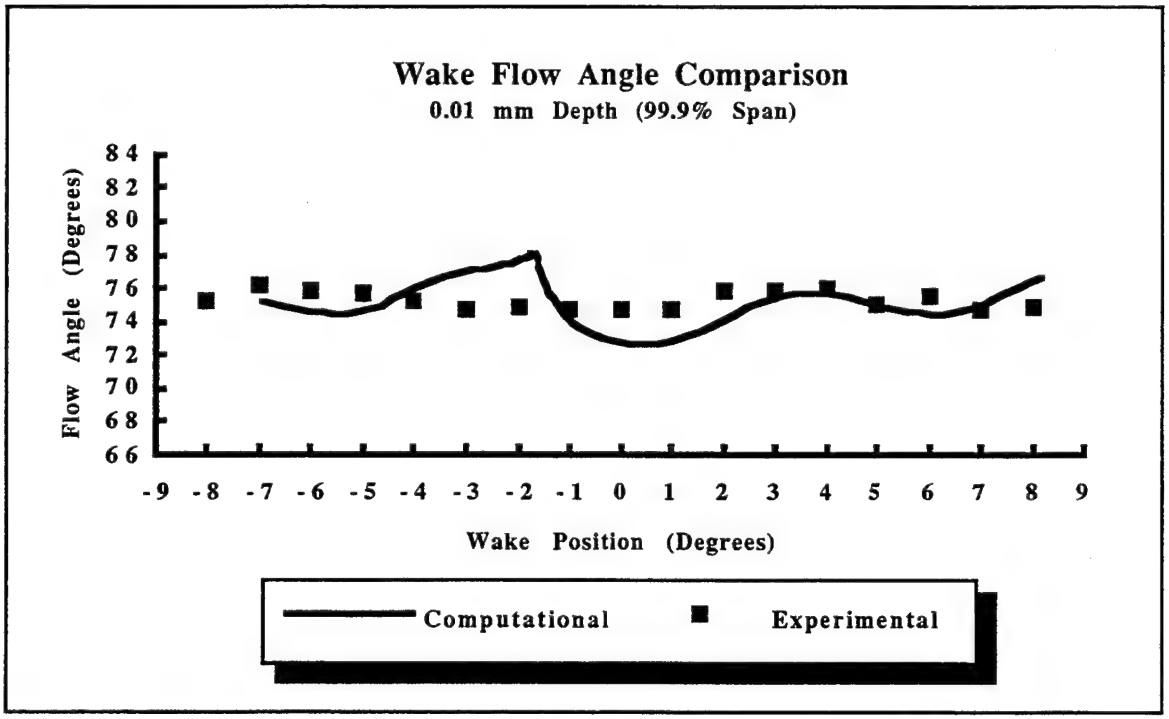

Figure 36. Wake Flow Angle Comparison At 0.01 mm Depth

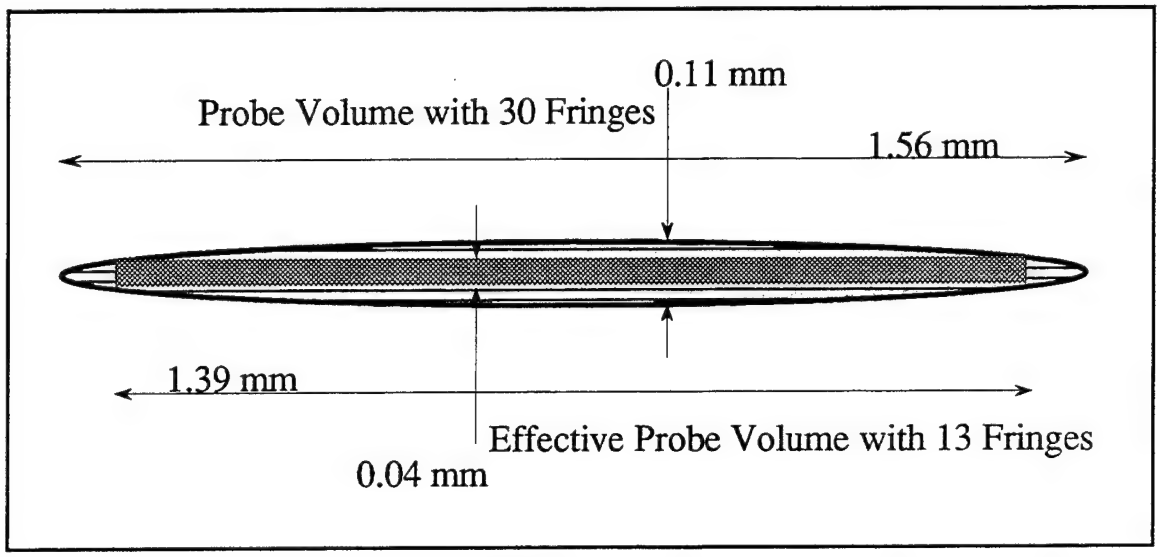

Figure 37. Probe Volume Dimensions

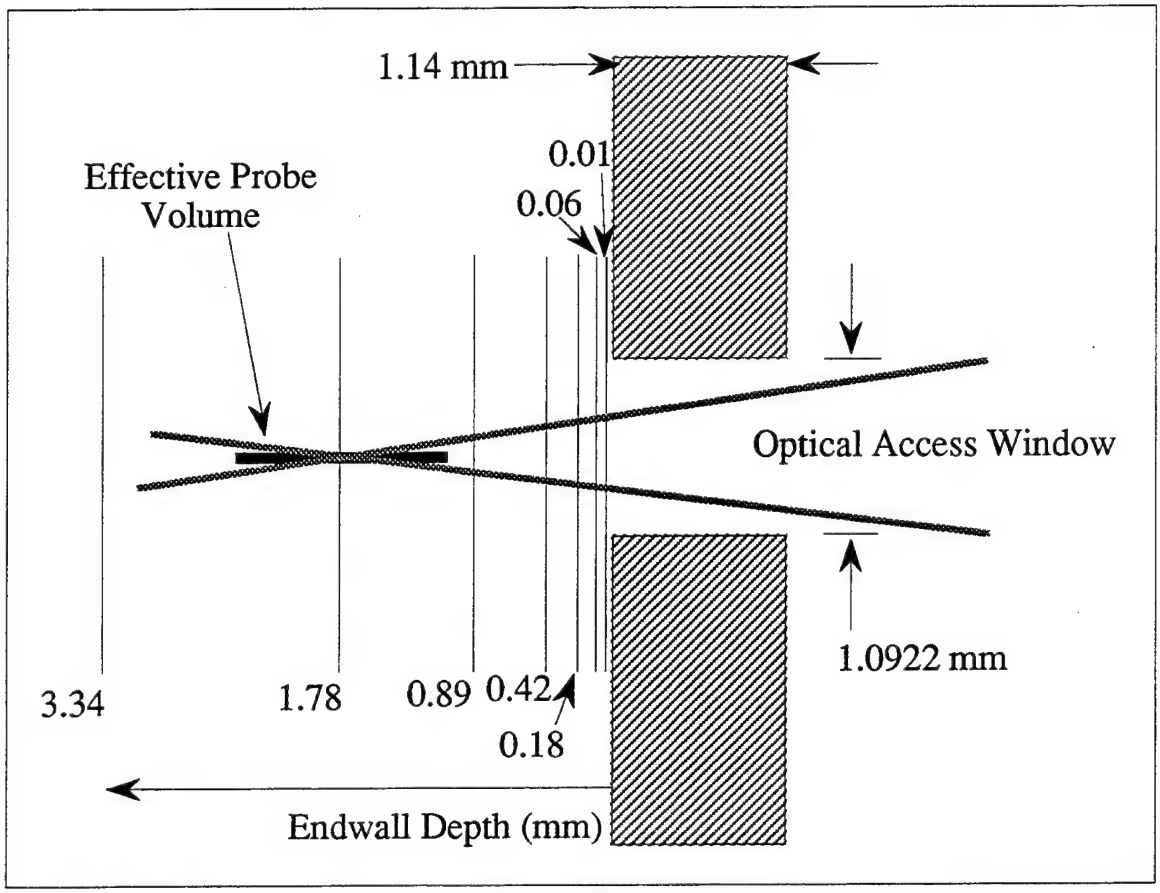

Figure 38. Endwall Measurement Schematic

D. NUMERICAL RESULTS

1. Convergence History

Solutions at pressure ratios of 0.5070, 0.6041 and 0.6815 fully converged after approximately 1,200 iterations. Figure 39 shows density residuals at 0.6815 pressure ratio after 10,200 iterations. Solutions for pressure ratios of 0.8077 and 0.9054 were initially obtained after 1,200 iterations, but convergence did not occur (i.e. three orders of magnitude reduction of the residuals) until approximately 3,000 iterations. Figures I1 through I5 of Appendix I contain density-residual convergence history for all examined pressure ratios.

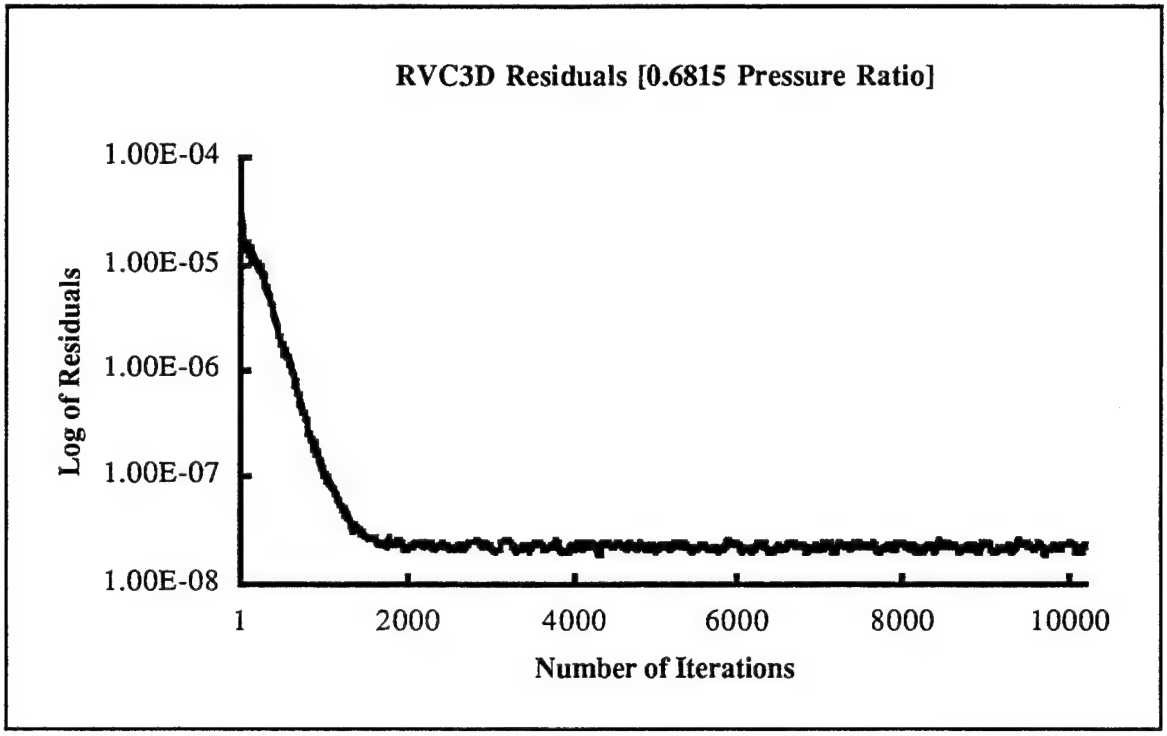

Figure 39. 0.6815 Pressure Ratio Convergence History (10,200 Iterations)

2. Turbulence Models

At a pressure ratio of 0.8077, the code was run with the following turbulence models;

RVC3D version 206 Cebeci-Smith

RVC3D version 206 Baldwin-Lomax

RVC3D version 208 Baldwin-Lomax

so as to assess the effect of different turbulence models on the solution. In all three cases, the code produced similar solutions.

3. Mach Number Contours

Figures 40 and 41 display exit plane Mach number contours at pressure ratios of 0.9054 and 0.5070 respectively. The Mach number contours between 25% and 75% span provide an indication of where the flow characteristics were well established. Boundary layers appear, as expected, to be thin near the endwall region and thicker near the hub. Spanwise wake curvature, due to secondary flows, is also apparent in the two figures with Figure 40 showing the greater curvature.

Figure 42 displays midspan Mach number contours for the blade passage at 0.5070 pressure ratio. The flow was strongly accelerated along the suction side. The acceleration of the flow to high local Mach numbers resulted in shocks at the throat and trailing edge. The wake was a merging of the pressure and suction side boundary layers. The trailing-edge shock extended across the wake from the adjacent (upper) blade, out to the exit plane of the grid. The shock interaction with the wake caused the wake to narrow down, resulting in a wake which was repeatedly diffused and then coalesced. The shock strength decreased away from the trailing edge as a result of this interaction with the wake, which could be both physical and computational in nature. Because of the relatively good agreement between experiment and computation of the blade surface pressure field, it was felt that the solution was realistic. Appendix J includes program listings for a graphical display of multiple grids and corresponding numerical solutions for use with PLOT3D.

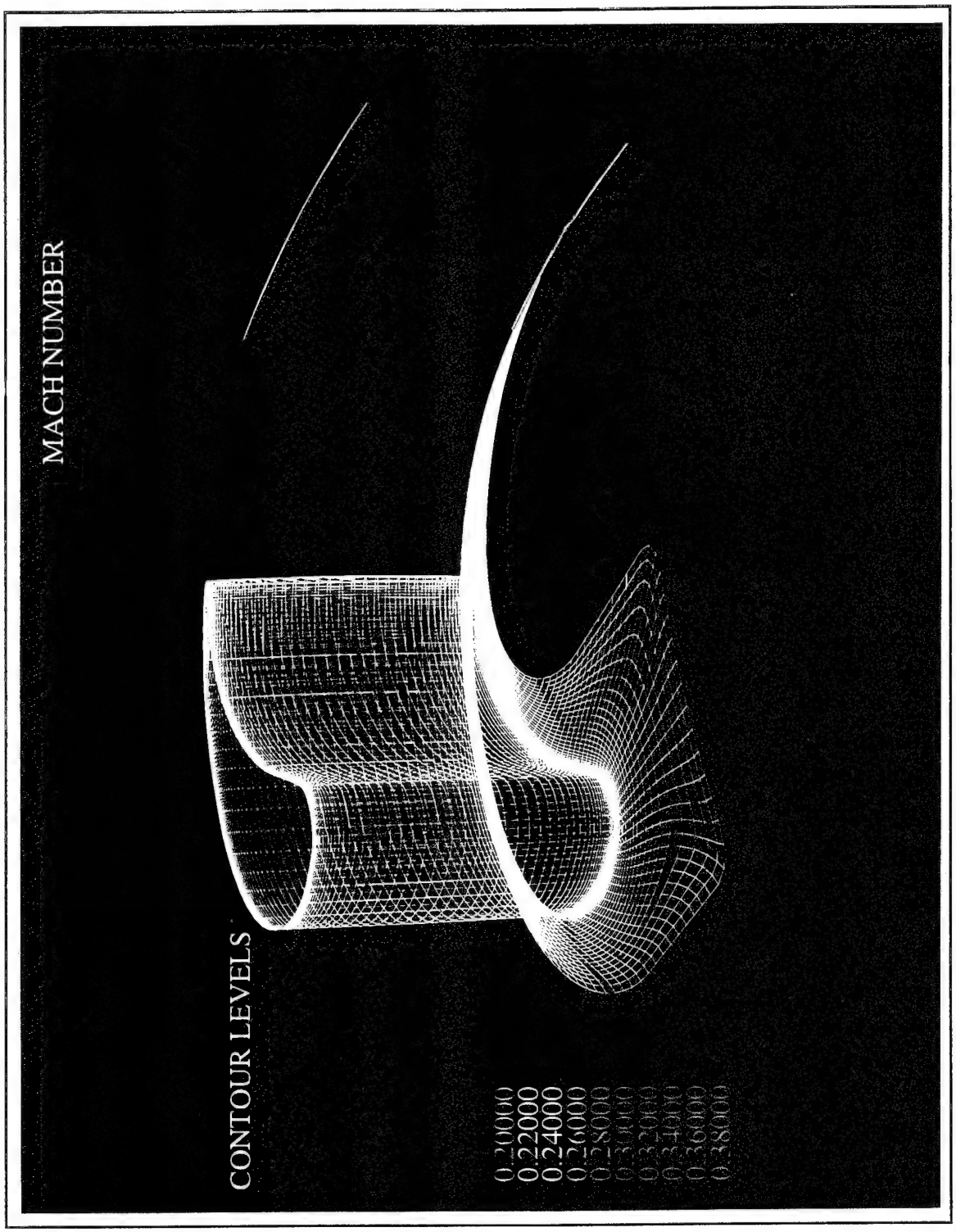

Figure 40. Exit Plane Mach Contours (0.9054 Pressure Ratio)

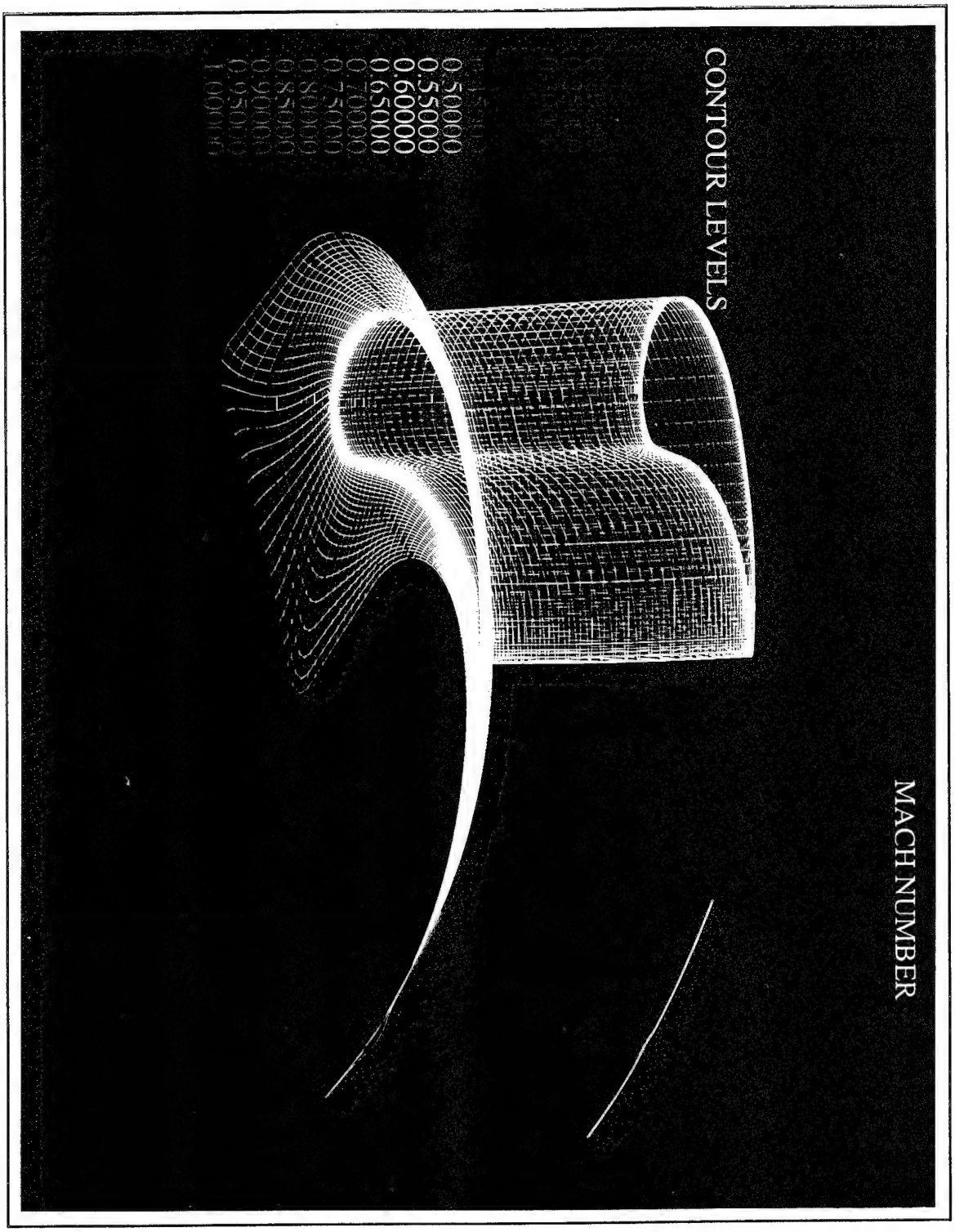

Figure 41. Exit Plane Mach Contours (0.5070 Pressure Ratio)

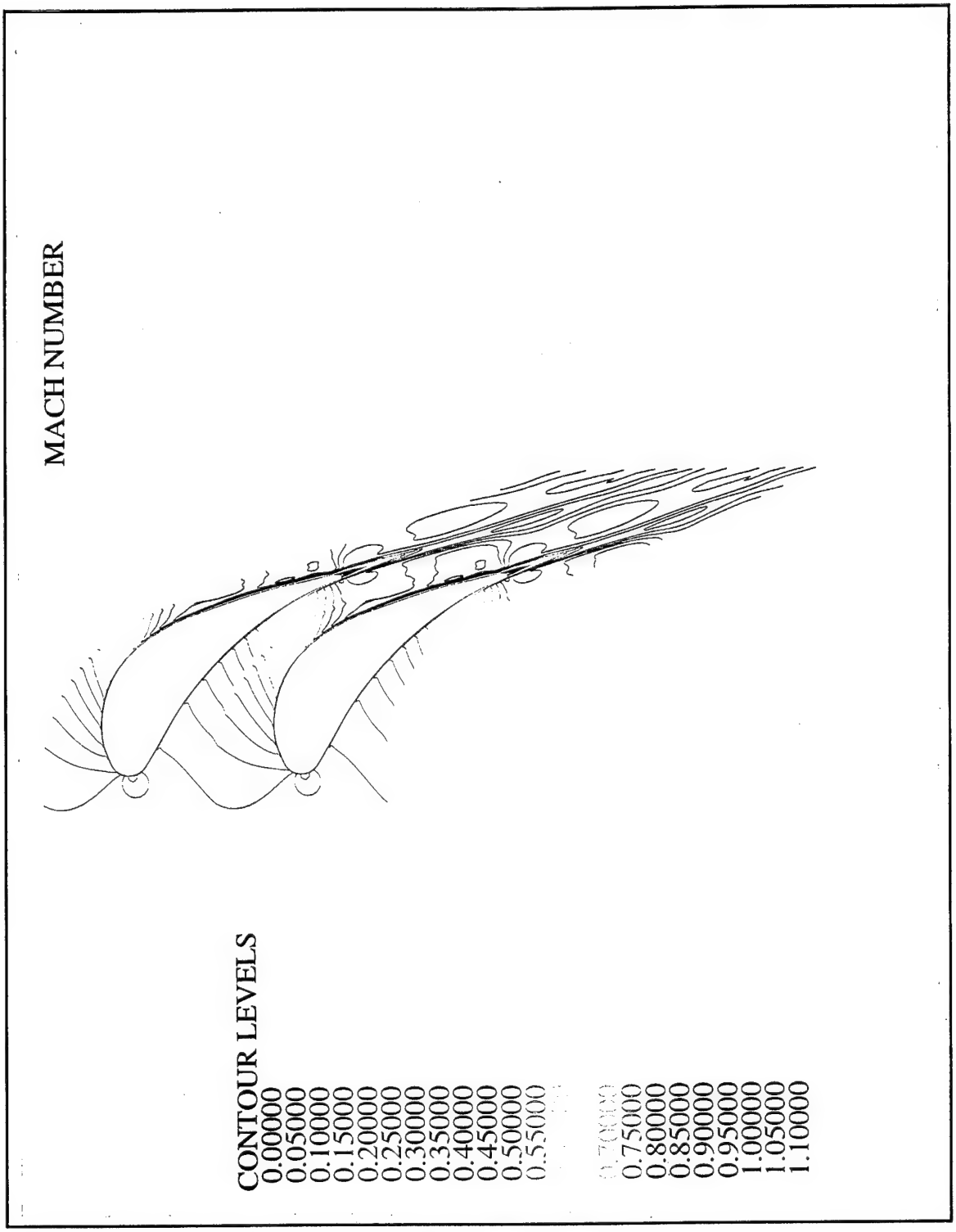

Figure 42. Midspan Mach Contours (0.5070 Pressure Ratio)

V. CONCLUSIONS AND RECOMMENDATIONS

An experimental and computational investigation was conducted of the flow through an annular turbine cascade. Computational pressure ratios (P_{rat}), defined as the downstream hub-static pressure (P_{hub}) divided by the upstream stagnation pressure (P_0), were chosen to coincide with experimental test conditions. Downstream computational and experimental measurement locations were chosen to coincide to provide a proper comparison.

An existing annular turbine cascade was modified to provide a capability to measure blade midspan surface pressures. Experimental measurements of blade midspan surface pressures were obtained and favorably compared with numerical predictions over a range of subsonic and transonic conditions. Measurements were repeatable with a maximum repeatability error of less than 0.87%. Numerical solutions converged on pressure within approximately 1,200 iterations.

The minimum and maximum pressure values on the suction surface close to the trailing edge should be investigated further to confirm the influence of the relatively blunt trailing edge. An inlet boundary layer survey, requiring a rig modification, should be performed to supplement data in Reference 6 and refine the inlet boundary conditions to the computational model.

To supplement blade midspan surface pressures, blade pressure taps could be installed at other spanwise locations to include the hub, tip, and possibly endwall locations. A tip gap could be created and a computational tip gap model introduced to investigate the endwall region. Blade tips, and the adjacent endwall, could be instrumented for pressure readings and a numerical and experimental comparison conducted to obtain insight into tip leakage flows. In addition, an LDV optical-access window could be installed over the tip region to measure tip-gap flow characteristics.

Successful measurements of two-dimensional velocity, flow angle, and turbulence intensity through a 1.0922 mm diameter casing-access hole were demonstrated. All LDV data were acquired one-half axial chord downstream over seven radial positions and 17 separate peripheral displacements. Experimental flow velocities were increased from those of Reference 6 mainly due to the availability and use of a digital burst correlator in place of a signal processor. Although all LDV data reported herein were acquired at 0.9054 pressure ratio, measurements were attempted at 0.80 pressure ratio and some data were obtained; however, low data rate and endwall hole vibrations prevented a complete survey.

The comparison of computational and experimental Mach number and flow angle yielded an average 12.7% difference in Mach number and 3.2% (2.3 degrees) difference in flow angle. All experimental measurements were repeatable to an average uncertainty ranging from 0.2% to 7.0% for velocity, flow angle, and turbulence intensity in both random and coincidence data processor modes. All numerical and experimental comparisons were based on a circumferential match of maximum Mach number at the 80.9% (3.34 mm) span location. An investigation of other circumferential matching options should be conducted to explore the effect on the degree of agreement (i. e. minimum Mach number circumferential matching).

LDV alignment and radial survey procedures were devised and repeated. The probe volume passed cleanly through the optical access hole and radial surveys were conducted to provide complete coverage for data recording. Probe volume dimensions were further refined to aid in estimates of radial-position accuracy. Introduction of a second fiber-optics probe for three component measurements would decrease the effective probe volume and increase radial position accuracy. The ability to resolve endwall flow characteristics and eventually flow tip losses appears to be promising.

The present hardware did not provide pressure equalization across the optical access hole. A rig modification is required to equalize the pressure at the measurement location and eliminate any influence the opening might have on the flow characteristics. Also, the coarse peripheral (wake) positioning mechanism needs modification to allow more precise adjustment. Experimental peripheral positioning uncertainties may contribute to differences in the compared data.

Future efforts with computational fluid dynamics should include modeling the inlet bellmouth and center body, and conducting a turbulence model sensitivity analysis in the endwall region. Increased grid resolution in the endwall region would be beneficial. The experimental 99.9% span location coincided with the final k grid point and may account for the 70.8% difference between the experimental and computed Mach numbers. Finally, a detailed investigation into transonic and sonic flow conditions could be conducted to examine the blade-passage and trailing-edge shock locations and subsequent interactions, both computationally and experimentally.

APPENDIX A. PRESSURE DATA ACQUISITION

Pressure data acquisition was accomplished using a Hewlett-Packard 9000 computer system with the following program:

```
10    !FILE NAME:  BILLSP
20    !DISK LABEL:  "'/AUSTIN"
30    !LAST MODIFIED 10/27/94 BY LT BILL DONOVAN
40    !THIS PROGRAM RECORDS AND REDUCES MEASURED PRESSURES FROM A
50    !SCANIVALVE CONNECTED TO 11 STATIC PRESSURE PORTS ON ATC
60    !       VARIABLES / PORT CONNECTIONS...
70    !       V=DESIRED S/V
80    !       A=PRESENT S/V PORT
90    !       C=CHANNEL
100   !       Voltage ( )=DVM VOLTAGE READING FOR EACH PORT
110   !       S=SCANNER NUMBER
120   !       Pinhg=BAROMETRIC PRESSURE IN INHG
130   !       Pamb=BAROMETRIC PRESSURE (psi)
140   !       AMBIENT PRESSURE...#1
150   !       CALIBRATION PRESSURE...#2
160   !       REFERENCE UPSTREAM TOTAL PRESSURE...PORT #4
170   !       INNER HUB STATIC PRESSURE...PORT #5
180   !       UPSTREAM STATIC PRESSURE...PORT #6
190   !       ATC PASSAGE PORTS #1-#11...S/V PORTS #9-#19
200   !       Prat= INNER HUB STATIC/ REFERENCE UPSTREAM TOTAL
210   !       Tstag=UPSTREAM STAGNATION TEMPERATURE IN DEGREES F
220   OPTION BASE 1
230   CLEAR SCREEN
240   PRINTER IS CRT
250   DISP "PLEASE WAIT WHILE RESETTING SCANIVALVE TO PORT #1"
260   PRINT
270   V=5
280   A=1
290   GOSUB Read
300   DIM Y(20)
310   DIM Voltage(50)
320   DIM P(50)
330   INPUT "ENTER MONTH, DAY, YEAR (I.E.02, 04, 94)", Y(3), Y(5), Y(7)
340   INPUT "ENTER RUN #: ", Y(9)
350   PRINTER IS 711
360   PRINT USING "K, DD, " " / " ", DD, " " / " ", DD", "DATE OF RUN: ", Y(3), Y(5), Y(7)
370   PRINT "DATA RUN ", Y(9)
380   PRINT USING "/, 5X, K, DDD, /, 2X, K, 15X, K, 17X, K", "SCANIVALVE # ", V,
      "Port", "Volts", "Psi"
390   PRINTER IS CRT
400   PRINT "       ZERO DVM ON SCANIVALVE #5, PORT #1..."
410   PRINT
420   PRINT "       SET 20 inhg FOR SCANIVALVE CALIBRATION..."
430   PRINT
440   PRINT "       ADJUST SPAN FOR DVM = 0.009823 VOLTS ON PORT #2..."
450   PRINT
460   PRINT "ENSURE DESIRED PRESSURE RATIO IS SET..."
470         INPUT "ENTER BAROMETRIC PRESSURE IN INHG", Pinhg
480         INPUT "ENTER HIGHEST SCANIVALVE PORT # NEEDED ", Nports
490         INPUT "ENTER UPSTREAM STAGNATION TEMP. IN DEG. F ", Tstag
```

```
500         Pamb=Pinhg*(0.4911541)
510         PRINT "**** PRESS CONTINUE WHEN READY TO TAKE DATA***"
520         PAUSE
530   !*****************************************************
540   !RECORD THE PRESSURE DATA FOR THIS RUN
550         OUTPUT 722; "F1R1T1M0Z1"          ! SETS UP HP3456A DVM
560         V=5                               !SCANIVALVE #5 DESIGNATED
570         S=1                               !HP3495A SCAN #1 DESIGNATED
580         FOR A=1 TO Nports
590               GOSUB Read
600               WAIT 2.0
610               OUTPUT 701; "C"             !CLEARS SCANNER #1
620               OUTPUT 701 USING "DDD"; V+9  !SCAN SET TO READ S/V
630               TRIGGER 722
640               ENTER 722; Voltage(A)
650               P(A)=(Voltage(A) - Voltage(1))*1000+Pamb
660   PRINTER IS CRT
670   PRINT USING "2X,DDD,7X,7DD.DDDDDDD,8X,7DD.DDDD"; A, Voltage(A), P(A)
680   PRINTER IS 711
690   PRINT USING "2X,DDD,7X,7DD.DDDDDDD,8X,7DD.DDDD"; A, Voltage(A), P(A)
700         NEXT A
710         Prat=P(5)/P(4)
720         PRINT "Prat = ", Prat
730         PRINT "UPSTREAM STAGNATION TEMPERATURE WAS (DEG F)", Tstag
740         PRINT "INPUT BAROMETRIC PRESSURE IN (inhg) WAS ", Pinhg
750   !**********SUBROUTINE TO POSITION AND READ S/V PORTS*********
760   Read: OUTPUT 707 USING "#,K";V
770         P0=SPOOL(707)
780         L=BINAND(P0,15)
790         T1=ROTATE(P0,4)
800         M1=BINAND(T1,7)
810         P(A)=10*M1+L
820         CLEAR 707
830         IF P(A)=A THEN Finish
840         OUTPUT 701; "C"
850         OUTPUT 701 USING "DDD";V-1
860         OUTPUT 701; "C"
870         WAIT 0.1
880         GOTO Read
890   Finish: RETURN
900         END
```

The following table relates each Scanivalve port to its respective pressure measurement.

Scanivalve Port Number	Pressure Measured
1	Ambient Pressure
2	Calibration Pressure (set at 20 inches hg)
3	Not Used
4	Upstream Total Pressure (P_0)
5	Downstream Hub Static Pressure (P_{hub})
6	Upstream Static Pressure (P_{static})
7	Not Used
8	Not Used
9	Blade Static Port #1 (at leading edge)
10	Blade Static Port #2 (suction side)
11	Blade Static Port #3 (suction side)
12	Blade Static Port #4 (suction side)
13	Blade Static Port #5 (suction side)
14	Blade Static Port #6 (suction side)
15	Blade Static Port #7 (suction side)
16	Blade Static Port #8 (at leading edge)
17	Blade Static Port #9 (pressure side)
18	Blade Static Port #10 (pressure side)
19	Blade Static Port #11 (pressure side)

Table A1. Pressure Data Acquisition Connections

APPENDIX B. GRID GENERATION INPUT FILE

Grid generation was completed on Silicon Graphics Indigo II workstations. The following TCGRID namelist file was utilized to obtain the final grid.

```
&nam1 im=150 jm=31 km=65 itl=20 icap=18 k2d=3 merid=0 &end
&nam2 nle=16 nte=10 dsle=.018 dste=.003 dshub=.0004 dstip=.0004
      dswte=.001 dswex=.060 dsthr=1. dsmin=.0004 dsmax=.025
      dsra=.45 rcorn=.098 &end
&nam3 iterm=100 idbg=0 0 0 0 0 0 0 0 aabb=.5 ccdd=.45 &end
&nam4 zbc=-1.5  -1.5   0.5 -1.5  -1.5   .5
      rbc= 3.895 3.895 3.895 4.585 4.585 4.585 &end
'TRANSONIC TURBINE'
      2       2
      -.975   0.0
      3.895   3.895
      -.975   0.0
      4.585   4.585
      2       51      31
      -7.8999996E-03 -9.9200001E-03 -1.2000000E-02 -1.4080000E-02
      -1.6100001E-02 -1.7999999E-02 -1.9710001E-02 -2.1190001E-02
      -2.2390001E-02 -2.3280000E-02 -8.1040002E-02 -0.1503800
      -0.2308900 -0.3219400 -0.4228500 -0.5328500 -0.6511000
      -0.7893000 -0.9275000 -0.9410600 -0.9527700 -0.9622700
      -0.9692700 -0.9735600 -0.9750000 -0.9735600 -0.9692700
      -0.9622700 -0.9527700 -0.9410700 -0.9275000 -0.9124900
      -0.8250000 -0.7200000 -0.6000000 -0.4560000 -0.3440000
      -0.2730000 -0.2200000 -0.1820000 -0.1160000 -5.9000000E-02
      -1.7000001E-02 0.0000000E+00 -1.8220000E-04 -7.2359998E-04
      -1.6100000E-03 -2.8100000E-03 -4.2900001E-03 -6.0000001E-03
      -7.8999996E-03 -0.2349885 -0.2351271 -0.2351733 -0.2351271
      -0.2349885 -0.2347600 -0.2344519 -0.2340719 -0.2336329
      -0.2331451 -0.1980565 -0.1643980 -0.1324210 -0.1023671
      -7.4464694E-02 -4.8926830E-02 -2.5946086E-02 -4.6726577E-03
      1.6618744E-02 1.9057767E-02 2.2061616E-02 2.5545571E-02
      2.9399229E-02 3.3504494E-02 3.7740692E-02 4.1976891E-02
      4.6082158E-02 4.9935814E-02 5.3417202E-02 5.6423619E-02
      5.8862645E-02 6.0659818E-02 6.9319643E-02 7.1887039E-02
      6.7522466E-02 5.1347882E-02 2.5673941E-02 0.0000000E+00
      -2.5673941E-02 -5.1347882E-02 -0.1026958 -0.1540437
      -0.2053915 -0.2320924 -0.2326265 -0.2331451 -0.2336329
      -0.2340719 -0.2344519 -0.2347600 -0.2349885 3.895000
      3.895000 3.895000 3.895000 3.895000 3.895000 3.895000
      3.895000 3.895000 3.895000 3.895000 3.895000 3.895000
      3.895000 3.895000 3.895000 3.895000 3.895000 3.895000
      3.895000 3.895000 3.895000 3.895000 3.895000 3.895000
      3.895000 3.895000 3.895000 3.895000 3.895000 3.895000
      3.895000 3.895000 3.895000 3.895000 3.895000 3.895000
      3.895000 3.895000 3.895000 3.895000 3.895000 3.895000
      3.895000 3.895000 -7.8999996E-03 -9.9200001E-03
      -1.2000000E-02 -1.4080000E-02 -1.6100001E-02 -1.7999999E-02
      -1.9710001E-02 -2.1190001E-02 -2.2390001E-02 -2.3280000E-02
```

-8.1040002E-02 -0.1503800 -0.2308900 -0.3219400 -0.4228500
-0.5328500 -0.6511000 -0.7893000 -0.9275000 -0.9410600
-0.9527700 -0.9622700 -0.9692700 -0.9735600 -0.9750000
-0.9735600 -0.9692700 -0.9622700 -0.9527700 -0.9410700
-0.9275000 -0.9124900 -0.8250000 -0.7200000 -0.6000000
-0.4560000 -0.3440000 -0.2730000 -0.2200000 -0.1820000
-0.1160000 -5.9000000E-02 -1.7000001E-02 0.0000000E+00
-1.8220000E-04 -7.2359998E-04 -1.6100000E-03 -2.8100000E-03
-4.2900001E-03 -6.0000001E-03 -7.8999996E-03 -0.1996249
-0.1997426 -0.1997819 -0.1997426 -0.1996249 -0.1994308
-0.1991690 -0.1988462 -0.1984733 -0.1980589 -0.1682508
-0.1396576 -0.1124929 -8.6961828E-02 -6.3258447E-02
-4.1563794E-02 -2.2041440E-02 -3.9694658E-03 1.4117776E-02
1.6189748E-02 1.8741548E-02 2.1701200E-02 2.4974918E-02
2.8462378E-02 3.2061070E-02 3.5659760E-02 3.9147221E-02
4.2420939E-02 4.5378406E-02 4.7932386E-02 5.0004359E-02
5.1531076E-02 5.8887679E-02 6.1068702E-02 5.7360962E-02
4.3620501E-02 2.1810250E-02 0.0000000E+00 -2.1810250E-02
-4.3620501E-02 -8.7241001E-02 -0.1308615 -0.1744820
-0.1971647 -0.1976183 -0.1980589 -0.1984733 -0.1988462
-0.1991690 -0.1994308 -0.1996249 4.585000 4.585000 4.585000
4.585000 4.585000 4.585000 4.585000 4.585000 4.585000
4.585000 4.585000 4.585000 4.585000 4.585000 4.585000
4.585000 4.585000 4.585000 4.585000 4.585000 4.585000
4.585000 4.585000 4.585000 4.585000 4.585000 4.585000
4.585000 4.585000 4.585000 4.585000 4.585000 4.585000
4.585000 4.585000 4.585000 4.585000 4.585000 4.585000
4.585000 4.585000 4.585000 4.585000 4.585000 4.585000

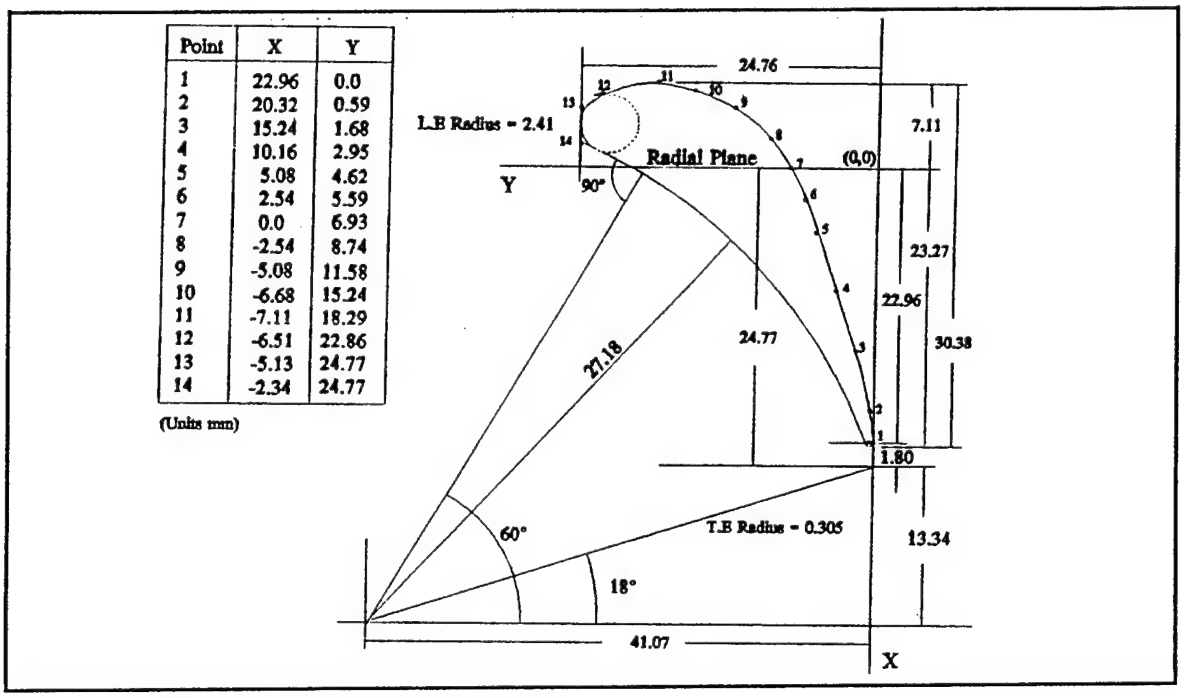

Figure B1. Blade Geometry From Ref. [6]

APPENDIX C. RVC3D SAMPLE INPUT AND EXECUTION

The following input namelist example was for a 0.6815 pressure ratio with subsonic exit boundary conditions and Cebeci-Smith turbulence modeling.

```
'TRANSONIC TURBINE Annular Cascade'
&nl1   im=150 jm=31 km=65 itl=20 iil=67 &end
&nl2   cfl=5.5 avisc1=0.0 avisc2=0.0 avisc4=0.50 ivdt=1 nstg=4 itmax=1200
       irs=1 epi=0.50 epj=0.60 epk=0.60 &end
&nl3   ibcin=3 ibcex=3 isymt=0 ires=10 icrnt=50
       iresti=0 iresto=1 ibcpw=0 iqin=0 &end
&nl4   emxx=0.13 emty=0.0 emrz=0.0 expt=0.0 prat=0.6815 ga=1.4
       om=0.000000 igeom=1 alex=-67.0 &end
&nl5   ilt=3 tw=1.00 renr=6.651e6 prnr=.7 prtr=.9 vispwr=.666666
       srtip=0.0 cmutm=14. jedge=31 kedge=20 iltin=2 dblh=0.0048 dblt=0.0178 &end
&nl6   io1=1 io2=165 oar=0. ixjb=0 njo=1 nko=3
       jo=1 ko=5 11 16 &end
```

Runs on the NPS Cray computer took approximately 12 hours for a 1,200 iteration convergence and were accomplished with the command:

```
>qsub myjob.nqs
```

where the file myjob.nqs was as follows:

myjob.nqs

```
#QSUB -q prem -lT 50000 -lM 9Mw
cd /d1/whdonova
./exec.rvc3d < rvc3d.in > rvc3d.out
```

Runs on the NASA Ames Research Center Cray computer took approximately 1 hour for a 1,200 iteration convergence and were accomplished with the command:

```
>qsub -lm 10Mw -lt 14400 rvc3d.com
```

where the file rvc3d.com was as follows:

rvc3d.com

```
cd /m/vn/v3/wdonovan
./exec.rvc3d < rvc3d.in > rvc3d.out
```

APPENDIX D. BLADE MIDSPAN SURFACE PRESSURE DATA

Prat = 0.6837	Date: 10/27/94, 1230 local, Run #1	Baro = 30.08 inhg	Tstag = 104°F
Scanivalve Port #	Scanivalve Port Value	Static Pressure (psi)	P/Po
1	P ambient	14.7739	
2	P calibration	24.5716	
4	Po (Ref. Upstream Stagnation)	22.2306	1.0000
5	P hub exit (Static @ 0.5c downstream)	15.1982	
6	P up static (Ref. Upstream Static)	22.2190	
9	P Static Port 1 (@ leading edge)	22.2524	1.0010
10	P Static Port 2	21.3661	0.9611
11	P Static Port 3	19.5768	0.8806
12	P Static Port 4	16.9327	0.7617
13	P Static Port 5	15.4186	0.6936
14	P Static Port 6	15.6884	0.7057
15	P Static Port 7	15.4516	0.6951
16	P Static Port 8 (@ leading edge)	22.2242	0.9997
17	P Static Port 9	22.0043	0.9898
18	P Static Port 10	21.0074	0.9450
19	P Static Port 11	20.0537	0.9021
Prat = 0.6828	Date: 10/27/94, 1245 local, Run #2	Baro = 30.08 inhg	Tstag = 105°F
Scanivalve Port #	Scanivalve Port Value	Static Pressure (psi)	P/Po
1	P ambient	14.7739	
2	P calibration	24.5786	
4	Po (Ref. Upstream Stagnation)	22.2571	1.0000
5	P hub exit (Static @ 0.5c downstream)	15.1969	
6	P up static (Ref. Upstream Static)	22.2622	
9	P Static Port 1 (@ leading edge)	22.2576	1.0000
10	P Static Port 2	21.3866	0.9609
11	P Static Port 3	19.5839	0.8799
12	P Static Port 4	16.9291	0.7606
13	P Static Port 5	15.3810	0.6911
14	P Static Port 6	15.6660	0.7039
15	P Static Port 7	15.4305	0.6933
16	P Static Port 8 (@ leading edge)	22.2670	1.0004
17	P Static Port 9	22.0659	0.9914
18	P Static Port 10	21.0580	0.9461
19	P Static Port 11	20.1035	0.9032
Prat = 0.6820	Date: 10/27/94, 1255 local, Run #3	Baro = 30.09 inhg	Tstag = 106°F
Scanivalve Port #	Scanivalve Port Value	Static Pressure (psi)	P/Po
1	P ambient	14.7813	
2	P calibration	24.5609	
4	Po (Ref. Upstream Stagnation)	22.2541	1.0000
5	P hub exit (Static @ 0.5c downstream)	15.1779	
6	P up static (Ref. Upstream Static)	22.2372	
9	P Static Port 1 (@ leading edge)	22.2562	1.0001
10	P Static Port 2	21.3422	0.9590
11	P Static Port 3	19.5633	0.8791
12	P Static Port 4	16.9163	0.7601
13	P Static Port 5	15.4302	0.6934
14	P Static Port 6	15.6781	0.7045
15	P Static Port 7	15.4566	0.6946
16	P Static Port 8 (@ leading edge)	22.2340	0.9991
17	P Static Port 9	22.0180	0.9894
18	P Static Port 10	21.0070	0.9440
19	P Static Port 11	20.0738	0.9020

Table D1. 0.6815 Pressure Ratio Series #1

Prat = 0.6779	Date: 11/02/94, 1430 local, Run #4	Baro = 29.84 inhg	Tstag = 98°F
Scanivalve Port #	Scanivalve Port Value	Static Pressure (psi)	P/Po
1	P ambient	14.6560	
2	P calibration	24.4824	
4	Po (Ref. Upstream Stagnation)	22.2493	1.0000
5	P hub exit (Static @ 0.5c downstream)	15.0818	
6	P up static (Ref. Upstream Static)	22.2322	
9	P Static Port 1 (@ leading edge)	22.2633	1.0006
10	P Static Port 2	21.3571	0.9599
11	P Static Port 3	19.5428	0.8784
12	P Static Port 4	16.8398	0.7569
13	P Static Port 5	15.3090	0.6881
14	P Static Port 6	15.5667	0.6996
15	P Static Port 7	15.3472	0.6898
16	P Static Port 8 (@ leading edge)	22.2201	0.9987
17	P Static Port 9	21.9913	0.9884
18	P Static Port 10	20.9822	0.9430
19	P Static Port 11	20.0285	0.9002
Prat = 0.6809	Date: 11/02/94, 1445 local, Run #5	Baro = 29.84 inhg	Tstag = 101°F
Scanivalve Port #	Scanivalve Port Value	Static Pressure (psi)	P/Po
1	P ambient	14.6560	
2	P calibration	24.4829	
4	Po (Ref. Upstream Stagnation)	22.1573	1.0000
5	P hub exit (Static @ 0.5c downstream)	15.0879	
6	P up static (Ref. Upstream Static)	22.1395	
9	P Static Port 1 (@ leading edge)	22.1270	0.9986
10	P Static Port 2	21.2561	0.9593
11	P Static Port 3	19.4558	0.8781
12	P Static Port 4	16.8161	0.7589
13	P Static Port 5	15.2810	0.6897
14	P Static Port 6	15.5741	0.7029
15	P Static Port 7	15.3099	0.6910
16	P Static Port 8 (@ leading edge)	22.1201	0.9983
17	P Static Port 9	21.9032	0.9885
18	P Static Port 10	20.8871	0.9427
19	P Static Port 11	19.9552	0.9006
Prat = 0.6801	Date: 11/02/94, 1455 local, Run #6	Baro = 29.84 inhg	Tstag = 102°F
Scanivalve Port #	Scanivalve Port Value	Static Pressure (psi)	P/Po
1	P ambient	14.6560	
2	P calibration	24.4737	
4	Po (Ref. Upstream Stagnation)	22.1854	1.0000
5	P hub exit (Static @ 0.5c downstream)	15.0893	
6	P up static (Ref. Upstream Static)	22.1707	
9	P Static Port 1 (@ leading edge)	22.1671	0.9992
10	P Static Port 2	21.2940	0.9598
11	P Static Port 3	19.4914	0.8786
12	P Static Port 4	16.8298	0.7586
13	P Static Port 5	15.3149	0.6903
14	P Static Port 6	15.5797	0.7023
15	P Static Port 7	15.3721	0.6929
16	P Static Port 8 (@ leading edge)	22.1570	0.9987
17	P Static Port 9	21.9304	0.9885
18	P Static Port 10	20.9124	0.9426
19	P Static Port 11	19.9889	0.9010

Table D2. 0.6815 Pressure Ratio Series #2

Prat = 0.5060	Date: 11/21/94, 1600 local, Run #1	Baro = 30.09 inhg	Tstag = 115°F
Scanivalve Port #	Scanivalve Port Value	Static Pressure (psi)	P/Po
1	P ambient	14.7788	
2	P calibration	24.6074	
4	Po (Ref. Upstream Stagnation)	30.5239	1.0000
5	P hub exit (Static @ 0.5c downstream)	15.4450	
6	P up static (Ref. Upstream Static)	30.8693	
9	P Static Port 1 (@ leading edge)	30.8956	1.0122
10	P Static Port 2	29.4056	0.9634
11	P Static Port 3	26.3156	0.8621
12	P Static Port 4	21.3339	0.6989
13	P Static Port 5	16.5247	0.5414
14	P Static Port 6	17.0462	0.5585
15	P Static Port 7	15.8206	0.5183
16	P Static Port 8 (@ leading edge)	30.8472	1.0106
17	P Static Port 9	30.4413	0.9973
18	P Static Port 10	28.7061	0.9404
19	P Static Port 11	27.0593	0.8865
Prat = 0.5080	Date: 11/21/94, 1605 local, Run #2	Baro = 30.09 inhg	Tstag = 115°F
Scanivalve Port #	Scanivalve Port Value	Static Pressure (psi)	P/Po
1	P ambient	14.7788	
2	P calibration	24.6073	
4	Po (Ref. Upstream Stagnation)	30.5541	1.0000
5	P hub exit (Static @ 0.5c downstream)	15.5215	
6	P up static (Ref. Upstream Static)	30.8504	
9	P Static Port 1 (@ leading edge)	30.9060	1.0115
10	P Static Port 2	29.4090	0.9625
11	P Static Port 3	26.3010	0.8608
12	P Static Port 4	21.3622	0.6992
13	P Static Port 5	16.6027	0.5434
14	P Static Port 6	17.0540	0.5582
15	P Static Port 7	15.9400	0.5217
16	P Static Port 8 (@ leading edge)	30.8135	1.0085
17	P Static Port 9	30.4450	0.9964
18	P Static Port 10	28.7116	0.9397
19	P Static Port 11	27.0684	0.8859
Prat = 0.5070	Date: 11/21/94, 1610 local, Run #3	Baro = 30.09 inhg	Tstag = 115°F
Scanivalve Port #	Scanivalve Port Value	Static Pressure (psi)	P/Po
1	P ambient	14.7788	
2	P calibration	24.6079	
4	Po (Ref. Upstream Stagnation)	30.6047	1.0000
5	P hub exit (Static @ 0.5c downstream)	15.5163	
6	P up static (Ref. Upstream Static)	30.9081	
9	P Static Port 1 (@ leading edge)	30.9457	1.0111
10	P Static Port 2	29.4551	0.9624
11	P Static Port 3	26.3531	0.8611
12	P Static Port 4	21.3499	0.6976
13	P Static Port 5	16.5516	0.5408
14	P Static Port 6	17.0929	0.5585
15	P Static Port 7	15.9170	0.5201
16	P Static Port 8 (@ leading edge)	30.7752	1.0056
17	P Static Port 9	30.3840	0.9928
18	P Static Port 10	28.6649	0.9366
19	P Static Port 11	27.0382	0.8835

Table D3. 0.5070 Pressure Ratio Series

Prat = 0.6050	Date: 11/21/94, 1535 local, Run #1	Baro = 30.09 inhg	Tstag = 102°F
Scanivalve Port #	Scanivalve Port Value	Static Pressure (psi)	P/Po
1	P ambient	14.7788	
2	P calibration	24.6010	
4	Po (Ref. Upstream Stagnation)	25.3685	1.0000
5	P hub exit (Static @ 0.5c downstream)	15.3474	
6	P up static (Ref. Upstream Static)	25.3969	
9	P Static Port 1 (@ leading edge)	25.3960	1.0011
10	P Static Port 2	24.2663	0.9566
11	P Static Port 3	21.9130	0.8638
12	P Static Port 4	18.3058	0.7216
13	P Static Port 5	15.7541	0.6210
14	P Static Port 6	16.1405	0.6362
15	P Static Port 7	15.6129	0.6154
16	P Static Port 8 (@ leading edge)	25.3701	1.0001
17	P Static Port 9	25.0731	0.9884
18	P Static Port 10	23.7612	0.9366
19	P Static Port 11	22.5170	0.8876
Prat = 0.6045	Date: 11/21/94, 1545 local, Run #2	Baro = 30.09 inhg	Tstag = 105°F
Scanivalve Port #	Scanivalve Port Value	Static Pressure (psi)	P/Po
1	P ambient	14.7788	
2	P calibration	24.5934	
4	Po (Ref. Upstream Stagnation)	25.3393	1.0000
5	P hub exit (Static @ 0.5c downstream)	15.3187	
6	P up static (Ref. Upstream Static)	25.3541	
9	P Static Port 1 (@ leading edge)	25.4161	1.0030
10	P Static Port 2	24.3015	0.9590
11	P Static Port 3	21.9296	0.8654
12	P Static Port 4	18.3235	0.7231
13	P Static Port 5	15.7793	0.6227
14	P Static Port 6	16.1046	0.6356
15	P Static Port 7	15.6232	0.6166
16	P Static Port 8 (@ leading edge)	25.2650	0.9971
17	P Static Port 9	24.9943	0.9864
18	P Static Port 10	23.6995	0.9353
19	P Static Port 11	22.4807	0.8872
Prat = 0.6026	Date: 11/21/94, 1555 local, Run #3	Baro = 30.09 inhg	Tstag = 105°F
Scanivalve Port #	Scanivalve Port Value	Static Pressure (psi)	P/Po
1	P ambient	14.7788	
2	P calibration	24.5966	
4	Po (Ref. Upstream Stagnation)	25.3541	1.0000
5	P hub exit (Static @ 0.5c downstream)	15.2796	
6	P up static (Ref. Upstream Static)	25.4145	
9	P Static Port 1 (@ leading edge)	25.3978	1.0017
10	P Static Port 2	24.2691	0.9572
11	P Static Port 3	21.9214	0.8646
12	P Static Port 4	18.3097	0.7222
13	P Static Port 5	15.7499	0.6212
14	P Static Port 6	16.1173	0.6357
15	P Static Port 7	15.6638	0.6178
16	P Static Port 8 (@ leading edge)	25.3317	0.9991
17	P Static Port 9	25.0652	0.9886
18	P Static Port 10	23.7501	0.9367
19	P Static Port 11	22.5026	0.8875

Table D4. 0.6041 Pressure Ratio Series

Prat = 0.8083	Date: 11/21/94, 1505 local, Run #1	Baro = 30.09 inhg	Tstag = 95°F
Scanivalve Port #	Scanivalve Port Value	Static Pressure (psi)	P/Po
1	P ambient	14.7788	
2	P calibration	24.6032	
4	Po (Ref. Upstream Stagnation)	18.5613	1.0000
5	P hub exit (Static @ 0.5c downstream)	15.0026	
6	P up static (Ref. Upstream Static)	18.5834	
9	P Static Port 1 (@ leading edge)	18.5658	1.0002
10	P Static Port 2	18.0638	0.9732
11	P Static Port 3	17.0140	0.9166
12	P Static Port 4	15.6507	0.8432
13	P Static Port 5	15.0818	0.8125
14	P Static Port 6	15.2191	0.8199
15	P Static Port 7	15.1762	0.8176
16	P Static Port 8 (@ leading edge)	18.5516	0.9995
17	P Static Port 9	18.4358	0.9932
18	P Static Port 10	17.8276	0.9605
19	P Static Port 11	17.3184	0.9330
Prat = 0.8071	Date: 11/21/94, 1515 local, Run #2	Baro = 30.09 inhg	Tstag = 96°F
Scanivalve Port #	Scanivalve Port Value	Static Pressure (psi)	P/Po
1	P ambient	14.7788	
2	P calibration	24.6037	
4	Po (Ref. Upstream Stagnation)	18.5866	1.0000
5	P hub exit (Static @ 0.5c downstream)	15.0020	
6	P up static (Ref. Upstream Static)	18.5665	
9	P Static Port 1 (@ leading edge)	18.5504	0.9981
10	P Static Port 2	18.0527	0.9713
11	P Static Port 3	17.0381	0.9167
12	P Static Port 4	15.6733	0.8433
13	P Static Port 5	15.0533	0.8099
14	P Static Port 6	15.2127	0.8185
15	P Static Port 7	15.1776	0.8166
16	P Static Port 8 (@ leading edge)	18.5620	0.9987
17	P Static Port 9	18.4420	0.9922
18	P Static Port 10	17.8390	0.9598
19	P Static Port 11	17.3165	0.9317
Prat = 0.8078	Date: 11/21/94, 1525 local, Run #3	Baro = 30.09 inhg	Tstag = 96°F
Scanivalve Port #	Scanivalve Port Value	Static Pressure (psi)	P/Po
1	P ambient	14.7788	
2	P calibration	24.6012	
4	Po (Ref. Upstream Stagnation)	18.5811	1.0000
5	P hub exit (Static @ 0.5c downstream)	15.0096	
6	P up static (Ref. Upstream Static)	18.5759	
9	P Static Port 1 (@ leading edge)	18.5878	1.0004
10	P Static Port 2	18.1007	0.9741
11	P Static Port 3	17.0542	0.9178
12	P Static Port 4	15.6716	0.8434
13	P Static Port 5	15.0769	0.8114
14	P Static Port 6	15.2120	0.8187
15	P Static Port 7	15.1707	0.8165
16	P Static Port 8 (@ leading edge)	18.5753	0.9997
17	P Static Port 9	18.4218	0.9914
18	P Static Port 10	17.8355	0.9599
19	P Static Port 11	17.3416	0.9333

Table D5. 0.8077 Pressure Ratio Series

Prat = 0.9063	Date: 11/21/94, 1430 local, Run #1	Baro = 30.09 inhg	Tstag = 90°F
Scanivalve Port #	Scanivalve Port Value	Static Pressure (psi)	P/Po
1	P ambient	14.7788	
2	P calibration	24.6056	
4	Po (Ref. Upstream Stagnation)	16.4287	1.0000
5	P hub exit (Static @ 0.5c downstream)	14.8888	
6	P up static (Ref. Upstream Static)	16.4464	
9	P Static Port 1 (@ leading edge)	16.4600	1.0019
10	P Static Port 2	16.2173	0.9871
11	P Static Port 3	15.7200	0.9569
12	P Static Port 4	15.1043	0.9194
13	P Static Port 5	14.8879	0.9062
14	P Static Port 6	14.9555	0.9103
15	P Static Port 7	14.9519	0.9101
16	P Static Port 8 (@ leading edge)	16.4225	0.9996
17	P Static Port 9	16.4047	0.9985
18	P Static Port 10	16.1224	0.9814
19	P Static Port 11	15.8879	0.9671
Prat = 0.9054	Date: 11/21/94, 1445 local, Run #2	Baro = 30.09 inhg	Tstag = 91°F
Scanivalve Port #	Scanivalve Port Value	Static Pressure (psi)	P/Po
1	P ambient	14.7880	
2	P calibration	24.5959	
4	Po (Ref. Upstream Stagnation)	16.4376	1.0000
5	P hub exit (Static @ 0.5c downstream)	14.8830	
6	P up static (Ref. Upstream Static)	16.4723	
9	P Static Port 1 (@ leading edge)	16.4365	0.9999
10	P Static Port 2	16.2328	0.9875
11	P Static Port 3	15.7218	0.9565
12	P Static Port 4	15.1136	0.9195
13	P Static Port 5	14.8797	0.9052
14	P Static Port 6	14.9571	0.9099
15	P Static Port 7	14.9630	0.9103
16	P Static Port 8 (@ leading edge)	16.4432	1.0003
17	P Static Port 9	16.3780	0.9964
18	P Static Port 10	16.1170	0.9805
19	P Static Port 11	15.8915	0.9668
Prat = 0.9046	Date: 11/21/94, 1455 local, Run #3	Baro = 30.09 inhg	Tstag = 93°F
Scanivalve Port #	Scanivalve Port Value	Static Pressure (psi)	P/Po
1	P ambient	14.7788	
2	P calibration	24.5980	
4	Po (Ref. Upstream Stagnation)	16.4384	1.0000
5	P hub exit (Static @ 0.5c downstream)	14.8704	
6	P up static (Ref. Upstream Static)	16.4480	
9	P Static Port 1 (@ leading edge)	16.4672	1.0018
10	P Static Port 2	16.2248	0.9870
11	P Static Port 3	15.7233	0.9565
12	P Static Port 4	15.1201	0.9198
13	P Static Port 5	14.8891	0.9058
14	P Static Port 6	14.9702	0.9107
15	P Static Port 7	14.9636	0.9103
16	P Static Port 8 (@ leading edge)	16.4591	1.0013
17	P Static Port 9	16.3869	0.9969
18	P Static Port 10	16.1301	0.9812
19	P Static Port 11	15.8869	0.9665

Table D6. 0.9054 Pressure Ratio Series

APPENDIX E. LDV DATA

Wake Position	Depth	V-theta	V-z	V total	Mach	Flow Angle	V-theta	V-z	T stag (°F)	95.0
(degrees)	(mm)	(m/s)	(m/s)	(m/s)	Number	(degrees)	turb. int.	turb. int.	P static (inhg)	30.03
-8	0.01	83.2	21.8	86.0	0.244	75.3	7.76	5.19	P stag (inhg)	3.13
-8	0.06	85.7	21.9	88.5	0.252	75.7	8.37	5.26	Prat	0.9056
-8	0.18	87.1	22.5	90.0	0.256	75.5	7.83	5.06	M exit	0.379
-8	0.42	92.5	22.6	95.2	0.271	76.3	7.60	5.08	T exit (°K)	299.4
-8	0.89	97.3	22.7	99.9	0.284	76.9	7.12	4.23	a exit (m/s)	346.84
-8	1.78	99.0	22.8	101.6	0.289	77.0	5.41	3.98	a stag (m/s)	351.79
-8	3.34	102.0	24.6	104.9	0.298	76.4	5.39	3.98	V exit (m/s)	131.46
Wake Position	Depth	V-theta	V-z	V total	Mach	Flow Angle	V-theta	V-z	T stag (°F)	95.0
(degrees)	(mm)	(m/s)	(m/s)	(m/s)	Number	(degrees)	turb. int.	turb. int.	P static (inhg)	30.03
-7	0.01	86.8	21.4	89.4	0.254	76.2	7.56	5.40	P stag (inhg)	3.13
-7	0.06	87.3	21.8	90.0	0.256	76.0	8.29	5.52	Prat	0.9056
-7	0.18	89.4	22.3	92.1	0.262	76.0	7.83	5.63	M exit	0.379
-7	0.42	92.0	22.6	94.7	0.269	76.2	7.69	5.17	T exit (°K)	299.4
-7	0.89	96.6	23.0	99.3	0.282	76.6	6.96	4.85	a exit (m/s)	346.84
-7	1.78	98.4	23.0	101.1	0.287	76.8	5.49	4.18	a stag (m/s)	351.79
-7	3.34	100.0	24.5	103.0	0.293	76.2	5.09	4.59	V exit (m/s)	131.46
Wake Position	Depth	V-theta	V-z	V total	Mach	Flow Angle	V-theta	V-z	T stag (°F)	95.0
(degrees)	(mm)	(m/s)	(m/s)	(m/s)	Number	(degrees)	turb. int.	turb. int.	P static (inhg)	30.03
-6	0.01	86.1	21.8	88.8	0.252	75.8	7.09	5.92	P stag (inhg)	3.13
-6	0.06	87.6	21.9	90.3	0.257	76.0	7.56	5.66	Prat	0.9056
-6	0.18	88.4	22.6	91.2	0.259	75.7	8.29	5.84	M exit	0.379
-6	0.42	91.7	23.3	94.6	0.269	75.7	7.58	5.71	T exit (°K)	299.4
-6	0.89	96.2	23.0	98.9	0.281	76.6	6.40	5.19	a exit (m/s)	346.84
-6	1.78	99.7	23.5	102.4	0.291	76.7	5.26	4.29	a stag (m/s)	351.79
-6	3.34	103.0	24.4	105.9	0.301	76.7	6.68	4.11	V exit (m/s)	131.46
Wake Position	Depth	V-theta	V-z	V total	Mach	Flow Angle	V-theta	V-z	T stag (°F)	96.0
(degrees)	(mm)	(m/s)	(m/s)	(m/s)	Number	(degrees)	turb. int.	turb. int.	P static (inhg)	30.03
-5	0.01	85.6	21.8	88.3	0.251	75.7	7.60	6.32	P stag (inhg)	3.13
-5	0.06	86.9	22.3	89.7	0.255	75.6	8.13	6.39	Prat	0.9056
-5	0.18	89.7	22.4	92.5	0.263	76.0	7.29	5.90	M exit	0.379
-5	0.42	91.9	22.8	94.7	0.269	76.1	7.34	5.95	T exit (°K)	299.9
-5	0.89	95.8	23.6	98.7	0.280	76.2	6.81	5.43	a exit (m/s)	347.15
-5	1.78	98.6	23.7	101.4	0.288	76.5	5.11	4.75	a stag (m/s)	352.10
-5	3.34	102.0	24.6	104.9	0.298	76.4	5.97	4.13	V exit (m/s)	131.58

Table E1. LDV Data (Wake Positions of -8, -7, -6, and -5 Degrees)

Wake Position	Depth	V-theta	V-z	V total	Mach	Flow Angle	V-theta	V-z	T stag (°F)	96.0
(degrees)	(mm)	(m/s)	(m/s)	(m/s)	Number	(degrees)	turb. int.	turb. int.	P static (inhg)	30.03
-4	0.01	86.1	22.8	89.1	0.253	75.2	7.35	6.45	P stag (inhg)	3.13
-4	0.06	87.3	22.4	90.1	0.256	75.6	7.04	6.50	Prat	0.9056
-4	0.18	88.5	24.1	91.7	0.260	74.8	7.56	6.25	M exit	0.379
-4	0.42	90.9	22.6	93.7	0.266	76.0	6.95	5.93	T exit (°K)	299.9
-4	0.89	96.6	24.6	99.7	0.283	75.7	6.78	5.44	a exit (m/s)	347.15
-4	1.78	98.9	24.4	101.9	0.289	76.1	4.42	4.63	a stag (m/s)	352.10
-4	3.34	103.0	25.7	106.2	0.302	76.0	5.66	3.87	V exit (m/s)	131.58
Wake Position	Depth	V-theta	V-z	V total	Mach	Flow Angle	V-theta	V-z	T stag (°F)	96.0
(degrees)	(mm)	(m/s)	(m/s)	(m/s)	Number	(degrees)	turb. int.	turb. int.	P static (inhg)	30.03
-3	0.01	85.4	23.4	88.5	0.251	74.7	7.34	6.57	P stag (inhg)	3.13
-3	0.06	86.4	22.8	89.4	0.254	75.2	7.26	6.11	Prat	0.9056
-3	0.18	87.9	22.5	90.7	0.258	75.6	6.74	6.33	M exit	0.379
-3	0.42	90.8	24.1	93.9	0.267	75.1	6.77	5.97	T exit (°K)	299.9
-3	0.89	95.0	24.4	98.1	0.279	75.6	6.27	5.36	a exit (m/s)	347.15
-3	1.78	100.0	24.6	103.0	0.293	76.2	4.50	4.68	a stag (m/s)	352.10
-3	3.34	103.0	26.1	106.3	0.302	75.8	3.91	3.62	V exit (m/s)	131.58
Wake Position	Depth	V-theta	V-z	V total	Mach	Flow Angle	V-theta	V-z	T stag (°F)	96.0
(degrees)	(mm)	(m/s)	(m/s)	(m/s)	Number	(degrees)	turb. int.	turb. int.	P static (inhg)	30.03
-2	0.01	87.7	23.7	90.8	0.258	74.9	7.83	6.19	P stag (inhg)	3.13
-2	0.06	87.4	23.8	90.6	0.257	74.8	7.98	5.92	Prat	0.9056
-2	0.18	89.2	24.1	92.4	0.262	74.9	7.75	6.04	M exit	0.379
-2	0.42	92.1	24.4	95.3	0.271	75.2	7.83	5.92	T exit (°K)	299.9
-2	0.89	94.9	24.3	98.0	0.278	75.6	6.68	5.44	a exit (m/s)	347.15
-2	1.78	100.0	24.4	102.9	0.292	76.3	4.54	4.92	a stag (m/s)	352.10
-2	3.34	104.0	25.6	107.1	0.304	76.2	3.73	4.03	V exit (m/s)	131.58
Wake Position	Depth	V-theta	V-z	V total	Mach	Flow Angle	V-theta	V-z	T stag (°F)	96.0
(degrees)	(mm)	(m/s)	(m/s)	(m/s)	Number	(degrees)	turb. int.	turb. int.	P static (inhg)	30.03
-1	0.01	88.5	24.0	91.7	0.260	74.8	8.36	5.66	P stag (inhg)	3.13
-1	0.06	89.0	23.5	92.1	0.262	75.2	7.42	5.40	Prat	0.9056
-1	0.18	90.4	23.9	93.5	0.266	75.2	7.75	5.54	M exit	0.379
-1	0.42	93.0	23.6	95.9	0.272	75.8	7.00	5.46	T exit (°K)	299.9
-1	0.89	97.0	24.5	100.0	0.284	75.8	6.37	4.96	a exit (m/s)	347.15
-1	1.78	99.6	24.8	102.6	0.291	76.0	4.72	4.05	a stag (m/s)	352.10
-1	3.34	105.0	26.3	108.2	0.307	75.9	3.75	3.93	V exit (m/s)	131.58

Table E2. LDV Data (Wake Positions of -4, -3, -2, and -1 Degrees)

Wake Position	Depth	V-theta	V-z	V total	Mach	Flow Angle	V-theta	V-z	T stag (°F)	96.0
(degrees)	(mm)	(m/s)	(m/s)	(m/s)	Number	(degrees)	turb. int.	turb. int.	P static (inhg)	30.03
0	0.01	90.2	24.7	93.5	0.266	74.7	8.47	5.12	P stag (inhg)	3.13
0	0.06	92.6	24.5	95.8	0.272	75.2	7.68	4.89	Prat	0.9056
0	0.18	92.6	24.5	95.8	0.272	75.2	7.64	4.68	M exit	0.379
0	0.42	98.4	24.9	101.5	0.288	75.8	7.03	4.54	T exit (°K)	299.9
0	0.89	101.7	24.5	104.6	0.297	76.5	6.10	4.13	a exit (m/s)	347.15
0	1.78	103.6	24.8	106.5	0.302	76.5	3.90	3.88	a stag (m/s)	352.10
0	3.34	106.8	27.1	110.2	0.313	75.7	2.87	3.23	V exit (m/s)	131.58
Wake Position	Depth	V-theta	V-z	V total	Mach	Flow Angle	V-theta	V-z	T stag (°F)	100.0
(degrees)	(mm)	(m/s)	(m/s)	(m/s)	Number	(degrees)	turb. int.	turb. int.	P static (inhg)	30.03
1	0.01	89.1	24.4	92.4	0.261	74.7	8.18	4.78	P stag (inhg)	3.13
1	0.06	91.1	24.3	94.3	0.267	75.1	7.73	4.63	Prat	0.9056
1	0.18	93.1	23.9	96.1	0.272	75.6	8.03	4.59	M exit	0.379
1	0.42	96.9	24.3	99.9	0.283	75.9	7.24	4.11	T exit (°K)	302.1
1	0.89	100.0	24.2	102.9	0.291	76.4	5.97	3.77	a exit (m/s)	348.40
1	1.78	104.0	24.2	106.8	0.302	76.9	3.96	3.68	a stag (m/s)	353.37
1	3.34	107.0	26.7	110.3	0.312	76.0	3.00	3.67	V exit (m/s)	132.05
Wake Position	Depth	V-theta	V-z	V total	Mach	Flow Angle	V-theta	V-z	T stag (°F)	100.0
(degrees)	(mm)	(m/s)	(m/s)	(m/s)	Number	(degrees)	turb. int.	turb. int.	P static (inhg)	30.03
2	0.01	91.4	23.2	94.3	0.267	75.8	8.33	4.42	P stag (inhg)	3.13
2	0.06	90.7	23.2	93.6	0.265	75.7	7.95	4.09	Prat	0.9056
2	0.18	93.0	22.8	95.8	0.271	76.2	8.18	4.45	M exit	0.379
2	0.42	96.4	23.3	99.2	0.281	76.4	7.30	3.68	T exit (°K)	302.1
2	0.89	101.0	23.6	103.7	0.293	76.8	6.27	3.30	a exit (m/s)	348.40
2	1.78	103.0	24.2	105.8	0.299	76.8	4.66	3.09	a stag (m/s)	353.37
2	3.34	106.0	26.3	109.2	0.309	76.1	3.95	3.66	V exit (m/s)	132.05
Wake Position	Depth	V-theta	V-z	V total	Mach	Flow Angle	V-theta	V-z	T stag (°F)	98.0
(degrees)	(mm)	(m/s)	(m/s)	(m/s)	Number	(degrees)	turb. int.	turb. int.	P static (inhg)	30.03
3	0.01	89.3	22.5	92.1	0.261	75.9	8.42	4.74	P stag (inhg)	3.13
3	0.06	90.4	22.3	93.1	0.264	76.1	7.89	4.64	Prat	0.9056
3	0.18	91.9	22.9	94.7	0.268	76.0	8.27	4.01	M exit	0.379
3	0.42	95.1	22.3	97.7	0.277	76.8	7.66	3.94	T exit (°K)	301.0
3	0.89	98.2	22.8	100.8	0.286	76.9	7.06	3.62	a exit (m/s)	347.78
3	1.78	102.0	23.2	104.6	0.297	77.2	5.28	3.18	a stag (m/s)	352.74
3	3.34	104.0	25.6	107.1	0.304	76.2	4.83	3.23	V exit (m/s)	131.82

Table E3. LDV Data (Wake Positions of 0, 1, 2, and 3 Degrees)

Wake Position	Depth	V-theta	V-z	V total	Mach	Flow Angle	V-theta	V-z	T stag (°F)	97.0
(degrees)	(mm)	(m/s)	(m/s)	(m/s)	Number	(degrees)	turb. int.	turb. int.	P static (inhg)	30.03
4	0.01	87.5	21.8	90.2	0.256	76.0	8.73	4.64	P stag (inhg)	3.13
4	0.06	88.1	22.2	90.9	0.258	75.9	8.12	4.53	Prat	0.9056
4	0.18	90.4	21.9	93.0	0.264	76.4	7.90	4.69	M exit	0.379
4	0.42	91.8	22.0	94.4	0.268	76.5	7.82	4.28	T exit (°K)	300.5
4	0.89	97.8	22.2	100.3	0.285	77.2	6.92	4.23	a exit (m/s)	347.46
4	0.89	101.0	22.9	103.6	0.294	77.2	6.08	3.82	a stag (m/s)	352.42
4	3.34	102.0	24.8	105.0	0.298	76.3	6.12	3.85	V exit (m/s)	131.70
Wake Position	Depth	V-theta	V-z	V total	Mach	Flow Angle	V-theta	V-z	T stag (°F)	96.0
(degrees)	(mm)	(m/s)	(m/s)	(m/s)	Number	(degrees)	turb. int.	turb. int.	P static (inhg)	30.03
5	0.01	85.2	22.7	88.2	0.250	75.1	7.28	5.66	P stag (inhg)	3.13
5	0.06	87.7	22.7	90.6	0.257	75.5	8.36	5.63	Prat	0.9056
5	0.18	89.4	22.6	92.2	0.262	75.8	7.60	5.65	M exit	0.379
5	0.42	92.9	22.8	95.7	0.272	76.2	7.83	5.25	T exit (°K)	299.9
5	0.89	97.4	23.3	100.1	0.284	76.5	6.93	5.12	a exit (m/s)	281.71
5	1.78	99.1	22.5	101.6	0.289	77.2	5.36	4.83	a stag (m/s)	285.73
5	3.34	99.8	24.2	102.7	0.292	76.4	5.24	4.07	V exit (m/s)	106.79
Wake Position	Depth	V-theta	V-z	V total	Mach	Flow Angle	V-theta	V-z	T stag (°F)	96.0
(degrees)	(mm)	(m/s)	(m/s)	(m/s)	Number	(degrees)	turb. int.	turb. int.	P static (inhg)	30.03
6	0.01	85.9	22.0	88.7	0.252	75.6	7.56	5.85	P stag (inhg)	3.13
6	0.06	85.1	22.8	88.1	0.250	75.0	7.13	6.05	Prat	0.9056
6	0.18	87.9	22.9	90.8	0.258	75.4	7.28	6.14	M exit	0.379
6	0.42	91.1	23.1	94.0	0.267	75.8	7.11	5.76	T exit (°K)	299.9
6	0.89	94.7	23.4	97.5	0.277	76.1	6.66	5.36	a exit (m/s)	347.15
6	1.78	99.5	23.7	102.3	0.291	76.6	5.12	4.71	a stag (m/s)	352.10
6	3.34	101.0	25.0	104.0	0.295	76.1	4.39	4.02	V exit (m/s)	131.58
Wake Position	Depth	V-theta	V-z	V total	Mach	Flow Angle	V-theta	V-z	T stag (°F)	96.0
(degrees)	(mm)	(m/s)	(m/s)	(m/s)	Number	(degrees)	turb. int.	turb. int.	P static (inhg)	30.03
7	0.01	83.9	22.9	87.0	0.247	74.7	7.39	6.52	P stag (inhg)	3.13
7	0.06	86.6	23.2	89.7	0.255	75.0	7.59	6.19	Prat	0.9056
7	0.18	86.8	23.0	89.8	0.255	75.2	7.68	6.10	M exit	0.379
7	0.42	89.5	23.3	92.5	0.263	75.4	6.53	6.07	T exit (°K)	299.9
7	0.89	94.9	24.2	97.9	0.278	75.7	6.79	5.39	a exit (m/s)	347.15
7	1.78	98.5	25.1	101.6	0.289	75.7	4.88	4.48	a stag (m/s)	352.10
7	3.34	102.0	24.9	105.0	0.298	76.3	4.24	4.80	V exit (m/s)	131.58

Table E4. LDV Data (Wake Positions of 4, 5, 6, and 7 Degrees)

Wake Position	Depth	V-theta	V-z	V total	Mach	Flow Angle	V-theta	V-z	T stag (°F)	96.0
(degrees)	(mm)	(m/s)	(m/s)	(m/s)	Number	(degrees)	turb. int.	turb. int.	P static (inhg)	30.03
8	0.01	85.8	23.1	88.9	0.252	74.9	7.68	6.08	P stag (inhg)	3.13
8	0.06	86.7	23.2	89.8	0.255	75.0	8.21	6.19	Prat	0.9056
8	0.18	88.4	23.3	91.4	0.260	75.2	6.94	6.66	M exit	0.379
8	0.42	91.9	23.7	94.9	0.270	75.5	7.08	6.18	T exit (°K)	299.9
8	0.89	95.3	24.1	98.3	0.279	75.8	6.68	5.50	a exit (m/s)	347.15
8	1.78	100.0	24.7	103.0	0.293	76.1	4.57	4.65	a stag (m/s)	352.10
8	3.34	103.0	25.5	106.1	0.301	76.1	3.83	3.86	V exit (m/s)	131.58

Table E5. LDV Data (Wake Position of 8 Degrees)

APPENDIX F. LDV REPEATABILITY DATA

Wake Position	Depth	V-theta	V-z	V total	Mach	Flow Angle	V-theta	V-z	T stag (°F)	96.0
(degrees)	(mm)	(m/s)	(m/s)	(m/s)	Number	(degrees)	turb. int.	turb. int.	P static (inhg)	29.99
Coincidence -8	0.01	90.4	22.4	93.1	0.264	76.1	8.74	4.61	P stag (inhg)	3.13
Coincidence -8	0.06	91.0	22.6	93.8	0.266	76.1	8.74	4.60	Prat	0.9055
Coincidence -8	0.18	92.3	22.2	94.9	0.270	76.5	8.66	4.54	M exit	0.379
Coincidence -8	0.42	96.4	22.1	98.9	0.281	77.1	8.28	4.48	T exit (°K)	299.9
Coincidence -8	0.89	99.5	22.2	101.9	0.289	77.4	7.58	4.27	a exit (m/s)	347.15
Coincidence -8	1.78	102.0	22.6	104.5	0.297	77.5	5.91	3.95	a stag (m/s)	352.10
Coincidence -8	3.34	104.0	25.5	107.1	0.304	76.2	4.88	4.24	V exit (m/s)	131.58
Wake Position	Depth	V-theta	V-z	V total	Mach	Flow Angle	V-theta	V-z	T stag (°F)	96.0
(degrees)	(mm)	(m/s)	(m/s)	(m/s)	Number	(degrees)	turb. int.	turb. int.	P static (inhg)	30.00
Random -8	0.01	89.8	22.4	92.6	0.263	76.0	8.97	4.74	P stag (inhg)	3.13
Random -8	0.06	91.4	22.5	94.1	0.267	76.2	8.28	4.67	Prat	0.9055
Random -8	0.18	92.7	22.5	95.4	0.271	76.4	8.51	4.54	M exit	0.379
Random -8	0.42	95.6	21.7	98.0	0.278	77.2	8.74	4.44	T exit (°K)	299.9
Random -8	0.89	99.6	22.2	102.0	0.290	77.4	7.52	4.23	a exit (m/s)	347.15
Random -8	1.78	101.0	22.8	103.5	0.294	77.3	5.83	3.58	a stag (m/s)	352.10
Random -8	3.34	104.0	25.8	107.2	0.304	76.1	5.16	3.65	V exit (m/s)	131.58
Wake Position	Depth	V-theta	V-z	V total	Mach	Flow Angle	V-theta	V-z	T stag (°F)	93.0
(degrees)	(mm)	(m/s)	(m/s)	(m/s)	Number	(degrees)	turb. int.	turb. int.	P static (inhg)	30.00
Coincidence 0	0.01	90.6	24.3	93.8	0.267	75.0	8.46	4.73	P stag (inhg)	3.13
Coincidence 0	0.06	92.4	23.9	95.4	0.272	75.5	7.85	5.17	Prat	0.9055
Coincidence 0	0.18	94.0	24.0	97.0	0.276	75.7	8.23	5.14	M exit	0.379
Coincidence 0	0.42	96.9	24.0	99.8	0.284	76.1	7.32	4.59	T exit (°K)	298.3
Coincidence 0	0.89	100.0	23.8	102.8	0.293	76.6	6.58	4.23	a exit (m/s)	346.21
Coincidence 0	1.78	104.0	24.7	106.9	0.304	76.6	4.33	3.33	a stag (m/s)	351.15
Coincidence 0	3.34	107.0	27.1	110.4	0.314	75.8	3.39	3.28	V exit (m/s)	131.23
Wake Position	Depth	V-theta	V-z	V total	Mach	Flow Angle	V-theta	V-z	T stag (°F)	87.0
(degrees)	(mm)	(m/s)	(m/s)	(m/s)	Number	(degrees)	turb. int.	turb. int.	P static (inhg)	30.00
Random 0	0.01	91.5	22.9	94.3	0.270	75.9	8.43	5.27	P stag (inhg)	3.13
Random 0	0.06	92.9	23.8	95.9	0.275	75.6	8.05	4.83	Prat	0.9055
Random 0	0.18	94.4	23.9	97.4	0.279	75.8	7.74	4.64	M exit	0.379
Random 0	0.42	97.5	24.1	100.4	0.287	76.1	6.87	4.56	T exit (°K)	295.1
Random 0	0.89	101.0	24.1	103.8	0.297	76.6	5.79	3.82	a exit (m/s)	344.33
Random 0	1.78	104.0	25.0	107.0	0.306	76.5	4.32	3.18	a stag (m/s)	349.24
Random 0	3.34	107.0	26.6	110.3	0.316	76.0	3.10	3.75	V exit (m/s)	130.51

Table F1. LDV Repeatability Data (Wake Positions of -8 and 0 Degrees)

Wake Position	Depth	V-theta	V-z	V total	Mach	Flow Angle	V-theta	V-z	T stag (°F)	95.0
(degrees)	(mm)	(m/s)	(m/s)	(m/s)	Number	(degrees)	turb. int.	turb. int.	P static (inhg)	30.00
Coincidence 7	0.01	88.5	24.5	91.8	0.261	74.5	8.06	5.59	P stag (inhg)	3.13
Coincidence 7	0.06	89.4	24.2	92.6	0.263	74.9	8.14	5.75	Prat	0.9055
Coincidence 7	0.18	92.1	24.5	95.3	0.271	75.1	7.76	5.74	M exit	0.379
Coincidence 7	0.42	93.9	24.4	97.0	0.276	75.4	7.07	5.58	T exit (°K)	299.4
Coincidence 7	0.89	98.3	24.6	101.3	0.288	76.0	6.25	5.25	a exit (m/s)	346.84
Coincidence 7	1.78	101.0	24.4	103.9	0.295	76.4	4.82	4.97	a stag (m/s)	351.79
Coincidence 7	3.34	103.0	25.5	106.1	0.302	76.1	4.33	4.70	V exit (m/s)	131.46
Wake Position	Depth	V-theta	V-z	V total	Mach	Flow Angle	V-theta	V-z	T stag (°F)	95.0
(degrees)	(mm)	(m/s)	(m/s)	(m/s)	Number	(degrees)	turb. int.	turb. int.	P static (inhg)	30.00
Random 7	0.01	88.5	24.3	91.8	0.261	74.6	8.22	5.95	P stag (inhg)	3.13
Random 7	0.06	89.9	24.6	93.2	0.265	74.7	7.68	6.06	Prat	0.9055
Random 7	0.18	91.4	24.5	94.6	0.269	75.0	7.42	6.09	M exit	0.379
Random 7	0.42	93.8	23.8	96.8	0.275	75.8	7.20	5.91	T exit (°K)	299.4
Random 7	0.89	98.1	24.3	101.1	0.287	76.1	6.21	5.49	a exit (m/s)	346.84
Random 7	1.78	101.0	24.4	103.9	0.295	76.4	4.61	4.66	a stag (m/s)	351.79
Random 7	3.34	103.0	25.3	106.1	0.302	76.2	4.18	4.50	V exit (m/s)	131.46

Table F2. LDV Repeatability Data (Wake Position of 7 Degrees)

APPENDIX G. COMPUTATIONAL DATA REDUCTION

Residual (fort.4) and P/P_0 (fort.7) files were produced from the solution (fort.3) files using the FORTRAN program **pxy.f**.

Program **pxy.f**

```
c*****************************************************************
c     pxy.f reads rvc3d files & writes ascii files for gnuplot
c     unit 1 = input xyz file
c     unit 3 = input q file
c     unit 7 = output blade pressures on 5 k-planes
c     unit 4 = output residual history
c*****************************************************************
parameter(ni=150,nj=31,nk=65)
      real x(ni,nj,nk),y(ni,nj,nk),z(ni,nj,nk)
      real qq(5,ni,nj,nk),resd(5000,5)
      real pk(5),xk(5)
      dimension kk(5)
c     k-values are hard-wired below (hub, 25%, 50%, 75%, tip)
     data kk/2,27,33,39,64/
c*****************************************************************
c     read grid coordinates
c*****************************************************************
read(1,*)im,jm,km
      read(1,*)(((x(i,j,k),i=1,im),j=1,jm),k=1,km),
     1      (((y(i,j,k),i=1,im),j=1,jm),k=1,km),
     2      (((z(i,j,k),i=1,im),j=1,jm),k=1,km)
c*****************************************************************
c     read restart file
c*****************************************************************
read(3,*)imax,jmax,kmax
      read(3,*)fsmach,alpha,re,time
c
       icheck=iabs(im-imax)+iabs(jm-jmax)+iabs(km-kmax)
      if(icheck.ne.0)then
     write(6,610)im,jm,km,imax,jmax,kmax
     stop
     endif
c
      read(3,*)((((qq(l,i,j,k),i=1,im),j=1,jm),k=1,km),l=1,5)
c
c     additional residual data
      read(3,*)itl,iil,phdeg,ga,om,nres,dum,dum,dum,dum
      read(3,*)((resd(nr,l),nr=1,nres),l=1,5)
c*****************************************************************
c     ps/p0 output to unit 3
c*****************************************************************
itr=im+1-itl
      ggm=ga*(ga-1.)
     j=1
```

```
c     normalize x by chord
      do 7 l=1,5
      k=kk(l)
      xmin=x(im/2,j,k)
      xmax=x(itl, j,k)
      do 5 i=itl,itr
      xmin=min(xmin,x(i,j,k))
    5 xmax=max(xmax,x(i,j,k))
      chord=xmax-xmin
      do 7 i=itl,itr
    7 x(i,j,k)=(x(i,j,k)-xmin)/chord

      write(7,305)(kk(l),l=1,5)
      do 20 i=itl,itr
      do 10 l=1,5
      k=kk(l)
      pk(l)=ggm*(qq(5,i,j,k)-.5*(qq(2,i,j,k)**2+qq(3,i,j,k)**2
     1+qq(4,i,j,k)**2)/qq(1,i,j,k))
   10 xk(l)=x(i,j,k)
   20 write(7,300)i,(xk(l),pk(l),l=1,5)
c*****************************************************************
c     residual history output to unit 4
c*****************************************************************
write(4,310) 1,(resd(1,l),l=1,5)
      do 30 j=2,nres
      it=10*(j-1)
   30 write(4,310)it,(resd(j,l),l=1,5)
c*****************************************************************
300  format(i5,10f10.5)
  305 format('   k=',5(17x,i3))
  310 format(i5,5(1x,e10.3))
  610 format(' ***** warning *****',/,
     1       ' im, jm, km, read from input',3i5,' do not match',/,
     2       ' im, jm, km, read from restart file',3i5)
      stop
      end
```

The **plane.f** program from Reference 6 was modified to compare two-dimensional experimental and computational Mach number and wake flow angle. Mach number, based on stagnation conditions, was redefined with respect to tangential and axial velocity components.

Program **plane.f**

```
c*************************************************************
c     Modified by Lt. William Donovan on 08 May 95 for Master's Thesis
c     plane.f reads rvc3d files & writes ascii files for plotting
c        exit plane mach number and flow angles
c        (2D comparison with experimental results)
c     unit 1 = input xyz file
c     unit 3 = input q file
c     unit 4 = output residual history
c     unit 7 = output (k #1) counter, theta, pt/p0,Mach, Angle
c     unit 8 = output (k #2) counter, theta, pt/p0,Mach, Angle
c     unit 9 = output (k #3) counter, theta, pt/p0,Mach, Angle
c     unit 10 = output (k #4) counter, theta, pt/p0,Mach, Angle
c     unit 11 = output (k #5) counter, theta, pt/p0,Mach, Angle
c
c*************************************************************
parameter(ni=150,nj=31,nk=65)
      integer um
      real x(ni,nj,nk),y(ni,nj,nk),z(ni,nj,nk), gama
      real qq(5,ni,nj,nk),resd(5000,5),q1,q2,q3,q4,q5,m(5)
      dimension kk(5),ang(5),theta(5),tt0(5),vtnd(5),vrnd(5),
     1  vznd(5),ptp0(5),deg(5)
c
c     k-values are hard-wired below (80.9%, 89.8%, 94.9%, 97.6%, 99.0%)
c     (use span.f to obtain %-k equivalency)
C     (k values of 61 and 64 obtained from a second program run)
c
      data kk/41,45,49,53,57/
c*************************************************************
c     read grid coordinates
c*************************************************************
read(1,*)im,jm,km
      read(1,*)(((x(i,j,k),i=1,im),j=1,jm),k=1,km),
     1       (((y(i,j,k),i=1,im),j=1,jm),k=1,km),
     2       (((z(i,j,k),i=1,im),j=1,jm),k=1,km)
c*************************************************************
c     read restart file
c*************************************************************
read(3,*)imax,jmax,kmax
      read(3,*)fsmach,alpha,re,time
c
       icheck=iabs(im-imax)+iabs(jm-jmax)+iabs(km-kmax)
      if(icheck.ne.0)then
      write(6,610)im,jm,km,imax,jmax,kmax
      stop
      endif
c
```

```
      read(3,*)((((qq(l,i,j,k),i=1,im),j=1,jm),k=1,km),l=1,5)
c
c     additional residual data
      read(3,*)itl,iil,phdeg,gama,om,nres,dum,dum,dum,dum
      read(3,*)((resd(nr,l),nr=1,nres),l=1,5)
c*****************************************************************
c     Pressure side of exit wake cut...
c*****************************************************************
k=kk(3)
      i=1
      do 10 j=jmax,1,-1
       um=um+1
       do 15 l=1,5
        k=kk(l)
c
c   Rename desired q values for use
c
          q1=qq(1,i,j,k)
          q2=qq(2,i,j,k)
          q3=qq(3,i,j,k)
          q4=qq(4,i,j,k)
          q5=qq(5,i,j,k)
c
c   Compute pt/p0 ratio
c
           ptp0(l)=gama*(gama-1)*q5+(gama-gama**2/2)/q1*(q2**2+q3**2+q4**2)
c
c   Compute T/Tt ratio and mach number
c
          tt0(l)=gama*(gama-1)/q1*(q5-0.5*(q2**2+q3**2+q4**2)/q1)
          m(l)=((1/tt0(l)-1)*2.0/(gama-1))**0.5
c
c   Compute Theta and Non-D velocities theta, r and z
c
          theta(l)=asin(y(i,j,k)/(z(i,j,k)**2+y(i,j,k)**2)**0.5)
          vtnd(l)=-q4*sin(theta(l))+q3*cos(theta(l))
          vrnd(l)=q4*cos(theta(l))+q3*sin(theta(l))
          vznd(l)=q2
          m(l)=(sqrt(vtnd(l)**2+vznd(l)**2))/q1
         deg(l)=theta(l)*57.296
c
c   Compute flow angle (degrees) using vtnd and vznd
c
          ang(l)=atan2(vtnd(l),vznd(l))*57.296
   15  continue
       write(7,300)um,deg(1),ptp0(1),m(1),ang(1)
       write(8,300)um,deg(2),ptp0(2),m(2),ang(2)
       write(9,300)um,deg(3),ptp0(3),m(3),ang(3)
       write(10,300)um,deg(4),ptp0(4),m(4),ang(4)
       write(11,300)um,deg(5),ptp0(5),m(5),ang(5)
   10 continue
c
c   Repeat above on other side of wake cut at imax
c     j=1 not used (duplicate location across wake)
c     jmax not repeated (same location as j=31 at i=1)
```

```
c
      jmaxm=jmax-1
      i=im
      do 30 j=2,jmaxm,1
       um=um+1
       do 25 l=1,5
        k=kk(l)
          q1=qq(1,i,j,k)
          q2=qq(2,i,j,k)
          q3=qq(3,i,j,k)
          q4=qq(4,i,j,k)
          q5=qq(5,i,j,k)
           ptp0(l)=gama*(gama-1)*q5+(gama-gama**2/2)/q1*(q2**2+q3**2+q4**2)
          tt0(l)=gama*(gama-1)/q1*(q5-0.5*(q2**2+q3**2+q4**2)/q1)
          m(l)=((1/tt0(l)-1)*2/(gama-1))**0.5
          theta(l)=asin(y(i,j,k)/(z(i,j,k)**2+y(i,j,k)**2)**0.5)
          vtnd(l)=-q4*sin(theta(l))+q3*cos(theta(l))
          vrnd(l)=q4*cos(theta(l))+q3*sin(theta(l))
          vznd(l)=q2
          m(l)=(sqrt(vtnd(l)**2+vznd(l)**2))/q1
         deg(l)=theta(l)*57.296
          ang(l)=atan2(vtnd(l),vznd(l))*57.296
   25  continue
       write(7,300)um,deg(1),ptp0(1),m(1),ang(1)
       write(8,300)um,deg(2),ptp0(2),m(2),ang(2)
       write(9,300)um,deg(3),ptp0(3),m(3),ang(3)
       write(10,300)um,deg(4),ptp0(4),m(4),ang(4)
       write(11,300)um,deg(5),ptp0(5),m(5),ang(5)
   30 continue
c*****************************************************************
c     residual history output to unit 4
c*****************************************************************
write(4,310) 1,(resd(1,l),l=1,5)
      do 40 j=2,nres
      it=10*(j-1)
   40 write(4,310)it,(resd(j,l),l=1,5)
c*****************************************************************
300  format(i5,5f8.3)
  310  format(i5,5(1x,e10.3))
  610  format(' ***** warning *****',/,
     1       ' im, jm, km, read from input',3i5,' do not match',/,
     2       ' im, jm, km, read from restart file',3i5)
      stop
      end
```

APPENDIX H. MACH NUMBER AND FLOW ANGLE COMPARISONS

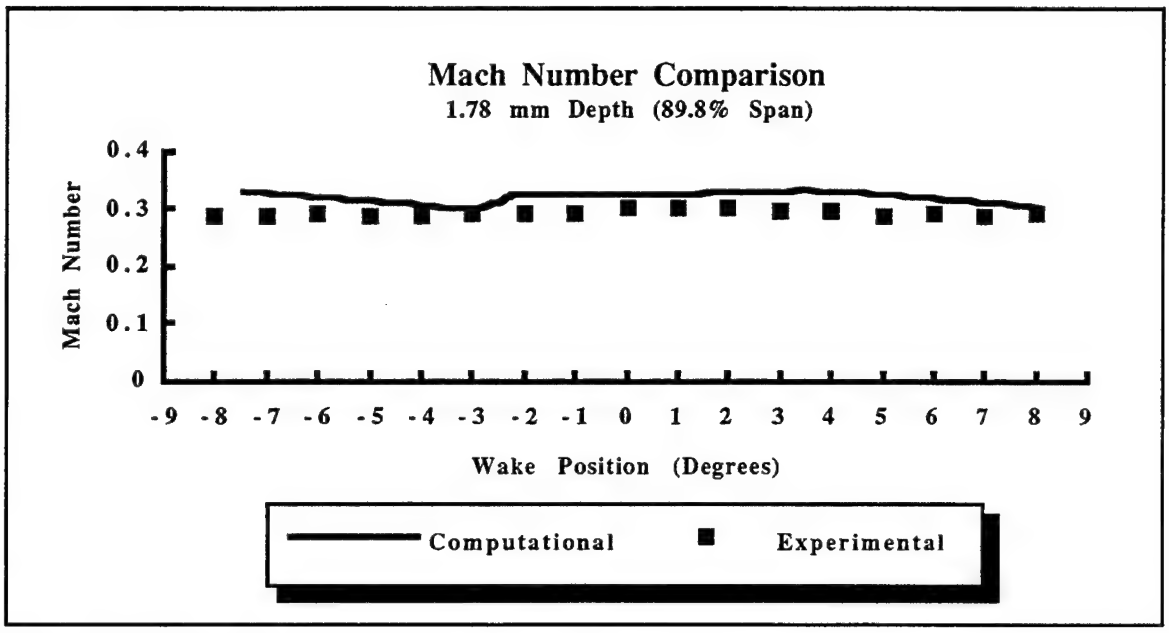

Figure H1. Mach Number Comparison At 1.78 mm Depth

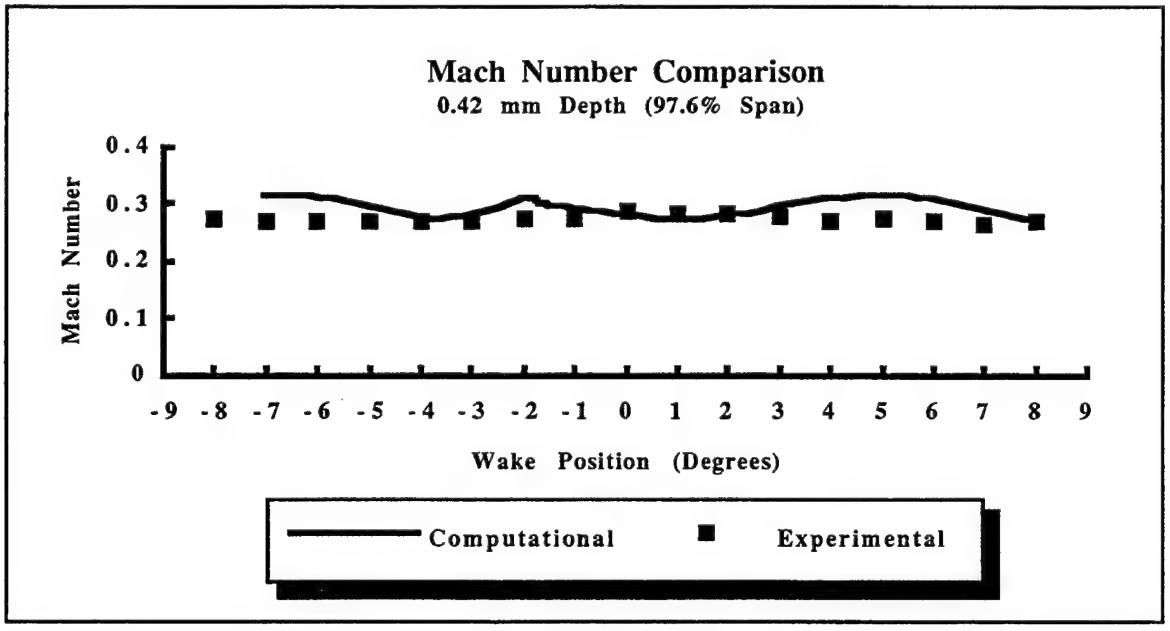

Figure H2. Mach Number Comparison At 0.42 mm Depth

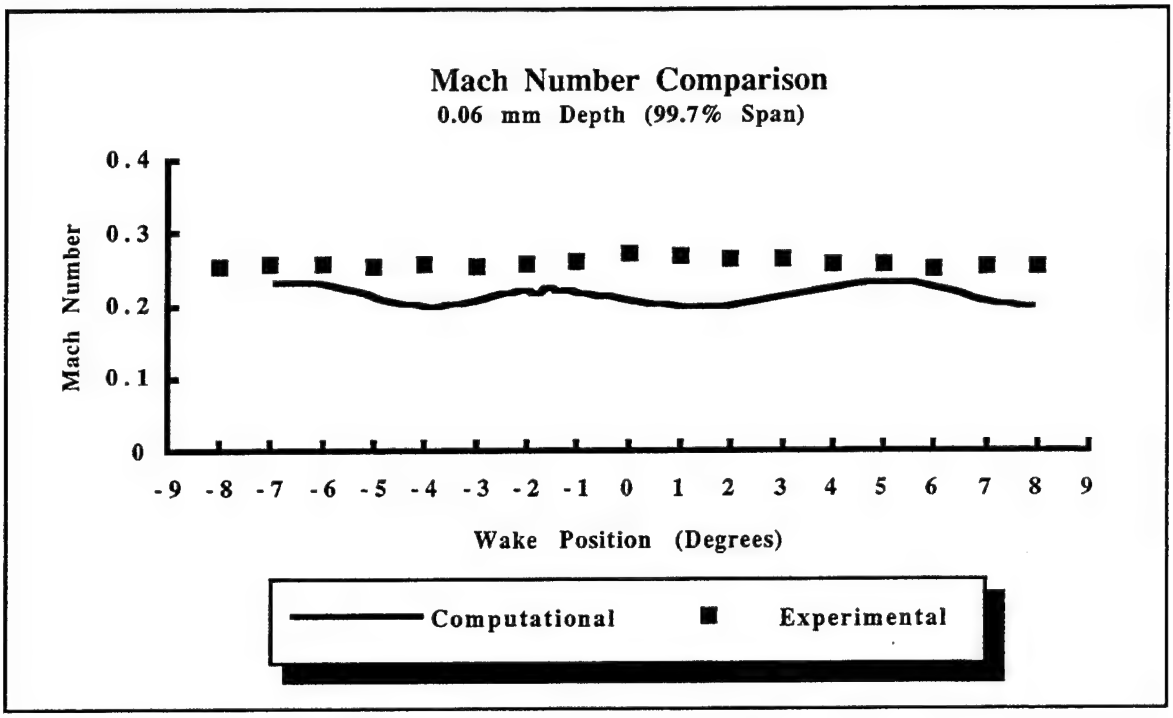

Figure H3. Mach Number Comparison At 0.06 mm Depth

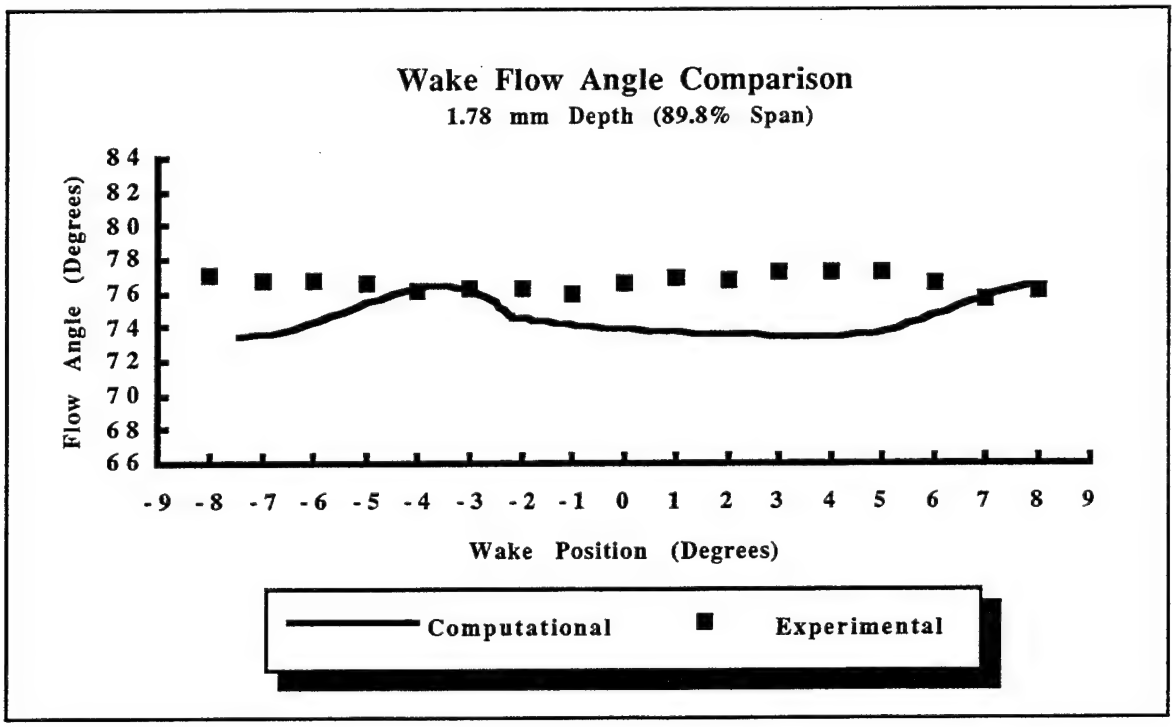

Figure H4. Flow Angle Comparison At 1.78 mm Depth

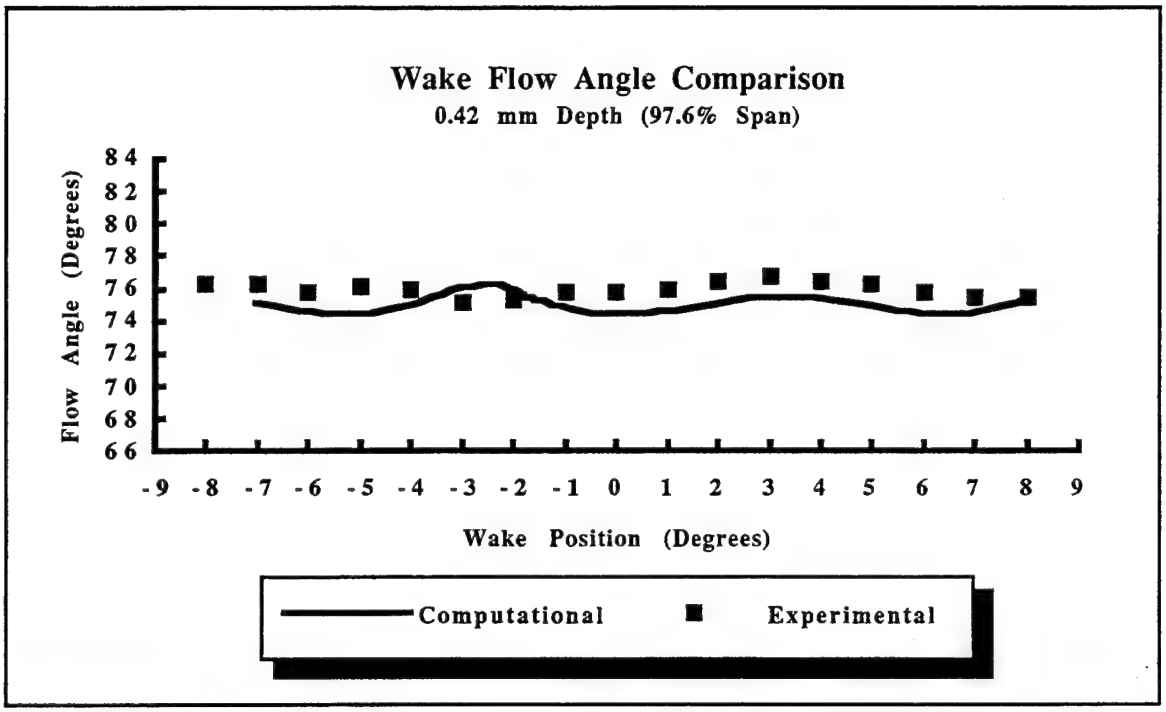

Figure H5. Flow Angle Comparison At 0.42 mm Depth

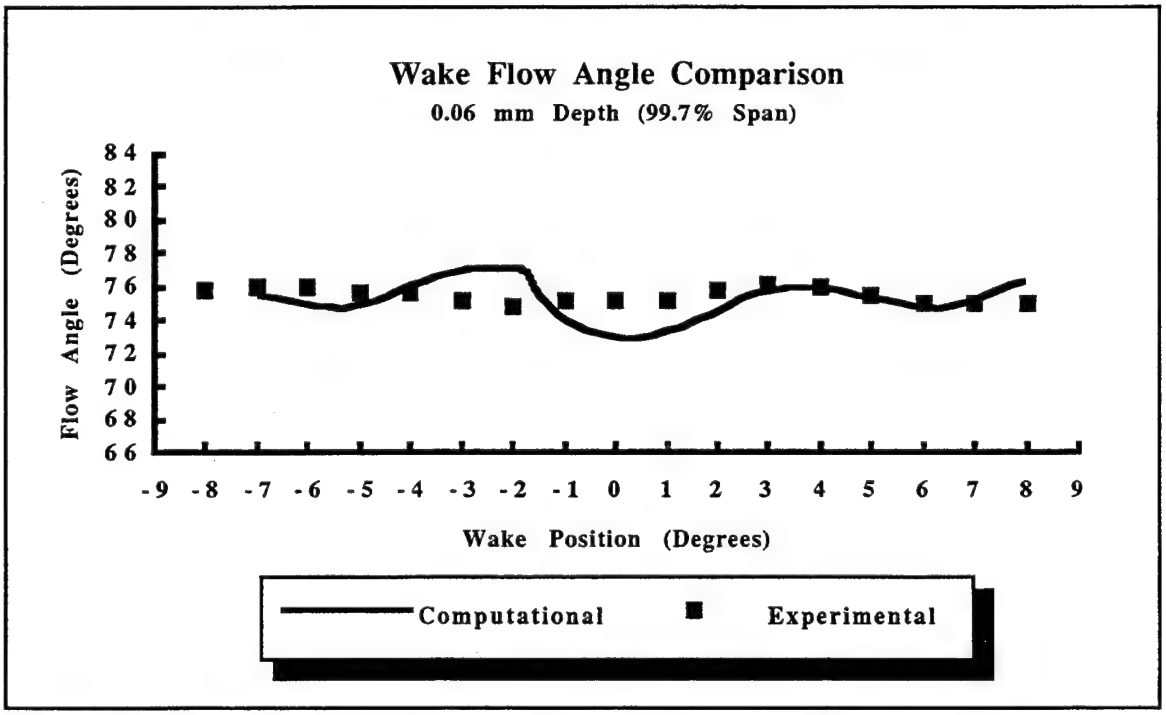

Figure H6. Flow Angle Comparison At 0.06 mm Depth

APPENDIX I. CONVERGENCE HISTORY

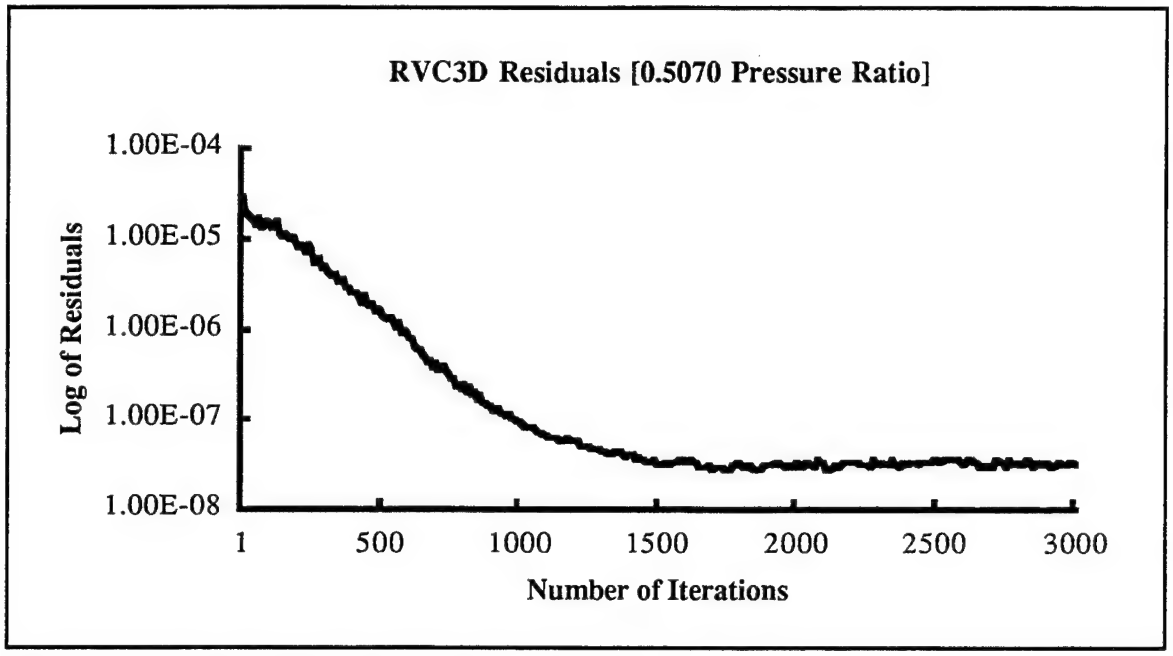

Figure I1. 0.5070 Pressure Ratio Convergence History

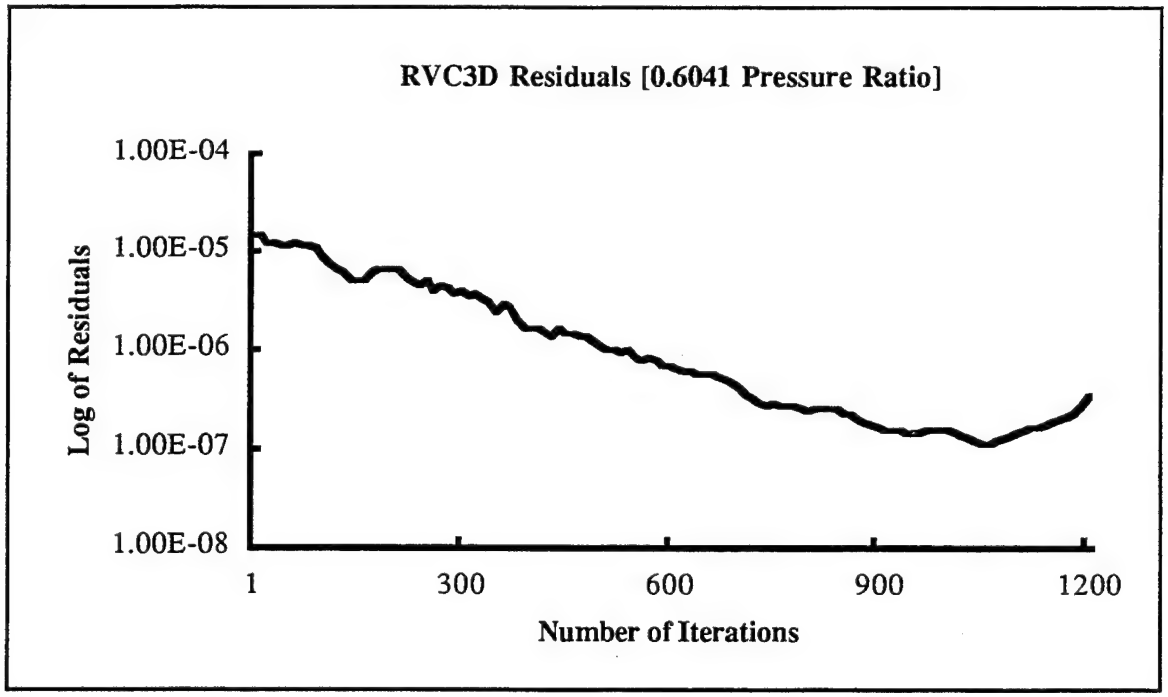

Figure I2. 0.6041 Pressure Ratio Convergence History

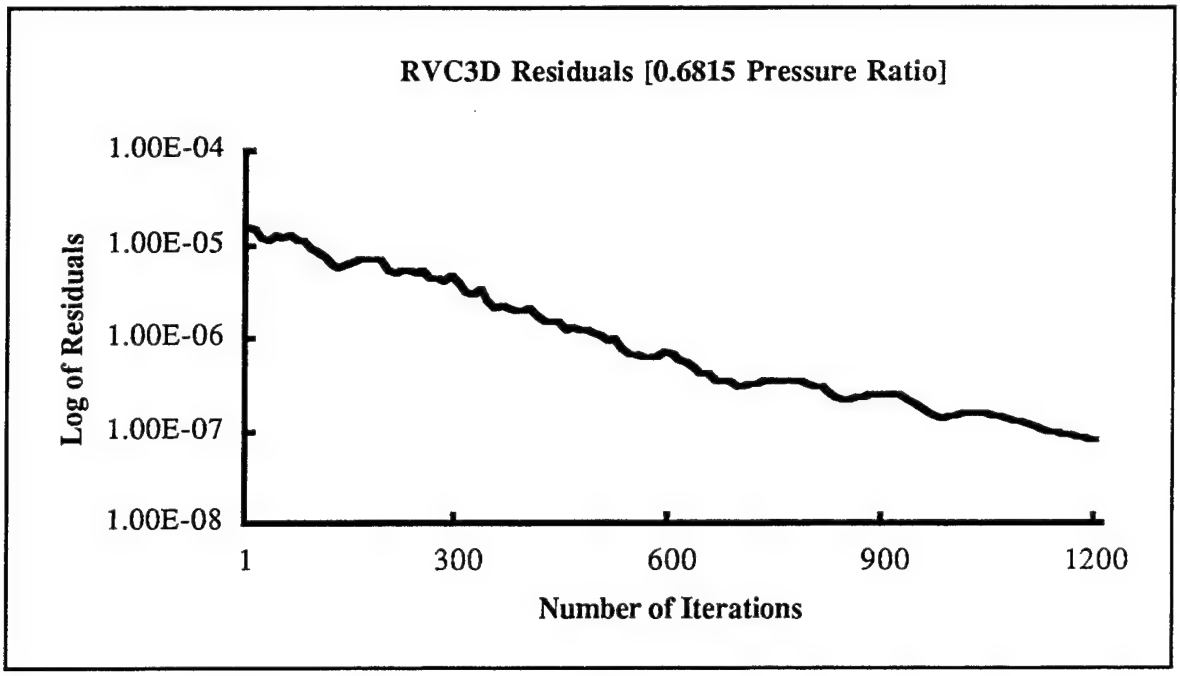

Figure I3. 0.6815 Pressure Ratio Convergence History

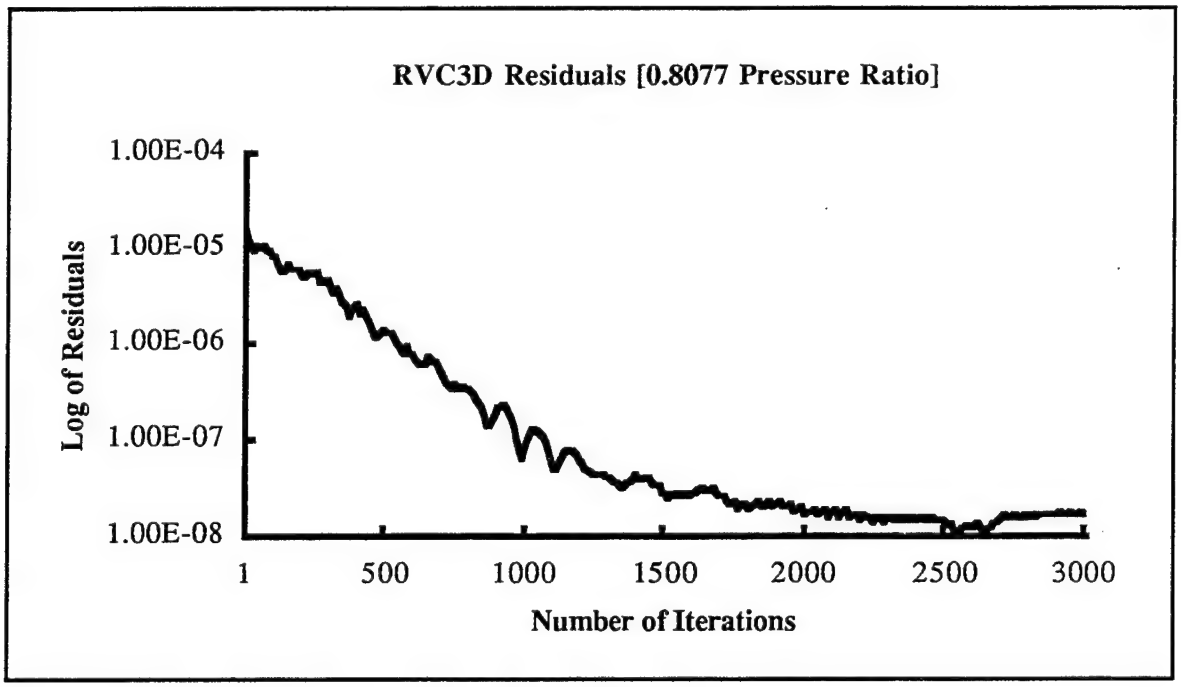

Figure I4. 0.8077 Pressure Ratio Convergence History

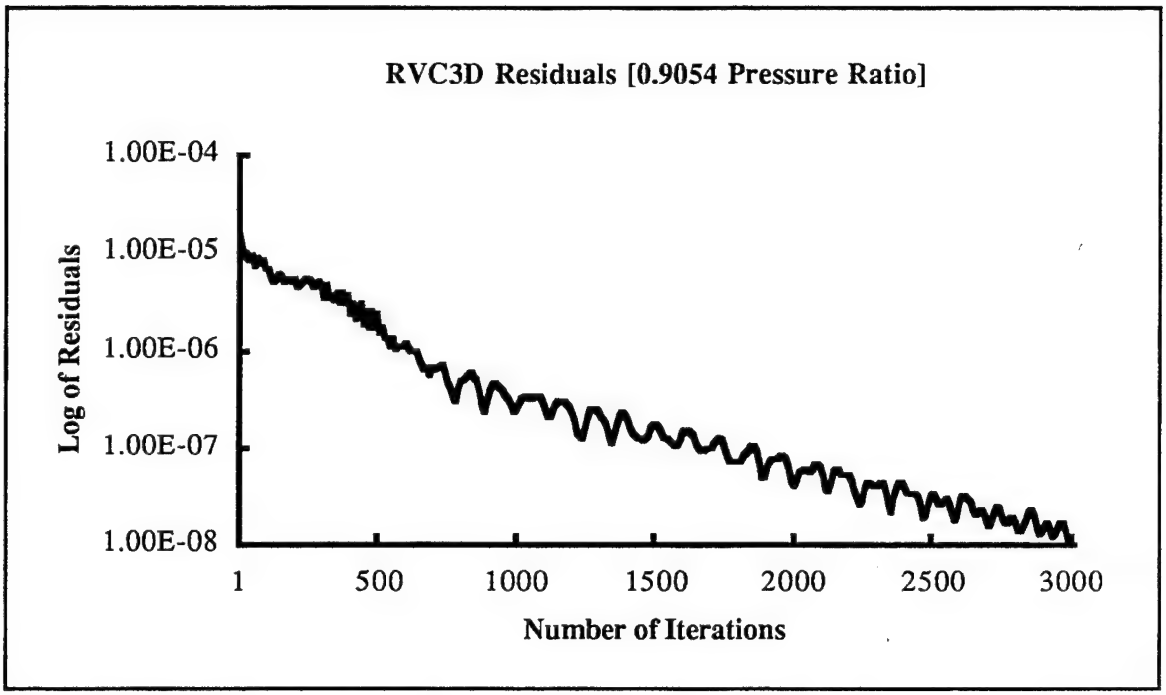

Figure I5. 0.9054 Pressure Ratio Convergence History

APPENDIX J. MULTIPLE GRID AND SOLUTION PLOTTING

Program **mgrid.f** read an x, y, z formatted grid file (fort.1) and converted it into a multiple grid file format (fort.21) for use with PLOT3D.

Program **mgrid.f**

```
ccccccccccccccccccccccccccccccccccccccccccccccccccccccccccccccccccccccccccc
c     Program to read a single PLOT3D file and convert
c     it to a mgrid file format
ccccccccccccccccccccccccccccccccccccccccccccccccccccccccccccccccccccccccccc
      real x(250,65,65),y(250,65,65),z(250,65,65)
      real yy(250,65,65),zz(250,65,65)
      read(1,*)idim,jdim,kdim
      read(1,*)(((x(i,j,k),i=1,idim),j=1,jdim),k=1,kdim),
     #         (((y(i,j,k),i=1,idim),j=1,jdim),k=1,kdim),
     #         (((z(i,j,k),i=1,idim),j=1,jdim),k=1,kdim)
      write(*,*)'Done reading fort.1'
c
c     calculate pitch
c
      jm=jdim
      im=idim
       r2=y(1,jm,1)**2+z(1,jm,1)**2
      sinp=(y(1,jm,1)*z(im,jm,1)-y(im,jm,1)*z(1,jm,1))/r2
      pitch=asin(sinp)
c
      do i=1,idim
        do j=1,jdim
          do k=1,kdim
                r=(z(i,j,k)**2+y(i,j,k)**2)**0.5
                theta=asin(y(i,j,k)/r)
                theta=theta+pitch
                yy(i,j,k)=r*sin(theta)
                zz(i,j,k)=r*cos(theta)
          enddo
        enddo
      enddo
c
      write(21)2
      write(21)(idim,jdim,kdim,igrid=1,2)
c     do 10 igrid=1,2
      write(21)(((x(i,j,k),i=1,idim),j=1,jdim),k=1,kdim),
     #         (((y(i,j,k),i=1,idim),j=1,jdim),k=1,kdim),
     #         (((z(i,j,k),i=1,idim),j=1,jdim),k=1,kdim)
c  10 continue
      write(21)(((x(i,j,k),i=1,idim),j=1,jdim),k=1,kdim),
     #         (((yy(i,j,k),i=1,idim),j=1,jdim),k=1,kdim),
     #         (((zz(i,j,k),i=1,idim),j=1,jdim),k=1,kdim)
      stop
      end
```

Program **mq.f** read a solution file (fort.3) and converted it into a multiple solution file format (fort.23) for use with PLOT3D.

Program **mq.f**

```
ccccccccccccccccccccccccccccccccccccccccccccccccccccccccccccccccccccccccc
c
c     Program to read a single PLOT3D file and convert
c     it to a Q_mgrid file format
c
ccccccccccccccccccccccccccccccccccccccccccccccccccccccccccccccccccccccccc
      real qq(250,65,65,5)
      read(3,*)idim,jdim,kdim
      read(3,*)fsmach,alpha,re,time
       read(3,*)((((qq(i,j,k,nx),i=1,idim),j=1,jdim),k=1,kdim),nx=1,5)
c
      write(23)2
      write(23)(idim,jdim,kdim,igrid=1,2)
      do 10 igrid=1,2
      write(23)fsmach,alpha,re,time
       write(23)((((qq(i,j,k,nx),i=1,idim),j=1,jdim),k=1,kdim),nx=1,5)
   10 continue
      stop
      end
```

LIST OF REFERENCES

1. Niehuis, R., Lucking, P. and Stubert, B., "Experimental and Numerical Study on Basic Phenomena of Secondary Flows in Turbines," presented and published for the AGARD Propulsion and Energetics Panel 74th (B) Specialists' Meeting, Luxembourg, 30 August-1 September 1989.

2. Goldman, L. J. and Seasholtz, R. G., "Laser Anemometer Measurements in an Annular Cascade of Core Turbine Vanes and Comparison With Theory," NASA Technical Paper 2018, July 1982.

3. Goldman, L. J. and Seasholtz, R. G., "Three Component Laser Anemometer Measurements in an Annular Cascade of Core Turbine Vanes With Contoured End Wall," NASA Technical Paper 2846, November 1988.

4. Goldman, L. J. and Seasholtz, R. G., "Laser Anemometer Measurements and Computations in an Annular Cascade of High Turning Core Turbine Vanes," NASA Technical Paper 3252, July 1992.

5. Thomas, G. D., "Measurement and Prediction of the Flow Through an Annular Turbine Cascade," Master's Thesis, Naval Postgraduate School, Monterey, CA, June 1993.

6. Spitz, J.D., "Laser Anemometry and Viscous Computation of the Flow Through an Annular Turbine Cascade," Master's Thesis, Naval Postgraduate School, Monterey, CA, March 1994.

7. Chima, R. V., "TCGRID," program documentation prepared at NASA Lewis Research Center, November 1990.

8. Chima, R. V., "RVC3D - Rotor Viscous Code 3-D," Users Manual and Documentation prepared at NASA Lewis Research Center, March 1992.

9. Chima, R. V. and Yokota, J. W., "Numerical Analysis of Three-Dimensional Viscous Flows in Turbomachinery," AIAA Journal, Vol. 28, No. 5, May 1990, pp. 798-806.

10. Chima, R. V., "Viscous Three-Dimensional Calculations of Transonic Fan Performance," presented and published for the AGARD 7th Propulsion and Energetics Panel Symposium on CFD Techniques for Propulsion Applications, San Antonio, TX, May 27-31, 1991. Also NASA TM-103800.

11. Saxer, A. P. and Giles, M. B., "Quasi-Three-Dimensional Nonreflecting Boundary Conditions for Euler Equation Calculations," Journal of Propulsion and Power, Vol. 9, No. 2, March-April 1993, pp. 263-271.

12. Chima, R. V., Private Communication, Feburary 16, 1995.

13. Walatka, P. P., Clucas, J., McCabe, R. K., Plessel, T. and Potter, R., FAST Users Manual, version 1.1a, July 1993.

14. Walatka, P. P., Buning, P. G., Pierce, L. and Elson, P. A., PLOT3D users manual, 1990. Also NASA TM 10167.

INITIAL DISTRIBUTION LIST

		No. Copies
1.	Defense Technical Information Center Cameron Station Alexandria, VA 22304-6145	2
2.	Library, Code 52 Naval Postgraduate School Monterey, CA 93943-5101	2
3.	Professor Daniel J. Collins Department of Aeronautics and Astronautics Code AA/CO Naval Postgraduate School 699 Dyer Road-Room 137 Monterey, CA 93943-5106	1
4.	Professor Garth V. Hobson Department of Aeronautics and Astronautics Code AA/HG Naval Postgraduate School 699 Dyer Road-Room 137 Monterey, CA 93943-5106	10
5.	Professor Raymond P. Shreeve Department of Aeronautics and Astronautics Code AA/SF Naval Postgraduate School 699 Dyer Road-Room 137 Monterey, CA 93943-5106	1
6.	Naval Air Systems Command AIR-4.4.T (Attn: Mr. C. Gordon) Washington, DC 20361-5360	1
7.	Naval Air Warfare Center Aircraft Division AIR-4.4.3.1(Attn: D. Parish) Propulsion and Power Engineering, Building 106 Patuxent River, MD 20670-5304	1
8.	William H. Donovan P.O. Box 980 Northville, NY 12134	3